Contrib. Plasma Phys. **54**, No. 1, 27 – 99 (2014) / **DOI** 10.1002/ctpp.201300066

Quantum Breathing Mode of Trapped Particles: From Nanoplasmas to Ultracold Gases

J. W. Abraham* and **M. Bonitz**

Institut für Theoretische Physik und Astrophysik, Christian-Albrechts-Universität zu Kiel, Leibnizstraße 15, D-24098 Kiel, Germany

Received 02 December 2013, accepted 09 December 2013
Published online 28 January 2014

Key words Non-Neutral plasmas, nanoplasmas, clusters, quantum dots, artificial atoms, ultracold gases, monopole mode, sum rules, Hartree-Fock, Thomas-Fermi

Particles spatially confined in trapping potentials have attracted increasing interest over the recent decade. Of particular importance are systems of charged particles, such as non-neutral plasmas, nanoplasmas, electrons in metal clusters, electrons in quantum-confined semiconductor structures ("artificial atoms"), electrons on the surface of liquid helium, ions in traps or highly charged particles (grains) in dusty plasmas. A second example of recent interest are systems with other kinds of pair interactions, including dipole interaction, which is important for excitons in quantum wells or ultracold Fermi and Bose gases in traps and optical lattices.

Trapped systems are fundamentally different from macroscopic systems since they are dominated by strong spatial inhomogeneity and finite size effects (the properties depend on the exact particle number). Furthermore, by changing the strength of the confinement potential, the many-particle state of the system can be externally controlled—from weak coupling (gas-like) to strong coupling (crystal-like). While trapped classical particles are meanwhile well understood and accessible to first-principle computer simulations, their quantum counterparts still pose big challenges, both for experiment and theory. Therefore, collective properties that can be easily measured or computed and allow to diagnose the many-particle state of the system are of prime importance. It has been found that the quantum breathing mode (monopole oscillation) is one of the most important such properties. In recent years a number of theoretical studies has demonstrated that the quantum breathing mode is ideally suited to measure the coupling strength (the degree of nonideality) of a trapped system, its kinetic and interaction energy and other key observables. This give rise to a novel kind of "spectroscopy" of trapped systems.

In this review these developments are summarized. The quantum breathing mode is studied for trapped fermions and bosons with Coulomb and dipole interaction, respectively. A systematic description of collective oscillations and especially the breathing mode is provided. Making use of time-dependent perturbation theory, it is shown how the corresponding breathing frequencies are connected to the properties of the initial equilibrium system. This gives rise to the application of the quantum mechanical sum rules. It is demonstrated how an improved version of the conventional sum rule formulas is suitable for an accurate description of the breathing mode in small systems. Finally, the dependence of the breathing mode on the particle number N is analyzed and the limit of large N is studied for one-dimensional and two-dimensional systems.

1 Introduction

1.1 Examples of trapped systems and common physical properties

The physics of confined systems is of major interest in many fields of research. Historically this topic was first studied in nuclear matter (shell structure of nuclei, collective excitations etc.), and many of the theoretical tools that are successfully used today, including the sum rule formalism [1–4] and numerical models have their origin there. Another line of research originated in plasma physics. While conventional plasmas are electrically neutral containing (at least) two oppositely charged components, it has long ago been realized that also a single charge component can be kept stable [5]. To this end one can use an electrical field (trapping potential) that compensates the mutual repulsion of the particles. The first systems where this was studied in detail were cold ionic plasmas

* Corresponding author. E-mail: abraham@theo-physik.uni-kiel.de, Phone: +49 431 880-4071, Fax: + 49 431 880-4094

in Paul or Penning traps, where it is possible to confine from small to large numbers of particles, for an overview see [6].

During the recent 20 years the topic of spatially confined finite systems regained new interest. The long row of prominent examples comprises correlated electrons in metal clusters, see e.g. [7] for an overview, ultracold quantum gases in traps or optical lattices, e.g. [8–10], quantum dots, e.g. [11–14], confined plasmas [15], trapped ions [16], and colloidal particles [17, 18]. These systems may differ in various of their properties including the types of particle species, the relevant length and time scales, the temperature and the number of effective spatial dimensions. Beyond that, the type of pair interaction—especially the distinction between long-range and short-range forces (which is particularly important to characterize the system)—may be very different. Trapped particles cover all possible cases of interaction range—from long-range Coulomb interaction (plasmas, ions) to short-range contact interaction, in the case of neutral atoms and molecules in ultracold gases. Intermediate types of interactions are common as well: ultracold atoms and molecules often possess an electrical or magnetic dipole moment, so in many cases the dipole-dipole interaction may be important [19, 20]. Other systems with dipole interaction include excitons in semiconductors or in electron-hole bilayers, e.g. [21, 22]. Here, variation of the layer separation can even lead to a smooth transition from Coulomb to dipole interaction, e.g. [23, 24]. Another example of different interaction are semiconductor quantum wells. As a result of the finite layer width the interaction between electrons or electrons and holes may differ both from Coulomb and dipole interaction, for a numerical analysis of the resulting potential and its implication on the phase diagram see Refs. [25, 26].

Interestingly, despite these differences in the physical details, many of the collective properties of all these systems are very similar and so are the theoretical descriptions of these many-body systems. In many cases, different interaction potentials do not qualitatively alter the behavior but lead to a rescaling of the parameters which can be accomplished by a suitable choice of coupling parameters (dimensionless interaction strength, cf. Sec. 2.1.1). On the other hand, the external trap is often well modelled by a parabolic potential (with the trap frequency Ω), at least for small amplitude excitations.

1.2 Quantum versus classical systems

When large particles are confined in a trap, such as micrometer-size dust particles, e.g. [27] or colloidal particles, quantum effects are irrelevant and a classical treatment is adequate. On the other hand, in the case of microparticles (electrons, ions, atoms), from a general theoretical point of view, a quantum mechanical description of the systems seems mandatory. However, if the repulsive interaction is very strong, than the combination of interaction and confinement force leads to a strong localization of the particles; they are nearly point-like (strong coupling limit), and the system is again well described with the classical equations of motion. This is the case, e. g., for trapped ions or small charged grains in a plasma with Coulomb or Yukawa interaction [28, 29]. Classical behavior dominates at sufficiently low density, even in the case of electrons in semiconductors (Wigner crystal regime [30]).

In Fig. 1, the spatial arrangement of 19 charged particles in a two-dimensional (2D) trap is illustrated for different coupling strengths (for a definition of the coupling parameter, see Sec. 2.1.1). It is shown how the system transitions between a liquid-like quantum state (at large trap frequency, corresponding to high density, left part) and a state that is characterized by strongly localized particles (small trap frequency, low density, middle figure). The figure shows that, even at temperature $T = 0$, the quantum nature of the particles causes them to have finite extensions that may lead a finite overlap of the orbitals. In case of particles in a confining field this effect can be tuned by the changing the trap frequency (and thus the density and the coupling strength). Note that, in the case of wave function overlap, also the spin statistics plays an important role. In the case of trapped bosons coherence effects may give rise to Bose condensation and superfluidity which may be inhomogeneously distributed among the shells and even externally controlled [31]. If the delocalization of the particles becomes negligibly small, the system can be considered point-like (right part of Fig. 1), i. e., the particles are well described in terms of the classical equations of motion and the many-particle state resembles a crystal. Of course, in classical systems as well, one can achieve a spatial delocalization of the particles, simply by increasing the temperature giving rise to melting, e.g. [32, 33]. This situation is briefly considered below when we compare the quantum mechanical breathing mode with the classical analogue in Sec. 3.2. The remaining parts of this work, however, concentrate on the zero-temperature case of quantum systems since here the main effects are seen more clearly. In this case "melting" of the particle ensemble is only possible due to quantum effects (so-called quantum melting [11]).

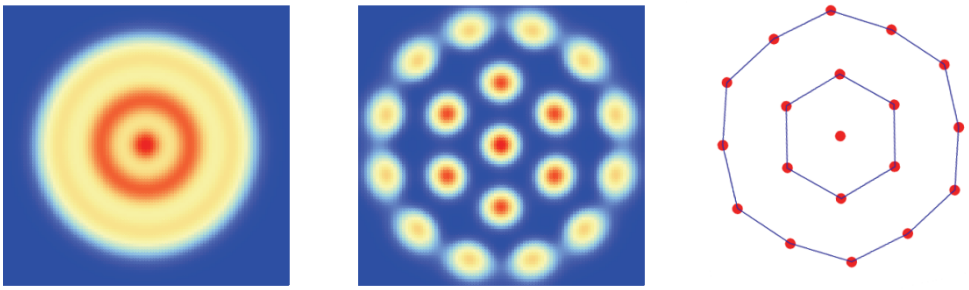

Fig. 1 Ground-state configurations (densities) of $N = 19$ charged particles in a 2D harmonic trap with different coupling strengths. Left: liquid-like state at weak coupling (high density). Center: crystal-like state at strong coupling with quantum mechanical finite extensions of the particles (low density). Right: classical point charges. The two left figures are obtained from Hartree-Fock simulations.

1.3 Normal modes as a novel spectroscopy tool for strongly correlated trapped systems

Strongly interacting systems in traps are complicated few- or many-body systems, due to the spatial inhomogeneity of their properties. In the quantum case, in addition, quantum diffraction and spin effects have to be accounted for simulataneously. This is theoretically extremely challenging. Also, from the experimental side, a diagnostics is very difficult since, usually no single-particle resolution is possible—with the exception of several classical systems with sufficiently large particles, such as colloids or dusty plasmas [18, 27, 34]). Therefore, typical diagnostics e.g. in ultracold gases, are related to studying the expansion of the whole particle ensemble after the trap is being turned off. Alternatively one can analyze the response of the whole system to an external excitation. Obviously, such a collective response yields only rather indirect information on the state of the system.

The situation is a bit similar to studying atoms (or molecules). These are also highly inhomogeneous systems where electrons are trapped by the Coulomb potential of the nucleus (or several nuclei or ions), and the quantum mechanical state of the electrons is very complicated problem. Here, by far the most successul and sensitive experimental approach consists in (absorption or emission) spectroscopy. The measured spectrum usually allows for detailed information on the type of atom and, at high density, also on the atom-atom interaction or on the level shift in the presence of a strong electromagnetic field. Now, we may proceed similarly with a finite ensemble of trapped atoms: in order to gain insight into static features or the time-dependent behavior of trapped systems, we may attempt to use properties of their low-lying collective oscillations [8, 35, 36]. The experimental and theoretical importance of these oscillations, which are also known as normal modes, is comparable to that of spectroscopy in atomic systems. In fact, as we will see below, a measurement of the normal modes is indeed a sensitive diagnostic. This concept has recently been worked out explicitly for 2D systems by McDonald *et al.* in Ref. [37]. There it was shown that the breathing frequency allows to directly infer important collective properties of the system, including its mean kinetic and potential energy. Details will be givn in Sec. 3.3.

This analogy to the spectroscopy in atomic or molecular systems is sketched in Fig. 2 and becomes immediately evident for quantum dots, which—due to their similarities to real atoms—are also termed "artificial atoms". The lowest normal modes are the monopole ("breathing") mode and the dipole (Kohn/sloshing) mode[1]. While there exists a complete analytical solution for the dipole mode [38, 39], the breathing mode demands a numerical approach in the general case. Particularly, due to the increasing success of time-dependent numerical methods, the quantum mechanical behavior of the breathing mode (BM) has been subject of several very recent investigations [37, 40–43]. In these works, the time-dependent response of the system to a monopole-type perturbation has been studied for finite numbers of various trapped interacting fermions and bosons with Coulomb or dipole interaction. The large variety of trapped systems in many field of physics has given rise to a large number of other works that are concerned with the quantum breathing mode. An early example is the systematic study of giant monopole resonances in nuclear matter systems [3, 4, 44–46]. But also in the rapidly growing field of quantum gases, including Bose-Einstein condensates [35, 47–50] and optically trapped Fermi gases [51–53], the BM plays an important role.

[1] If the Hamiltonian of the system is rotationally invariant, there is also a collective rotation mode of the system as a whole with frequency zero. This trivial excitation is not relevant in the present context and will not be considered.

For classical systems consisting of strongly interacting point masses, the breathing mode and other normal modes are well understood [16, 28, 29, 54, 55]. According to the definition of the term "normal mode", all particles oscillate with the same frequency and a fixed phase relation around their initial positions. In particular, the normal modes can occur independently from eath other, i. e., collective oscillations may be formed by complex superpositions of the normal modes. For the example of three confined particles in a plane, some basic normal modes—rotational oscillations, oscillations of the center of mass (sloshing mode), and a uniform radial expansion and contraction of the system (breathing mode)—are illustrated in Fig. 3. As has been shown [29, 55], the normal mode spectrum of a crystallized system at zero temperature can be obtained by diagonalizing the Hessian matrix of the potential terms. Beyond that, an extension for finite temperatures in the framework of the classical Bogoliubov-Born-Green-Kirkwood-Yvon (BBGKY) hierarchy is to be found in Ref. [28].

If quantum effects cannot be neglected, the theoretical description becomes more complex. Furthermore, as was reported in Refs. [42, 56], the quantum breathing mode is characterized by some unique properties. The authors analyzed the time-dependent breathing motion of small quantum systems, covering different types of interactions, and distinguishing, in addition, between bosonic and fermionic particles. An important result of this analysis is the fact that the *quantum breathing mode is characterized by a superposition of two sinusoidal oscillations* with different frequencies. As it is not possible to excite these oscillations independently of each other, this is a remarkable difference from the classical case. While one of the frequencies—called $\omega_{\rm rel}$—is strongly dependent on the coupling parameter of the system, λ, the other one, $\omega_{\rm cm}$, has a universal value. The occurence of two frequencies has its origin in a separation of the Hamiltonian in center-of-mass and relative coordinates. In fact, the frequency $\omega_{\rm rel}$ is even accompanied by an infinite set of higher frequencies (harmonics), which, however, have very low spectral weights if the system is in the ground state or equilibrium and is only weakly excited.

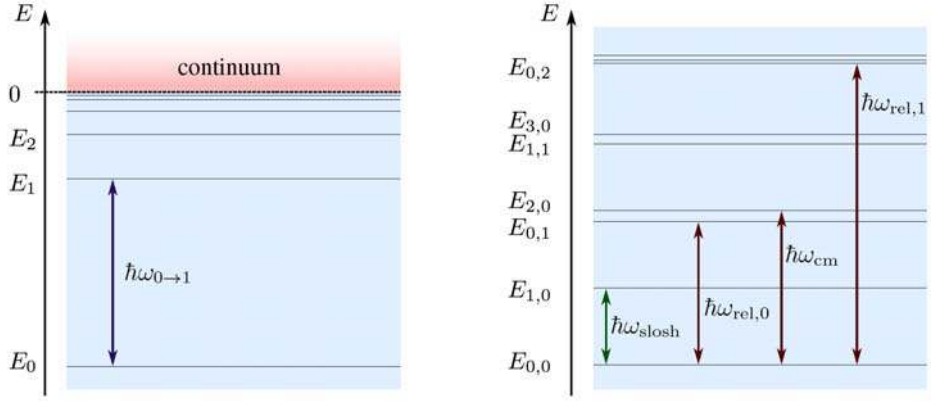

Fig. 2 **Left**: schematic energy spectrum of a real atom (example for one electron). Absorption or emission spectroscopy accesses the allowed transition energies between two energies $\hbar\omega_{m\to n} = E_n - E_m$. **Right**: schematic energy spectrum of an "artificial atom"—a finite system of N particles in a 2D harmonic trap. The excitation energies are N-particle energies and correspond to normal modes (collective excitations) of all particles. These modes correspond to specific well defined perturbations of all particles, such as "sloshing" and monopole oscillations, see. Fig. 3, for an illustration in the classical case. The excitation energies $E_{n,m}$ are characterized by two quantum numbers, correponding to excitations of the center-of-mass and relative subsystem, respectively, see Sec. 2.

The normal modes are usually excited by weak perturbations of the ground-state configurations, so that the reactions of the systems can be considered in the linear response regime. The frequencies of the oscillations are thus to be found in the spectra of the ground states. Consequently, it becomes clear again how the normal mode analysis is able to take over the role of spectroscopy in atomic systems. The excitation process of a real atom can be recapitulated in Fig. 2. For comparison, this figure also illustrates the normal mode excitation in quantum dots ("artificial atoms"). From one of the most famous examples—the hydrogen atom—the discrete nature of the energy levels as well as the ionized continuum states are well known. A quantum dot models the features of a real atom, but due to the harmonic trap potential, there exist only bound states with unique distributions of the energy levels. As will be shown in Sec. 2.2, the total energies of the system are composed of two terms that can

be attributed to the aforementioned separation of the Hamiltonian in center-of-mass an relative coordinates. On the one hand, the figure shows the excitation of the sloshing/dipole mode with just a single frequency (left green arrow). On the other hand, the first three breathing/monopole excitations are illustrated (red arrows). In contrast to atomic systems, the spacings between the energy levels can be shifted by modifying the coupling parameter λ [for a definition, see Sec. 2], e.g. via changing the steepness of the trapping potential. If the particles do not interact with each other ($\lambda = 0$), the first two energies of the monopole excitation are equal. By contrast, in the classical limit, $\lambda \to \infty$, the spacing between these energies attains a maximum. Furthermore, except for the first excitation energy, the corresponding oscillations have vanishing spectral weights in this case. As has been shown for up to 20 fermions with Coulomb interaction in 1D in Ref. [41], not only the coupling parameter, but also the particle number has a considerable influence on the spacing of the energy levels.

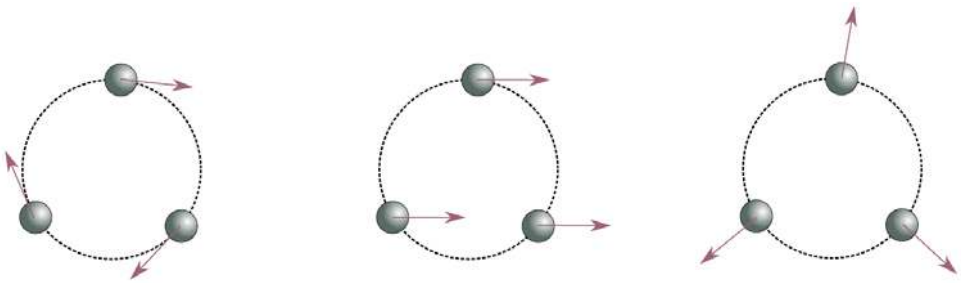

Fig. 3 Illustration of classical normal modes: rotational mode (left), dipole (sloshing, center of mass) mode, breathing/monopole mode (right). Note that in a quantum system, in addition to the quasi-classical relative breathing modes there exists a second (center of mass) breathing mode (not shown), see Sec. 2.

1.4 Outline of this paper and notational remarks

A central goal of this work is the phenomenological explanations given above on a firm theoretical basis. In fact, in recent years impressive theoretical progress has been made in many fields and by applying a variety of methods. It is, therefore, of high interest to review the common but very diverse approaches to calculate the frequencies of the breathing mode and to provide additional details that are often skipped in the original literature. To compute the breathing frequencies of large strongly correlated quantum systems in a harmonic trap, a sum rule formalism is introduced which allows for a—although approximate—reliable prediction of the breathing frequencies with the help of time- independent methods. Two models and a first-principle simulation approach are used:

a.: the Hartree-Fock approximation,

b.: the Thomas-Fermi approximations,

c.: path integral Monte Carlo simulations.

We present simulation results for the following cases:

i.: one-dimensional fermions with Coulomb and dipole interaction,

ii.: two dimensional fermions with Coulomb interaction,

iii.: two-dimensional bosons with dipole interaction.

These settings are of high fundamental theoretical and experimental interest. Systems of interacting electrons in two spatial dimensions are realized in quantum dots, for example. As it is possible to set up the number of participating particles precisely, starting with just one electron [14], quantum dots are a well suited environment for the study of few-body physics. By contrast, typical examples for larger systems are cold fermionic or bosonic quantum gases [8, 9]. They can be realized in one to three effective spatial dimensions [35, 36, 57]. As the gases consist of atoms or molecules, the binary interactions are modelled in terms of contact and dipole interaction potentials [49, 58, 59]. Typical simplifications for the theoretical description of Bose gases are, for example,

the application of hydrodynamic theory [59]. Furthermore, for the numerical investigation of Bose-Einstein condensation, the Schrödinger equation is commonly replaced by the Gross-Pitaevskii equation [9]. Such a mean-field description allows one to reduce the N-particle problem to an effective single-particle problem. In this work, however, the BM of dipolar bosons is studied with the equilibrium results from first-principles Quantum Monte Carlo simulations. These simulations are considered exact, but the analysis is restricted to relatively small particle numbers ($N < 1000$).

The fundamental idea of the derivations in this work is the application of time-dependent perturbation theory, as it allows to systematically describe the normal modes based essentially on the equilibrium properties of the system (linear response theory). Comparing with results from time-dependent calculations, it is shown that the breathing mode is accurately described by various time-independent methods. With these methods, it is possible to work out the peculiarities of finite systems as well as to consider large systems which will be done by means of the Thomas-Fermi theory.

This review is organized as follows. The presentation of the theory starts with an introduction to the quantum mechanical description of the breathing mode (Sec. 2), including the formalism of time-dependent perturbation theory. Furthermore, the two-particle system is extensively studied since it can be solved exactly and allows to benchmark approximations. For the determination of the breathing frequencies in larger systems, the theory of the sum rules and an approximate solution of an operator equation are presented (Sec. 3). Concerning the numerical solutions of the many-body problem, remarks on single-particle basis sets and brief descriptions of exact methods are given in Sec. 4. Thereafter, the Hartree-Fock approximation and the Thomas-Fermi approximation are explained in detail (Secs. 5 and 6). The numerical results are separately considered for the 1D case (Sec. 7) and the 2D case (Sec. 8). Finally, the results are summarized and an outlook is provided (Sec. 9).

2 Quantum Mechanical Description of the Breathing Mode

In this section, the underlying equations for the quantum mechanical description of the breathing mode are presented. The consideration starts with a general approach, which can also be applied for the investigation of other collective modes. After a specification of the breathing mode, this section provides an overview of some basic properties of the expected breathing frequencies, and shows how the computation can be approached. Finally, a thorough review of the two-particle system is given, providing the understanding of the peculiarities of the breathing mode.

2.1 Basic equations

A quantum system of N particles in d-dimensional space is described by an N-body wave function Ψ. Neglecting relativistic effects, its time-evolution is governed by the time-dependent Schrödinger equation (TDSE)

$$\mathrm{i}\hbar\frac{\mathrm{d}}{\mathrm{d}t}|\Psi(t)\rangle = \hat{H}(t)|\Psi(t)\rangle \ . \tag{1}$$

The characteristics of the system are determined by the explicit form of the Hamilton operator $\hat{H}(t)$. Remaining on a general level of description, $\hat{H}(t)$ can be constructed as a sum of a stationary part $\hat{H}_0$ and an explicitly time-dependent part. Since the normal modes are usually excited from an initial equilibrium state, it is natural to start the description of the system by specifying $\hat{H}_0$. For simplicity, all N particles are assumed to have equal (effective) masses $m_i = m$ and—in case of charged particles—equal charges $q_i = q$. The dynamics of the system are determined by repulsive interactions and an external trapping potential, driving the particles to the center of the trap. The corresponding equilibrium Hamiltonian has the general form

$$\hat{H}_0 = \hat{T} + \hat{V} + \hat{W} \ , \tag{2}$$

where the single-particle operators $\hat{T}$ and $\hat{V}$ refer to the kinetic energy and the external trap energy, respectively, and the two-particle operator $\hat{W}$ represents the binary interactions. Setting the external potential to be harmonic with a trap frequency Ω and introducing the coordinates $\mathbf{r} = (\mathbf{r}_1, \ldots, \mathbf{r}_N)$, the Hamiltonian finally takes the

form[2]

$$H_0(\mathbf{r}) = \sum_{i=1}^{N} \left\{ -\frac{\hbar^2}{2m} \frac{\partial^2}{\partial \mathbf{r}_i^2} + \frac{1}{2} m\Omega^2 \mathbf{r}_i^2 \right\} + \sum_{i<j} w(|\mathbf{r}_i - \mathbf{r}_j|) \; . \tag{3}$$

The major interest of this work is to investigate charged particles with Coulomb interaction, i. e.,

$$w(|\mathbf{r}_i - \mathbf{r}_j|) = \frac{q^2}{\epsilon |\mathbf{r}_i - \mathbf{r}_j|} \; . \tag{4}$$

The constant ϵ is the proportionality constant of the Coulomb potential. In SI units, it is given by $\epsilon = 4\pi\varepsilon_0\varepsilon$, where ε is the dielectric constant of the background material.

Another physically relevant interaction considered in this work is the long-range part of the dipole interaction. It is given by [58]

$$w(\mathbf{r}) = \frac{C_{\mathrm{dd}}}{4\pi} \frac{1 - 3(\mathbf{r}\cdot\mathbf{n})^2/|\mathbf{r}|^2}{|\mathbf{r}|^3} = \frac{C_{\mathrm{dd}}}{4\pi} \frac{1 - 3\cos^2(\theta)}{|\mathbf{r}|^3} \; , \tag{5}$$

where $\mathbf{n}$ is a unit vector in the direction of the dipole axis, θ is the angle between the dipole axis and $\mathbf{r}$, and C_{dd} is a proportionality constant. It depends on the physical situation and especially on the character of the dipoles being electric or magnetic. In this work, dipolar particles are investigated in 1D chains and 2D "pancake-shaped" geometries. It is always assumed that an external field aligns the dipoles perpendicular to their distance vectors. As a consequence, the expression for the interaction between two dipolar particles can be reduced to

$$w(|\mathbf{r}_i - \mathbf{r}_j|) = \frac{C_{\mathrm{dd}}}{4\pi} \frac{1}{|\mathbf{r}_i - \mathbf{r}_j|^3} \; . \tag{6}$$

It shall be remarked that this type of interaction is a very basic model. For the modeling of Bose-Einstein condensates, one often takes into account the finite extension of the particles by adding a contact potential $\propto \; \delta(\mathbf{r}_i - \mathbf{r}_j)$ [60]. Following Ref. [20], however, it is assumed that the interaction is so strong that one can neglect the cores of the particles.

A final remark is made to keep the notations consistent throughout the following sections. It is assumed that $\hat{H}_0$ is diagonalized by the N-body wave functions $\{|k\rangle \mid k = 0, 1, \dots\}$ with the corresponding eigenvalues $\{E_k \mid k = 0, 1, \dots\}$.

2.1.1 Coupling parameter and dimensionless units

For both notational convenience and an appropriate numerical handling, it is useful to rewrite the TDSE in dimensionless units. With the standard oscillator length $l_0 = [\hbar/(m\Omega)]^{1/2}$, one can define new spatial coordinates $\tilde{\mathbf{r}}_i = \mathbf{r}_i/l_0$. After rescaling the time by $\tilde{t} = \Omega t$, inserting the new quantities in Eq. (1), and omitting the tilde symbol, one arrives at the rescaled Hamiltonian

$$H_0(\mathbf{r}) = \sum_{i=1}^{N} \left\{ -\frac{1}{2} \frac{\partial^2}{\partial \mathbf{r}_i^2} + \frac{1}{2} \mathbf{r}_i^2 \right\} + \lambda_{\mathrm{C/dd}} \sum_{i<j} \frac{1}{|\mathbf{r}_i - \mathbf{r}_j|^{\alpha}} \; , \tag{7}$$

where, a dimensionless coupling parameter has been introduced. For Coulomb interaction ($\alpha = 1$), it takes the form

$$\lambda_{\mathrm{C}} = \frac{q^2}{\epsilon l_0 \hbar\Omega} \geq 0 \; , \tag{8}$$

whereas, for repulsive dipole interaction ($\alpha = 3$), it is given by

$$\lambda_{\mathrm{dd}} = \frac{C_{\mathrm{dd}}}{4\pi l_0^3 \hbar\Omega} \geq 0 \; . \tag{9}$$

[2] The statement $\sum_{i<j}$ means a summation over $j = 2, \dots, N$ and $i = 1, \dots, (j-1)$.

Since $\lambda_{\mathrm{C/dd}}$ is a prefactor of the interaction potential, it determines the strength of interaction effects. Defining the scales for the trap energy E_0, the Coulomb interaction energy, E_{C} and the dipole interaction energy E_{dd} as

$$E_0 = \frac{1}{2} m\Omega^2 l_0^2 \,, \qquad E_{\mathrm{C}} = \frac{q^2}{2\epsilon l_0} \,, \qquad E_{\mathrm{dd}} = \frac{C_{\mathrm{dd}}}{2 \cdot 4\pi l_0^3} \,, \tag{10}$$

the coupling parameter can directly be interpreted as

$$\lambda_{\mathrm{C/dd}} = \frac{E_{\mathrm{C/dd}}}{E_0} \,. \tag{11}$$

In experiments, $\lambda_{\mathrm{C/dd}}$ can be directly controlled by the trap frequency of the confining field.[3]

From now on, lengths, times and energies of numerical results will be given in units of l_0, Ω^{-1} and $\hbar\Omega$, respectively. Nevertheless, for the sake of clarity, the units are explicitly written out for most values in the text. Furthermore, it is always written λ instead of λ_{C} or λ_{dd}. It can be seen from the context to which interaction the coupling parameter corresponds.

Coupling in the macroscopic uniform electron gas. For a later discussion, it will be interesting to compare the coupling parameter to the relevant quantities of a macroscopic uniform electron gas [32]. In such a system, one of the important characteristic parameters is the average interparticle distance $\overline{r} \propto n^{-1/d}$, where n is the density of the d-dimensional system. With this, one defines the mean Coulomb energy (per particle) for the electrons (charge e) and the mean kinetic energy of a classical system

$$E_{\mathrm{C}} = \frac{e^2}{4\pi\varepsilon\overline{r}} \,, \qquad E_{\mathrm{kin}} = \frac{d}{2k_{\mathrm{B}}T}, \tag{12}$$

where k_{B} is the Boltzmann constant and T is the temperature. In contrast, in a degenerate Fermi system, the kinetic energy is given by

$$E_{\mathrm{kin}} = \frac{3}{5} E_{\mathrm{F}} \tag{13}$$

with the Fermi energy E_{F}. Defining the Coulomb coupling parameter as the ratio of the mean Coulomb energy and the kinetic energy, we obtain, for a classical and a Fermi system, resprectively,

$$\Gamma = \frac{E_{\mathrm{C}}}{k_{\mathrm{B}}T} \,, \qquad r_{\mathrm{s}} = \frac{\overline{r}}{a_{\mathrm{B}}} \propto \frac{E_{\mathrm{C}}}{E_{\mathrm{F}}} \,, \tag{14}$$

where we introduced the Bohr radius a_{B} as the relevant quantum length scale. The parameter r_{s} is also called Brueckner parameter. Finally, with the help of the degeneracy parameter

$$\chi = \left(\frac{\Lambda}{\overline{r}} \right)^d \,, \tag{15}$$

measuring the ratio of the de Broglie wavelength Λ and the interparticle distance, one can discriminate between quantum-like ($\chi \geq 1$) and classical ($\chi < 1$) behavior.

2.1.2 Excitation of collective modes

So far, only the initial Hamiltonian has been considered. The excitation of collective modes can be achieved by a short perturbation of the system. Such a perturbation is formally included in the Hamiltonian as

$$\hat{H}(t) = \hat{H}_0 + \eta\delta(t)\hat{Q} \,. \tag{16}$$

[3] Of course, there are also other possible dimensionless forms of the TDSE, involving different coupling parameters. In this work, the given form of Eq. (7) is used. It has the advantage that it is straightforward to numerically implement this Hamiltonian in the standard oscillator basis.

In this equation, $\hat{Q}$ is a perturbation operator which is not further specified at this point. It is just assumed that the action of $\hat{Q}$ is delta-like in time and that the small parameter η guarantees a weak perturbation.

Of course, the excitation process which is defined by Eq. (16) is just an idealization of a real process. In both experimental and numerical situations, the duration and the strength of the excitation are always finite. However, the above definition has the advantage that it allows for a mathematical definition of collective modes in terms of time-dependent perturbation theory. As will be seen in the results, the perturbative treatment is justified. For the time-dependent calculations presented in Refs. [42, 56], it was stated that the action of the excitation operator should be very short. Here, the mathematical foundation in terms of δ-like perturbations is given.

At $t = 0$, the system is assumed to be in the state $|n\rangle$. The wave function of the perturbed system has to obey the TDSE

$$\mathrm{i}\frac{\mathrm{d}}{\mathrm{d}t}|\Psi(t)\rangle = \left(\hat{H}_0 + \eta\delta(t)\hat{Q}\right)|\Psi(t)\rangle \ . \tag{17}$$

At any time t, the wave function can by expanded by

$$|\Psi(t)\rangle = \sum_k c_k(t)\exp\left\{-\mathrm{i}E_k t\right\}|k\rangle \ . \tag{18}$$

For sufficiently small η, one can make use of time-dependent perturbation theory up to the first order to calculate the coefficients $c_k(t)$. According to the derivation in Appendix A.1.2, the perturbation $\eta\delta(t)\hat{Q}$ leads to time-independent coefficients

$$c_k = \delta_{kn} - \mathrm{i}\eta\langle k|\hat{Q}|n\rangle \ . \tag{19}$$

The expectation value of an observable $\hat{A}$ which is not explicitly time-dependent is given by

$$\langle\hat{A}\rangle(t) = \sum_{ij} c_i^* c_j \exp\left\{\mathrm{i}\left(E_i - E_j\right)t\right\}\langle i|\hat{A}|j\rangle \ . \tag{20}$$

This equation shows that the expectation value of $\hat{A}$ can only oscillate with the frequencies

$$\omega_{ij} = |E_i - E_j| \ . \tag{21}$$

These frequencies correspond to the normal modes of the system. However, a given frequency ω_{ij} can only be observed if each of the terms c_i, c_j and $\langle i|\hat{A}|j\rangle$ is non-zero.

2.1.3 Definition of the quantum breathing mode

The quantum breathing mode is defined as the collective oscillation which is induced by the monopole operator

$$\hat{Q} = \hat{\mathbf{r}}^2 = \sum_{i=1}^{N}\hat{\mathbf{r}}_i^2 \ . \tag{22}$$

A perturbation with this operator can be realized by a short switch of the trap frequency. In this work, the system is always assumed to be initially in the lowest eigenstate $|0\rangle$ of $\hat{H}_0$. This corresponds to a temperature $T = 0$. An appropriate observable for the determination of the breathing frequencies is $\langle\hat{\mathbf{r}}^2\rangle$. This quantity is proportional to the trap energy $\langle\hat{V}\rangle$. Inserting the expansion coefficients from Eq. (19) into Eq. (20) for this special case, one finds

$$\langle\hat{\mathbf{r}}^2\rangle(t) = \langle 0|\hat{\mathbf{r}}^2|0\rangle - 2\eta\sum_i |\langle 0|\hat{\mathbf{r}}^2|i\rangle|^2\sin(\omega_{i0}t) + \mathcal{O}(\eta^2) \ . \tag{23}$$

The structure of this result is quite simple. The first term is constant. It represents the expectation value of the unperturbed system. The second term is a superposition of oscillations induced by the perturbation. The amplitudes of these oscillations are determined by the strength of the perturbation η and the matrix elements $\langle 0|\hat{\mathbf{r}}^2|i\rangle$. As a special consequence, only frequencies with non-vanishing matrix elements can be observed. In other words, a frequency can only contribute to the oscillations if its corresponding transition is not forbidden by the selection rules of the monopole operator. Furthermore, all contributions in the second order of η can be neglected, because η is small.

2.2 Limiting cases and analytical results

According to the derivation in Sec. 2.1.3, the breathing motion comprises a variety of possible frequencies. In Refs. [41, 42, 56], however, it was shown that the breathing mode is dominated by just two frequencies. One of these has the universal value $2\,\Omega$. It is independent of the particle number, the coupling strength and the dimension of the system. The universality of this frequency can be explained with a formal decoupling of the wave function into a center-of-mass and a relative part,

$$|\Psi(t)\rangle = |\Psi_{\rm cm}(t)\rangle \otimes |\Psi_{\rm rel}(t)\rangle \ . \tag{24}$$

Such a decoupling is induced by the splitting of the Hamiltonian [61],

$$\hat{H}(t) = \hat{H}_{\rm cm}(t) + \hat{H}_{\rm rel}(t) \ , \tag{25}$$

where the contributions read

$$\hat{H}_{\rm cm}(t) = \frac{N}{2}\hat{\mathbf{P}}^2 + \frac{N}{2}\hat{\mathbf{R}}^2 + \eta\delta(t)N\hat{\mathbf{R}}^2 \ , \tag{26}$$

$$\hat{H}_{\rm rel}(t) = \sum_{i<j}\left\{\frac{1}{2N}\hat{\mathbf{p}}_{ij}^2 + \frac{1}{2N}\hat{\mathbf{r}}_{ij}^2 + \hat{w}(|\hat{\mathbf{r}}_{ij}|) + \eta\delta(t)\frac{1}{N}\hat{\mathbf{r}}_{ij}^2\right\} \ . \tag{27}$$

Here, the center-of-mass and relative coordinates have been introduced, according to the scheme

$$\hat{\mathbf{O}} = \frac{1}{N}\sum_{i=1}^{N}\hat{\mathbf{o}}_i \ , \qquad \hat{\mathbf{o}}_{ij} = \hat{\mathbf{o}}_i - \hat{\mathbf{o}}_j \ . \tag{28}$$

The above separation does not only achieve a splitting of the time-independent part of the Hamiltonian, but also of the excitation operator $\sum_{i=1}^{N}\hat{\mathbf{r}}_i^2$. Hence, the monopole operator excites the breathing motion in both independent subsystems at the same time. The time-dependent expectation value of the trap energy consequently takes the form

$$\langle\hat{V}\rangle(t) = \langle\Psi_{\rm cm}(t)|\hat{V}_{\rm cm}(t)|\Psi_{\rm cm}(t)\rangle + \langle\Psi_{\rm rel}(t)|\hat{V}_{\rm rel}(t)|\Psi_{\rm rel}(t)\rangle \ . \tag{29}$$

The corresponding expression for the kinetic energy $\langle\hat{T}\rangle(t)$ follows analogously. The interaction energy, however, has no contributions originating from the center-of-mass system, because the operator $\hat{W}$ only appears in the relative system.

The above insights allow for a further specification of the expected breathing oscillation. Equation (26) describes an ideal quantum mechanical oscillator problem for the observables $\hat{T}_{\rm cm} = N\hat{\mathbf{P}}^2/2$ and $\hat{V}_{\rm cm} = N\hat{\mathbf{R}}^2/2$. Factoring out the particle number N with a rescaling of the coordinates, one can show that the eigenvalues of this system are given by $E_{\rm cm}^k = (k + d/2)\,\hbar\Omega$. Hence, one can conclude with Eq. (23) and the selection rules of the monopole operator that the center-of-mass system contributes to the breathing motion with the frequency $2\,\Omega$. The frequencies of the relative motion, however, are more complex. Depending on the coupling parameter λ, the dominating frequency attains the values $\sqrt{3}\,\Omega \leq \omega_{\rm rel} \leq 2\,\Omega$, for Coulomb interaction, and $2\,\Omega \leq \omega_{\rm rel} \leq \sqrt{5}\,\Omega$, for dipole interaction [42, 55, 56]. This frequency is the first frequency that is allowed by a monopole excitation in the relative system. For $\lambda = 0$, $\omega_{\rm rel}$ reaches the ideal quantum limit, because the interaction vanishes. In this case, the frequency $2\,\Omega$ is degenerate. By contrast, the classical limit with the frequencies $\sqrt{3}\,\Omega$ and $\sqrt{5}\,\Omega$, respectively, is reached for $\lambda \to \infty$, i. e., dominating interaction energy. In this case, the particles can be described like classical point masses. To conclude, the separable structure of the TDSE gives some important insight into the expected behavior of the system. As will be shown in Sec. 2.4, one can particularly make use of it in the case of $N = 2$ interacting particles. For larger particle numbers, however, computations are usually performed in the full system without the splitting.

2.2.1 Quantum virial theorem

As it is important for some derivations, it is briefly remarked that the quantum virial theorem holds in the considered systems [62]. This theorem states that there is a fixed relation between the ground-state expectation values

of the kinetic energy and all potential terms. This relation is given by

$$2\langle\hat{T}\rangle - 2\langle\hat{V}\rangle + \alpha\langle\hat{W}\rangle = 0\ . \tag{30}$$

Additionally, the virial theorem also holds for the subsystems given by the center-of-mass coordinate and the relative coordinates,

$$2\langle\hat{T}_{\mathrm{rel}}\rangle - 2\langle\hat{V}_{\mathrm{rel}}\rangle + \alpha\langle\hat{W}\rangle = 0 \qquad \text{and} \qquad \langle\hat{T}_{\mathrm{cm}}\rangle - \langle\hat{V}_{\mathrm{cm}}\rangle = 0\ . \tag{31}$$

2.2.2 Sloshing mode

Although this work is concerned with the breathing mode, it is recapitulated that the system possesses another mode, which can be described analytically. This mode, which is known as the sloshing mode, corresponds to the dipole excitation operator,

$$\hat{Q} = \sum_{i=1}^{N} \hat{\mathbf{r}}_i = N\hat{\mathbf{R}}\ . \tag{32}$$

This operator induces an oscillation of the center of mass coordinate $\langle\hat{\mathbf{R}}\rangle$. The mode has the universal frequency $1\,\Omega$ and can be used as a sensitive test for the conserving properties of an approximation [39]. To demonstrate the universal capabilities of the methods introduced in Sec. 5 (time-dependent Hartree-Fock and perturbation theory), this result is numerically reproduced in Sec. 7.1.1.

2.3 Calculation of the breathing frequencies

The purpose of this work is to show how the breathing frequency ω_{rel} can be determined in dependence of the particle number and the coupling strength for systems with Coulomb interaction and systems with dipole interaction. Having laid the mathematical foundation of the quantum breathing mode, one can conclude how to generally approach the calculation of the breathing frequencies.

On the one hand, one can perform time-dependent calculations like in Refs. [41,42,56]. For that purpose, one calculates the ground state of the system, excites the breathing mode and propagates the system for a sufficiently long time. Finally, the breathing frequencies can be extracted from the spectrum of some time-dependent quantities, for example, the potential energy $\langle\hat{V}\rangle$. As the investigation with time-dependent methods is the natural approach, the presentation of the results in Sec. 7 starts with a comprehensive study of the time-dependent behavior and its peculiarities. Besides, recent works on the breathing mode from different authors [37,40] confirm the relevance of time-dependent methods in current research.

On the other hand, Eq. (23) suggests to avoid time-dependent calculations because the spectrum of the initial state already yields all possible frequencies. As a consequence, each method that is suited to calculate the spectrum of the initial ground state—or at least a sufficient part of it—can be used to determine the breathing frequencies. Compared to the methods of Refs. [42,56], this is a new ansatz. A major part of this work is devoted to the presentation of several ground-state methods. Not only do such methods save the computational time of the propagation, they also yield useful formulas for the physical interpretation of the breathing mode. Before continuing with applications in the quantum case, some of the most important classical results are repeated in the following subsection.

2.3.1 Breathing frequencies in the classical limit

In the classical limit of strongly interacting particles that can be treated like point masses, the breathing mode is well understood. For completeness, a summary of the theoretical approaches is given in the following. Analogous to Eq. (7), the Hamiltonian of the classical system (with $m \equiv 1$) takes the form

$$H_0(\mathbf{r}) = \sum_{i=1}^{N} \frac{1}{2}\mathbf{p}_i^2 + U(\mathbf{r})\ , \qquad U(\mathbf{r}) = \sum_{i=1}^{N} \frac{1}{2}\Omega^2\mathbf{r}_i^2 + \sum_{j<k} \frac{1}{|\mathbf{r}_j - \mathbf{r}_k|^\alpha} \tag{33}$$

where U denotes the total potential energy. For a ground state with vanishing kinetic energy ($\mathbf{p}_i = 0$), the forces on each particle with the coordinate $\mathbf{r}_i^*$ must vanish, i. e.,

$$0 = \nabla_i U(\mathbf{r})|_{\mathbf{r}=\mathbf{r}^*} \ . \tag{34}$$

For small excitations from the ground state, the potential may be approximated harmonically,

$$U(\mathbf{r}) \approx U(\mathbf{r}^*) + \frac{1}{2}(\mathbf{r}-\mathbf{r}^*)^{\mathrm{T}} \mathcal{H}^{\mathbf{r}^*} (\mathbf{r}-\mathbf{r}^*) \ , \tag{35}$$

where the real symmetric and positive semidefinite $dN \times dN$ matrix $\mathcal{H}^{\mathbf{r}^*} = \nabla\nabla^{\mathrm{T}} U(\mathbf{r})|_{\mathbf{r}=\mathbf{r}^*}$ is the so-called Hessian. The eigenvalue problem

$$\omega^2 \tilde{\mathbf{r}} = \mathcal{H}^{\mathbf{r}^*} \tilde{\mathbf{r}} \tag{36}$$

yields dN linearly independent eigenvectors $\tilde{\mathbf{r}}_i$ and corresponding eigenvalues ω_i^2 [29, 55]. Expressing the collective motion with the expansion

$$\mathbf{r}(t) = \mathbf{r}^* + \sum_{i=1}^{dN} c_i(t) \tilde{\mathbf{r}}_i \ , \tag{37}$$

one can derive the scalar solutions

$$c_i = A_i \cos(\omega_i t + B_i) \tag{38}$$

for all $i \leq dN$ [55]. These terms contain all normal modes and their corresponding frequencies. For the breathing mode, the values $\omega_{\mathrm{BM}} = \sqrt{3}\,\Omega$ and $\omega_{\mathrm{BM}} = \sqrt{5}\,\Omega$ are well known for the cases $\alpha = 1$ and $\alpha = 3$, respectively [29, 42, 55, 63].

The above considerations correspond to the zero-temperature limit, because it has been assumed that the particles have no kinetic energy. A more general approach including finite temperatures can be found in Ref. [28]. Introducing the ratio of the thermal kinetic energy and the energy of the harmonic trap potential, $p \sim (k_{\mathrm{B}}T/E_{\mathrm{trap}})$, the authors arrive at the general formula

$$\omega_{\mathrm{BM}} = \Omega \left((2-\alpha)(p-1)+4\right)^{1/2} \ . \tag{39}$$

This result reveals that the breathing frequency of non-interacting quantum systems, $2\,\Omega$, has a classical analogue in the high-temperature limit with $p = 1$.

2.4 Review of the two-particle system

Before the methods for many-particle systems are presented, the two-particle system shall be reviewed. The corresponding Schrödinger equation can essentially be simplified. Furthermore, one can gain insight into some properties that also hold for larger systems. Since the numerical techniques for the following results are quite simple, they need not be described in detail here. The purpose of this section is to provide a qualitative picture of the quantum breathing mode.

The first time-dependent investigations for the breathing mode of two particles in a trap are presented in Refs. [42, 56]. In this section, an alternative time-independent approach is followed. According to the separation procedure discussed in Sec. 2.2, the stationary relative problem in coordinate representation reads

$$E_{\mathrm{rel}} \Psi_{\mathrm{rel}}(\mathbf{r}) = \left\{ -\nabla_{\mathbf{r}}^2 + \frac{1}{4}\mathbf{r}^2 + \frac{\lambda}{|\mathbf{r}|^\alpha} \right\} \Psi_{\mathrm{rel}}(\mathbf{r}) \ , \tag{40}$$

where the coordinate $\mathbf{r} := \mathbf{r}_1 - \mathbf{r}_2$ has been defined. In this equation, it is advantageous that the interaction term is of single-particle type, i. e., one can avoid the numerical effort of handling the two-particle interaction operator.

After rescaling $\mathbf{r} = \sqrt{2}\tilde{\mathbf{r}}$, and omitting the tilde symbol, one obtains an equation with the standard oscillator prefactors of the kinetic and trap energy terms,

$$E_{\mathrm{rel}}\Psi_{\mathrm{rel}}(\mathbf{r}) = \left\{-\frac{1}{2}\nabla_{\mathbf{r}}^2 + \frac{1}{2}\mathbf{r}^2 + \frac{\lambda}{2^{\alpha/2}|\mathbf{r}|^\alpha}\right\}\Psi_{\mathrm{rel}}(\mathbf{r}) \,. \tag{41}$$

If the dimension of the system is $d \geq 2$, one can take advantage of the radial symmetry, expressing $\mathbf{r}$ in hyperspherical coordinates $(\rho, \phi_1, \ldots, \phi_{d-1})$ [64]. In these coordinates, the Laplace operator reads

$$\nabla_{\mathbf{r}}^2 = \frac{\partial^2}{\partial\rho^2} + \frac{d-1}{\rho}\frac{\partial}{\partial\rho} + \frac{1}{\rho^2}\nabla_\phi^2 \,, \tag{42}$$

where ∇_ϕ^2 is the Laplace operator on the unit hypersphere S_{d-1} [65]. With the separation ansatz

$$\Psi_{\mathrm{rel}}\left(\rho, \phi_1, \ldots, \phi_{d-1}\right) = R_l(\rho) Y_l\left(\phi_1, \ldots, \phi_{d-1}\right), \tag{43}$$

one can reduce the problem to the radial equation

$$\left\{-\frac{1}{2}\left[\frac{\mathrm{d}^2}{\mathrm{d}\rho^2} + \frac{d-1}{\rho}\frac{\mathrm{d}}{\mathrm{d}\rho} - \frac{l(l+d-2)}{\rho^2}\right] + \frac{1}{2}\rho^2 + \frac{\lambda}{2^{\alpha/2}\rho^\alpha}\right\} R_l(\rho) = E_{\mathrm{rel}} R_l(\rho) \,. \tag{44}$$

The functions Y_l with $l = 0, 1, 2, \ldots$ are normalized hyperspherical harmonics with the eigenvalues $l(l+d-2)$ [64, 66]. For a further simplification, one can make the ansatz

$$R_l(\rho) = \frac{u_l(\rho)}{\rho^{(d-1)/2}} \,, \tag{45}$$

resulting in the equation

$$\left\{-\frac{1}{2}\frac{\mathrm{d}^2}{\mathrm{d}\rho^2} + \frac{\rho^2}{2} + \frac{\left(l + (d-2)/2\right)^2 - 1/4}{2\rho^2} + \frac{\lambda}{2^{\alpha/2}\rho^\alpha}\right\} u_l(\rho) = E_{\mathrm{rel}} u_l(\rho) \,. \tag{46}$$

Compared to Eq. (40), one has reduced the problem to compute a 1D wave function instead of a d-dimensional one. In the following subsections, 1D and 2D systems are investigated in detail.

2.4.1 Solution for the one-dimensional system

The introduction of spherical coordinates is only meaningful for systems with dimensions $d \geq 2$. The starting point for the numerical investigation of 1D systems is thus Eq. (41), describing the 1D wave function $\Psi_{\mathrm{rel}}(r)$. It can be solved with standard numerical techniques. In this work, the results were obtained with an expansion of the wave function in FEDVR basis functions[4]. With this procedure, one has to solve an eigenvalue problem for the matrix representation of Eq. (41). Hence, one obtains a set of eigenfunctions with corresponding eigenvalues from which the breathing frequencies can be extracted.

Before showing the results for different interaction types, the influence of the particle statistics shall be discussed. For bosonic particles, the relative wave function must fulfill

$$\Psi_{\mathrm{rel}}(r) = \Psi_{\mathrm{rel}}(-r) \,. \tag{47}$$

This is also the case for fermions with anti-parallel spin projections. Nevertheless, such a symmetric wave function will be referred to as bosonic in the following. On the other hand, for fermionic particles with parallel spin projections,

$$\Psi_{\mathrm{rel}}(r) = -\Psi_{\mathrm{rel}}(-r) \tag{48}$$

is demanded. One can immediately conclude that such an anti-symmetric wave function—that will be called fermionic—must vanish at the origin. Hence, it is sufficient to solve Eq. (41) on the positive interval $[0, \infty[$ with the condition that the wave function vanishes at the boundaries. This condition is a priori fulfilled with the FEDVR basis functions, but for numerical reasons, the interval is finite. For bosons, by contrast, the wave function can be non-zero at the origin. Hence, one has to do the calculations on the complete interval $]-\infty, \infty[$, demanding that the wave function vanishes at $\pm\infty$. Since this approach also yields fermionic eigenfunctions, one has to select the desired particle species by the spatial symmetry.

[4] Details of the FEDVR basis are given in Sec. 4.2.2

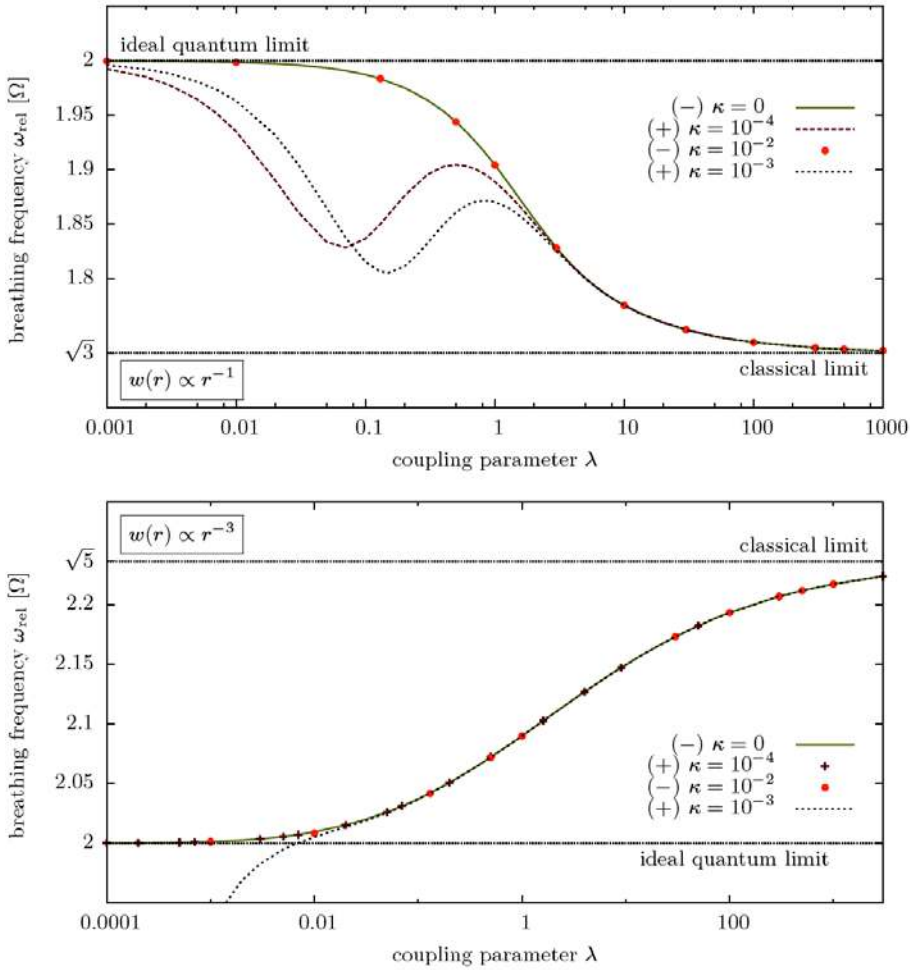

Fig. 4 Breathing frequency $\omega_{\rm rel}$ vs. coupling parameter λ for two particles in a 1D system with Coulomb interaction (top) and dipole interaction (bottom). Both potentials are screened, according to Eq. (49). The plus (minus) signs denote symmetric (anti-symmetric) wave functions. The curves with $\kappa = 0$ originate from calculations on the interval $[0, \infty]$. For symmetric wave functions, the screening parameter κ leads to strongly non-monotonic behavior. This effect is weakened in the dipolar case.

If one solves the problem on the complete interval, one has to overcome the problem of the divergence in the potential $w(r) = 1/|r|^\alpha$. One solution to this problem is the physically motivated replacement of the pure Coulomb/dipole potential by the screened potential

$$w(r) = \frac{1}{(r^2 + \kappa^2)^{\alpha/2}} \tag{49}$$

with the small parameter κ. Here, κ is intended to approximately represent the extension of the wave function in the other spatial dimensions [67, 68]. The screened potential, however, leads to a non-monotonic behavior of the breathing frequency for bosonic particles. In Ref. [56], this issue was thoroughly discussed. In Fig. 4, the κ-dependence of the breathing frequency is illustrated for Coulomb and dipole interaction. The influence of κ can be understood as follows. As κ appears as an additional constant in the denominator of the interaction potential, it only has an influence if the distance of the particles r is small. For strongly separated particles, however, κ becomes negligible. As the average particle distance depends on the coupling parameter λ, there is a strongly coupled regime for each κ in which its influence on the frequency vanishes. The smaller the value of κ is, the smaller is also the value of λ for which κ can be neglected. In the weakly interacting regime (small λ), however,

the error induced by the screening leads to a non-monotonic behavior of the breathing frequencies. As can be seen from the figure, this behavior is only apparent for bosonic particles. For fermions, having vanishing wave functions at the origin, the dominating influence of κ is suppressed. Furthermore, in the case of dipolar bosons, the influence of κ is strongly reduced.

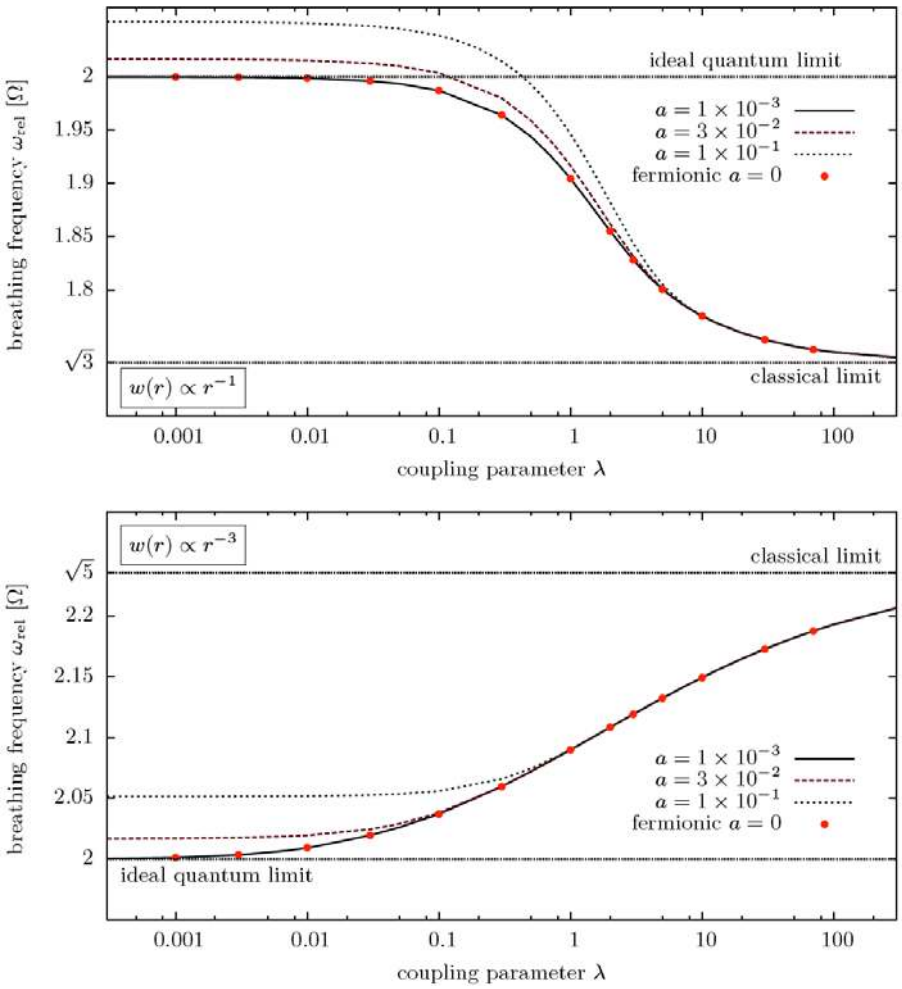

Fig. 5 Breathing frequency $\omega_{\rm rel}$ vs. coupling parameter λ for two particles in a 1D system with Coulomb interaction (top) and dipole interaction (bottom). Both interactions include an additional hard-core term as introduced by Eq. (50). As the Bose-Fermi mapping holds, there is no difference between bosonic and fermionic curves. For small core extensions a, the results converge to those from fermionic systems with pure Coulomb/dipole interaction ($a = 0$).

In Ref. [56], the authors mention that they expect the same results for bosons and fermions in 1D systems due to the Bose-Fermi mapping [69]. They explain that their calculations with the screened potential are not able to fulfill these expectations. To add a thought to their analysis, one can again cite Ref. [69], noticing that the one-one correspondence between 1D Bose and Fermi systems holds under the restriction that the interactions have an impenetrable core. Hence, another useful possibility for the numerical simulation of the 1D system is to employ a hard-core potential

$$w(r) = \begin{cases} \infty & |r| \leq a \\ 1/|r|^{\alpha} & |r| > a \,, \end{cases} \tag{50}$$

forbidding the particles to approach each other closer than twice the extension of the core a. For the numerical implementation, it is sufficient to replace infinity by a very large number for the case $|r| \leq a$. One only has

to check that the wave function is close to zero in the forbidden region. In Fig. 5, the results for the potential (50) are shown for Coulomb and dipole interaction. As expected, the Bose-Fermi mapping holds for every core extension. Apparently, in the limit $a \to 0$, the bosonic results converge to the fermionic results with $a = 0$. From this analysis, one can conclude that a hard-core interaction potential is a possible alternative to the regularization with κ, because such a potential forces the relative wave function to vanish around the origin. Hence, symmetric and anti-symmetric wave functions can be handled at the same time. Finally, to emphasize the differences of the proposed modified interaction potentials in 1D systems, Fig. 6 shows the relative wave functions and densities of two Coulomb interacting bosons and fermions with the κ-regularization and the additional hard-core term, respectively.

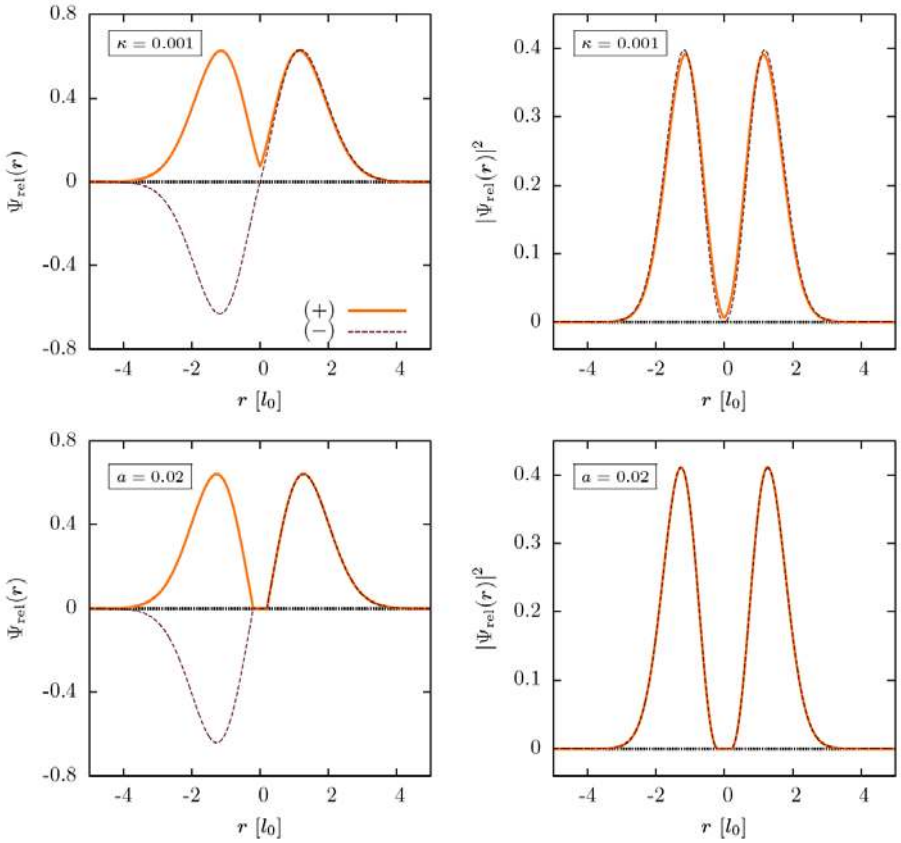

Fig. 6 Comparison of the relative wave functions (left column) and the corresponding densities (right column) of two charged particles with a screened potential as in Eq. (49) (top row) and a hard-core potential as in Eq. (50) (bottom row). Only in the case of a hard-core potential, the bosonic density $(+)$ is equivalent to the fermionic density $(-)$. The data were produced for the coupling $\lambda = 1$.

As mentioned before, the breathing mode comprises the frequencies $\omega_{\rm rel}$ and $\omega_{\rm cm}$ as well as weakly contributing higher frequencies. The mathematical reason is found in Eq. (20), stating that, in principle, all frequencies $E_i - E_0$ can occur. These higher frequencies are the last feature that shall be analyzed in the framework of the 1D two-particle system. Starting the consideration with the center-of-mass system, it is easy to see that this subsystem yields no other frequencies than $\omega_{\rm cm} = 2\,\Omega$. This can be explained with the selection rules of the monopole operator, because the system is non-interacting. The relative system, however, is perturbed with the interaction potential. Therefore, transitions to higher states are not forbidden anymore. In order to interpret the spectra of time-dependent quantities, it is important to know the values of the higher frequencies. Figure 7 presents an overview of the λ-dependent behavior of the higher breathing frequencies for Coulomb interaction as well as dipole interaction. One can see that the quantum limits of the i-th possible breathing frequency takes the value

$2i\,\Omega$. Similarly, the classical limits attain the values $\sqrt{3}i\,\Omega$ for Coulomb interaction and $\sqrt{5}i\,\Omega$ for dipole interaction. But still, it is important to note that for intermediate couplings, the frequencies do *not* scale exactly with the factor i. It remains to investigate the weights of the higher frequencies. From Eq. (23), one can conclude that the expectation value of the quantity $\hat{\mathbf{r}}_{12}^2 := (\hat{\mathbf{r}}_1 - \hat{\mathbf{r}}_2)^2$ has breathing oscillations with the weights $|\langle 0_{\rm rel}|\hat{\mathbf{r}}_{12}^2|i_{\rm rel}\rangle|^2$. Here, $|i_{\rm rel}\rangle$ are the eigenstates of the Hamiltonian $\hat{H}_{\rm rel}$. In Fig. 8, the λ-dependent weights are shown for the example of two Coulomb-interacting fermions of parallel spin. One can see that for each coupling, the weight of the first excited breathing frequency is several orders of magnitude larger than those of higher frequencies. While the contributions of the higher frequencies have their maximum for intermediate couplings $1 \leq \lambda \leq 10$, in the limiting cases, only the first frequency remains. Noticing the increasing weight of the first frequency with λ, one can also understand that the frequency $2\,\Omega$ from the center-of-mass system is a pure quantum effect, as its constant weight is always negligible in the classical limit $\lambda \to \infty$.

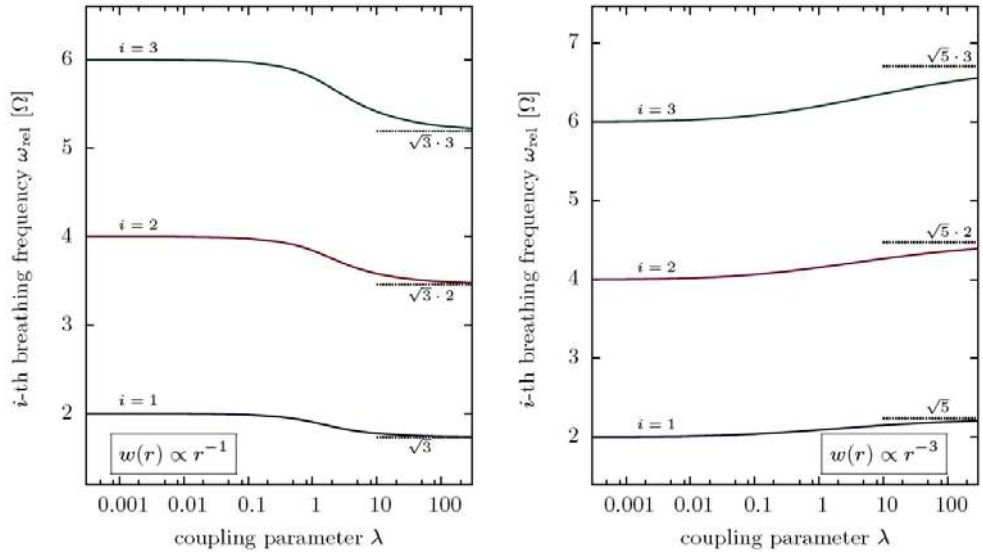

Fig. 7 Transition of the first and two higher breathing frequencies of the relative system from weak to strong coupling in the case of two particles with Coulomb interaction (left) and dipole interaction (right) in 1D. Keeping the notation from Eq. (20), the index i denotes the corresponding transition from the energy eigenvalue $E_{\rm rel,0}$ to $E_{{\rm rel},i}$.

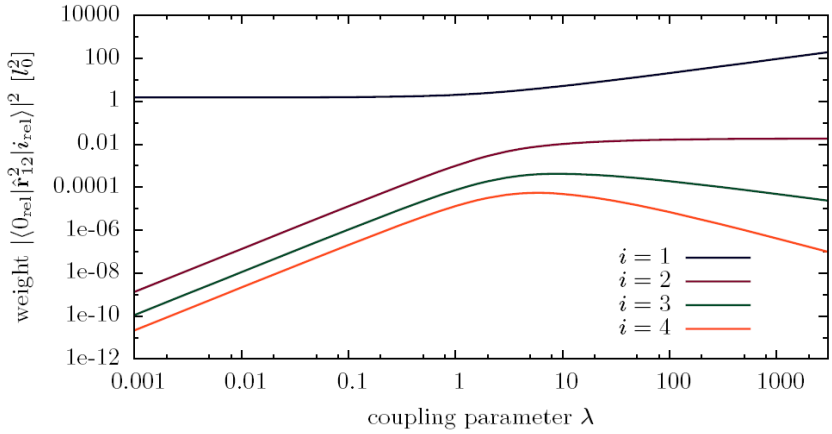

Fig. 8 Spectral weights of the i-th breathing oscillation of the quantity $\hat{\mathbf{r}}_{12}^2 := (\hat{\mathbf{r}}_1 - \hat{\mathbf{r}}_2)^2$ in the relative subsystem. These data have been produced for a 1D two-particle system with Coulomb interaction.

Having analyzed the higher frequencies for the two-particle system in 1D, one can expect that the behavior is similar for other system parameters. However, this has to be checked as far as this is possible. As will be seen

later in this work, for the application of the sum rule formulas, it is an important property that the contributions from higher frequencies are very small.

2.4.2 Solution for two and higher dimensions

For dimensions $d > 1$, it is useful to solve Eq. (46), which is an essential simplification of the full problem. Concentrating on the 2D system, the equation takes the form

$$\left\{ -\frac{1}{2}\frac{\mathrm{d}^2}{\mathrm{d}\rho^2} + \frac{\rho^2}{2} + \frac{l^2 - 1/4}{2\rho^2} + \frac{\lambda}{2^{\alpha/2}\rho^\alpha} \right\} u_l(\rho) = E_{\mathrm{rel}} u_l(\rho) \ . \tag{51}$$

Compared to the 1D system, this equation includes the additional centripetal term $\frac{l^2-1/4}{2\rho^2}$. In the case of Coulomb interaction, Taut has found analytical solutions of Eq. (51) for an infinite and countable set of trap frequencies, i. e., selected coupling parameters [70]. Similarly to the non-interacting harmonic oscillator, Taut's idea is to make an ansatz with a sum of polynomials, yielding a recurrence relation for the coefficients of the polynomials.

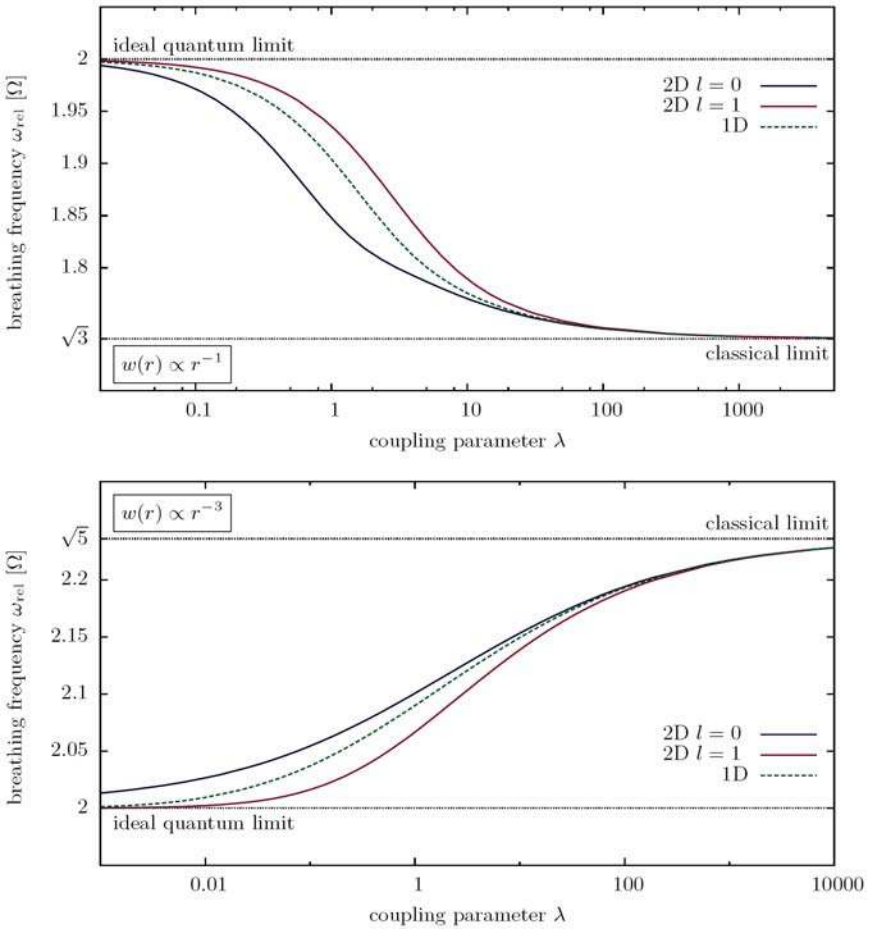

Fig. 9 Breathing frequency ω_{rel} vs. coupling parameter λ for two particles in a 2D system with Coulomb interaction (top) and dipole interaction (bottom). The curves with $l = 0$ ($l = 1$) represent symmetric (anti-symmetric) wave functions. For comparison, the frequencies of 1D systems with anti-symmetric wave functions and pure Coulomb/dipole interaction are also plotted.

This ansatz, however, forces the trap frequency to obtain selected values, and one cannot get pairs of the ground state and the first monopole-allowed state. That is why the problem is treated numerically in this work. With negligible computational effort taking no more than seconds or minutes, one can calculate the full spectra for

arbitrary couplings. Contrary to the 1D system, the symmetry of the wave function is conveniently determined by the quantum number l. To understand this, one can recall that in 2D, the spherical harmonic is proportional to $\exp(\mathrm{i}l\phi)$ for $l = 0, \pm1, \pm2, \ldots$ [66, 70]. Exchanging the positions of the two particles, the difference vector $\mathbf{r}$ changes its sign, i. e., it points to the opposite direction. That means that the coordinate r remains the same, while ϕ goes over to $\phi + \pi$. As a consequence, the spherical harmonic is multiplied by

$$\exp(\mathrm{i}l\pi) = (-1)^l \ , \tag{52}$$

yielding symmetric wave functions for even l and anti-symmetric wave functions for odd l. The ground states for both cases are found for $l = 0$ and $l = \pm1$, respectively.

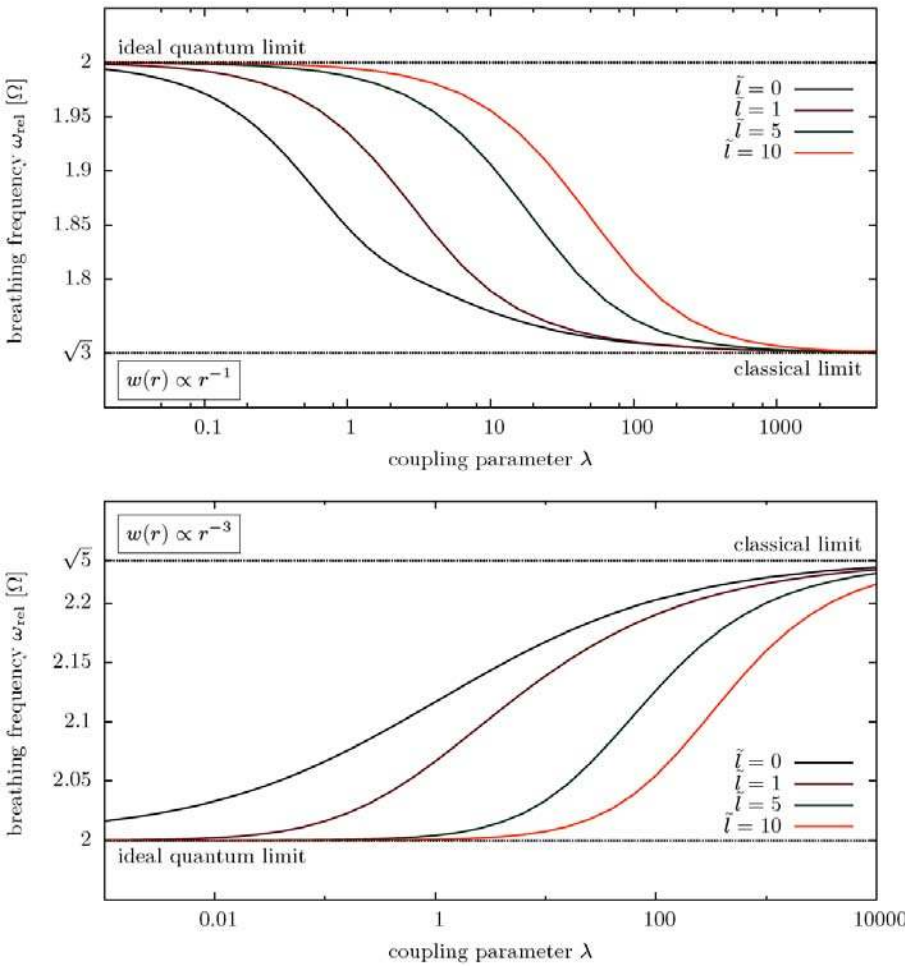

Fig. 10 Dependence of the breathing frequency on the parameter $\tilde{l}$ for Coulomb interaction (top) and dipole interaction (bottom). With increasing $\tilde{l}$, the frequencies are shifted towards the ideal quantum regime.

In Fig. 9, the breathing frequencies are plotted for Coulomb and dipole interaction. As expected, the values transition from the ideal quantum limit into the classical limit. Compared to the frequencies of a 1D system, the breathing frequencies are shifted in the classical direction for $l = 0$ and in the direction of the ideal quantum system for $l = 1$. To understand this on a more general level, one can take another look at Eq. (46) for the d-dimensional system, focusing on the centripetal term

$$\frac{(l + (d-2)/2)^2 - 1/4}{2\rho^2} \ . \tag{53}$$

This term results from the kinetic energy operator. It can be interpreted as an additional contribution to the (effective) interaction potential[5]

$$\tilde{w}(\rho) = \frac{(l+(d-2)/2)^2 - 1/4}{2\rho^2} + \frac{\lambda}{2^{\alpha/2}\rho^\alpha} \,. \tag{54}$$

If l or d is strongly increased, the second term of $\tilde{w}$ can be neglected. In this case, the breathing frequency possesses the value $2\,\Omega$ [71]. The influence of l and d can be summarized in the quantity $\tilde{l} = |l + (d-2)/2|$, which can assume the values 0, 0.5, 1, 1.5, ... For example, the 1D system and the 3D system with $l = 0$ have the same value $\tilde{l} = 0.5$ and thus the same breathing frequencies. As is confirmed in Fig. 10, the breathing frequencies are shifted to the ideal limit with increasing $\tilde{l}$.

To summarize, it has been shown how to generalize the breathing frequency of two particles to arbitrary dimensions d and quantum numbers l. One always has to solve a 1D equation. In the above considerations, the case $d = 1$ has been excluded from the treatment of Eq. (46). Nevertheless, one can formally include this case, setting $l = 0$ and assuming that the boundary condition $u_0(r = 0) = 0$ holds due to the Bose-Fermi mapping.

3 The Breathing Frequency in Terms of Equilibrium Expectation Values

As has been shown in the last section, the possibility to induce breathing oscillations of a trapped system by a δ-like perturbation opens the route towards time-independent calculations and measurements. Using the terminology of statistical physics, these methods will be called "equilibrium methods" to distinguish them from time-propagation approaches. While in general any thermodynamics ensemble (mixed state) is suitable as a starting point, in the following, we will concentrate on systems in the ground state. We will derive a variety of expecation values of relevant quantum mechanical observables that are directly related to the breathing mode. These expectation values can be computed from the wave function of the system. If needed, the obtained results are straightforwardly extended to mixed states (e.g. to the canonical or grand canonical ensembles) by replacing the wave functions by the proper density operator.

The direct way to calculate the breathing frequencies exactly is to determine the spectrum of the full system Hamiltonian $\hat{H}_0$. This can be, in principle, accomplished with the configuration interaction method (CI) that allows for a diagonalization of the Hamiltonian, see Sec. 4.3. The computational effort of this method, however, can only be handled for very small particle numbers. To overcome this problem, one can use approximate formulas for the breathing frequencies, allowing to employ other analytical or computational approaches. In this section, some equilibrium approaches are presented, namely the sum rules and the solution of an operator equation.

3.1 Sum rule approach

The quantum mechanical sum rules are an important tool to gain spectral information from equilibrium states and to compute dynamical properties of many-body systems. At the same time, sum rules are a powerful method to verify the consistency of theoretical models and computational schemes. For spatially homogeneous systems sum rules put important constraints on the density response, dielectric function and the plasmon spectrum. Here the most important sum rule is the f-sum rule, e.g. [72], for an overview see Ref. [73] and references therein.

Sum rules are equally important for spatially inhomogeneous finite systems in traps. They can be used to calculate mean excitation energies which, in turn, yield approximations for the breathing frequency. Two famous examples for the sum rules, the Thomas-Reiche-Kuhn sum rule for the coordinate operator $\hat{\mathbf{r}}$ [74,75] and the Bethe sum rule for the operator $\exp(\mathrm{i}\hat{\mathbf{k}} \cdot \hat{\mathbf{r}})$ [76], have been known already since the early days of quantum mechanics. Generalizations of these expressions have been extensively studied, see Ref. [77], for an example. Especially in nuclear physics, the sum rules have been an important tool for the investigation of collective resonances of nuclei [1–4]. In this section, the sum rules are introduced and it is shown how to make use of them for the calculation of the breathing frequencies. For all of the following considerations, the notations for the unperturbed Hamiltonian $\hat{H}_0$ (see Sec. 2) are used. The validity of the derived sum rules, however, extends to a large variety of other systems.

[5] The introduction of an effective potential is a common method for the solution of the central-force problem in classical mechanics.

3.1.1 Weighted moments

The central quantities for the calculation of average excitation energies are the so-called weighted moments [1]. For any operator $\hat{Q}$ and any integer number k, they are defined by

$$m_k = \sum_{i=1}^{\infty} (E_i - E_0)^k \, |\langle 0|\hat{Q}|i\rangle|^2 \; . \tag{55}$$

For the case $k = 1$, one usually finds the term "energy-weighted moment" in the literature. For other values of k, for example, $k = -1$ and $k = 3$, one uses the terminology "inverse energy-weighted moment" and "cubic energy-weighted moment", respectively. For the following considerations, the suggestive notation $\omega_{ij} = E_i - E_j$ will be used, as the oscillator units allow one to express the frequencies in terms of energies. Furthermore, it is assumed that E_a is the lowest energy excited by the operator $\hat{Q}$. More technically speaking, that means that the matrix elements fulfill $\langle 0|\hat{Q}|i\rangle = 0$, for all $0 < i < a$ and $\langle 0|\hat{Q}|a\rangle \neq 0$.

Containing the exact excitation energies, the moments can be used to define average excitation energies

$$E_{k,l} = \left(\frac{m_k}{m_{k-l}} \right)^{1/l} , \tag{56}$$

for positive integer numbers l. In the literature, one typically finds the quantities [1]

$$E_{k,2} = \sqrt{\frac{m_k}{m_{k-2}}} \qquad \text{and} \qquad E_{k,1} = \frac{m_k}{m_{k-1}} \; . \tag{57}$$

The average excitation energies fulfill the relation

$$\cdots \geq E_{k+2,1} \geq E_{k+2,2} \geq E_{k+1,1} \geq E_{k+1,2} \geq \ldots \tag{58}$$

and, especially, [3] the limit $\lim_{k\to-\infty} E_{k,1} = \omega_{a0}$. All $E_{k,l}$ are upper bounds for the exact excitation energy ω_{a0}.

Expressing the excitation energies in terms of weighted moments is advantageous because of the fact that various moments can be calculated with rather simple formulas instead of the direct evaluation of the sum in Eq. (55). Those formulas are called "sum rules" and they always refer to a special physical system, an integer number k, and an operator $\hat{Q}$. In some cases, however, the sum rules even hold for a general class of systems [1]. The next subsections deal with the calculation of the sum rules and their applicability to the breathing mode. Henceforth, the notation $E_{k,l}$ will be replaced by $\mathrm{sr}(k, k-l)$.

3.1.2 Selected sum rules

In the following, some selected sum rules with significance for this work are presented. They can be used to calculate the moments m_1 and m_{-1}.

Sum rules for energy-weighted moments: The first moment of interest is the energy-weighted moment m_1. It can be expressed with a double commutator, involving the Hamiltonian $\hat{H}_0$. Following the derivation in Ref. [77], one can write

$$\begin{aligned} m_1 &= \sum_{i=1}^{\infty} \omega_{i0} \, \langle 0|\hat{Q}|i\rangle \langle 0|\hat{Q}|i\rangle^* = \sum_{i=1}^{\infty} \omega_{i0} \, \langle 0|\hat{Q}|i\rangle \langle i|\hat{Q}|0\rangle \\ &= \sum_{i=0}^{\infty} \langle 0|[\hat{Q}, \hat{H}_0]|i\rangle \langle i|\hat{Q}|0\rangle = \langle 0|[\hat{Q}, \hat{H}_0]\hat{Q}|0\rangle, \end{aligned} \tag{59}$$

for any Hermitean operator $\hat{Q}$, i. e., $\hat{Q} = \hat{Q}^\dagger$. Analogously, one finds

$$m_1 = \sum_{i=1}^{\infty} \omega_{i0} \, \langle 0|\hat{Q}|i\rangle \langle i|\hat{Q}|0\rangle = -\sum_{i=0}^{\infty} \langle 0|\hat{Q}|i\rangle \langle i|[\hat{Q}, \hat{H}_0|0\rangle = -\langle 0|\hat{Q}[\hat{Q}, \hat{H}_0]|0\rangle \; . \tag{60}$$

These two results can be combined, resulting in the sum rule for the operator $\hat{Q}$,

$$m_1 = \frac{1}{2}\langle 0|[\hat{Q},[\hat{H}_0,\hat{Q}]]|0\rangle \ . \tag{61}$$

For further simplifications of the double commutator in this equation, it is assumed that $\hat{Q}$ is a one-particle operator of the form

$$\hat{Q} = \sum_{i=1}^{N} \hat{q}(\hat{\mathbf{r}}_i) \ . \tag{62}$$

Noting the commutativity of all potentials in the Hamiltonian $\hat{H}_0$ from Eq. (3) with the operator $\hat{Q}$, i. e.,

$$[\hat{Q},\hat{V}] = [\hat{Q},\hat{W}] = 0, \tag{63}$$

one finds

$$[\hat{H}_0,\hat{Q}] = [\hat{T},\hat{Q}] \ . \tag{64}$$

This is a property that holds for a variety of physical situations in which the potentials only have a spatial dependence. The commutator in Eq. (64) can immediately be reduced to

$$[\hat{T},\hat{Q}] = \frac{1}{2}\sum_{i=1}^{N}\left[\hat{\mathbf{p}}_i^2,\hat{q}(\hat{\mathbf{r}}_i)\right] = \frac{1}{2}\sum_{i=1}^{N}\left[\hat{\mathbf{p}}_i,\hat{q}(\hat{\mathbf{r}}_i)\right]\hat{\mathbf{p}}_i + \hat{\mathbf{p}}_i\left[\hat{\mathbf{p}}_i,\hat{q}(\hat{\mathbf{r}}_i)\right] \ . \tag{65}$$

For further calculations, it is useful to switch to the coordinate representation of the operators,

$$\hat{\mathbf{p}}_i \to \mathbf{p}_i = -\mathrm{i}\frac{\partial}{\partial \mathbf{r}_i} \ , \qquad \hat{q}(\hat{\mathbf{r}}_i) \to q(\mathbf{r}_i) \ . \tag{66}$$

Making use of the commutator relation

$$[\mathbf{p}_i, q(\mathbf{r}_i)] = -\mathrm{i}\frac{\partial q(\mathbf{r}_i)}{\partial \mathbf{r}_i} \ , \tag{67}$$

one can calculate the coordinate representation of the commutator in Eq. (65),

$$[T(\mathbf{r}),Q(\mathbf{r})] = -\frac{1}{2}\sum_{i=1}^{N}\mathrm{i}\frac{\partial q(\mathbf{r}_i)}{\partial \mathbf{r}_i}\mathbf{p}_i + \frac{\partial^2 q(\mathbf{r}_i)}{\partial \mathbf{r}_i^2} \ . \tag{68}$$

As a next step, one calculates

$$[Q(\mathbf{r}),[T(\mathbf{r}),Q(\mathbf{r})]] = -\frac{\mathrm{i}}{2}\sum_{i=1}^{N}\frac{\partial q(\mathbf{r}_i)}{\partial \mathbf{r}_i}[q(\mathbf{r}_i),\mathbf{p}_i] = \frac{1}{2}\sum_{i=1}^{N}\left(\frac{\partial q(\mathbf{r}_i)}{\partial \mathbf{r}_i}\right)^2 \ . \tag{69}$$

Applying this result to the monopole excitation operator $\hat{Q} = \hat{\mathbf{r}}^2$, one arrives at the monopole sum rule

$$\sum_{i=1}^{\infty}\omega_{i0}\,|\langle 0|\hat{\mathbf{r}}^2|i\rangle|^2 \ = 2\,\langle 0|\hat{\mathbf{r}}^2|0\rangle \ . \tag{70}$$

It is often practical for the computations to take the trap energy operator $\hat{V} = \hat{\mathbf{r}}^2/2$ instead of $\hat{\mathbf{r}}^2$, yielding the sum rule

$$\sum_{i=1}^{\infty}\omega_{i0}\,|\langle 0|\hat{V}|i\rangle|^2 \ = \ \langle 0|\hat{V}|0\rangle \ . \tag{71}$$

Without proof, some interesting relations are also mentioned here. For the kinetic energy operator, one can derive

$$\sum_{i=1}^{\infty} \omega_{i0} \, \langle i|\hat{T}|0\rangle\langle 0|\hat{V}|i\rangle \; = - \, \langle 0|\hat{T}|0\rangle \; . \tag{72}$$

Similarly, for the interaction operator, one obtains

$$\sum_{i=1}^{\infty} \omega_{i0} \, \langle i|\hat{W}|0\rangle\langle 0|\hat{V}|i\rangle \; = -\frac{1}{2} \, \langle 0|\hat{W}|0\rangle \tag{73}$$

in the case of Coulomb interaction ($\alpha = 1$) and

$$\sum_{i=1}^{\infty} \omega_{i0} \, |\langle 0|\hat{W}|i\rangle|^2 = -\frac{3}{2} \, \langle 0|\hat{W}|0\rangle \tag{74}$$

in the case of dipole interaction ($\alpha = 3$). Further, it is remarked that the quantum virial theorem manifests itself in the sum rules. With the diagonality of the Hamiltonian,

$$\langle i|\hat{H}_0|j\rangle = \delta_{ij} E_i \; , \tag{75}$$

one can conclude

$$0 = \sum_{i=1}^{\infty} \omega_{i0} \, \langle 0|\hat{H}_0|i\rangle\langle 0|\hat{V}|i\rangle = \sum_{i=1}^{\infty} \omega_{i0} \, \langle 0|\hat{T} + \hat{V} + \hat{W}|i\rangle\langle 0|\hat{V}|i\rangle = -\langle\hat{T}\rangle + \langle\hat{V}\rangle - \frac{\alpha}{2}\langle\hat{W}\rangle \; . \tag{76}$$

This result can be used for consistency checks.

Sum rules for inverse energy-weighted moments. Another important sum rule can be derived for the inverse energy-weighted moment. To do so, one considers the Hamiltonian under the perturbation of the Hermitean one-body operator $\hat{Q}$,

$$\hat{H}_0 + \eta\hat{Q} \; . \tag{77}$$

Here, η is assumed to be small enough to ensure that time-independent perturbation theory can be applied (see Appendix A.1.1). With the perturbed wave function, the η-dependent expectation value of any operator $\hat{F}$ is given by

$$\langle\hat{F}\rangle_\eta = \langle 0|\hat{F}|0\rangle - \eta \sum_{i=1}^{\infty} \left\{ \frac{\langle 0|\hat{F}|i\rangle\langle i|\hat{Q}|0\rangle + \langle 0|\hat{Q}|i\rangle\langle i|\hat{F}|0\rangle}{\omega_{i0}} \right\} + \mathcal{O}(\eta^2) \; . \tag{78}$$

For the special case $\hat{F} = \hat{Q}$, one obtains [3]

$$m_{-1} = \sum_{i=1}^{\infty} \frac{|\langle i|\hat{Q}|0\rangle|^2}{\omega_{i0}} = -\frac{1}{2} \lim_{\eta\to 0} \frac{\langle\hat{Q}\rangle_\eta - \langle\hat{Q}\rangle_0}{\eta} = -\frac{1}{2}\frac{\partial}{\partial\eta}\langle\hat{Q}\rangle_{\eta=0} \; . \tag{79}$$

For one of the following ideas, it is also interesting to consider a Hamiltonian that contains an operator $\gamma c\hat{Q}$, where c is an arbitrary constant and γ is a tunable parameter. A slight increase of the parameter γ to the value $(1+\eta)\gamma$ can be interpreted as a perturbation with the operator $\eta c\hat{Q}$. Similarly to the derivation of Eq. (79), one can show

$$m_{-1} = -\frac{1}{2c}\frac{\partial}{\partial\gamma}\langle\hat{Q}\rangle_\gamma \; . \tag{80}$$

This means that the sum m_{-1} can be calculated with a simple derivative of the ground-state expectation value of $\hat{Q}$. The simplest calculation of such a derivative can be performed with a finite difference of the results from two separate computations. Of course, any other more sophisticated standard technique can be applied, too.

In order to apply Eq. (80) to the breathing mode with the Hamiltonian $\hat{H}_0$, one can write $\hat{H}_0(\gamma) = \hat{T}+\gamma\hat{V}+\hat{W}$, where $\hat{H}_0 = \hat{H}_0(1)$ is valid. Since $\hat{V} = \hat{\mathbf{r}}^2/2$, one identifies $c = 1/2$ and $\hat{Q} = \hat{\mathbf{r}}^2$. Finally, one obtains

$$m_{-1} = -\frac{\partial}{\partial\gamma}\langle\hat{\mathbf{r}}^2\rangle_{\gamma=1} \,. \tag{81}$$

In this equation, the expectation value $\langle\cdot\rangle$ is taken with respect to the ground-state wave function of the Hamiltonian $\hat{H}_0(\gamma)$, and the derivative is evaluated at the point $\gamma = 1$.

3.1.3 Upper bounds for the breathing frequency

Using the moments m_{-1} and m_1 from formulas (81) and (70), one can write the simple formula

$$\omega_{a0} \leq \left\{-2\frac{\langle\mathbf{r}^2\rangle}{[\partial\langle\mathbf{r}^2\rangle/\partial\gamma]_{\gamma=1}}\right\}^{1/2} , \tag{82}$$

for the first excitation frequency of the operator $\hat{\mathbf{r}}^2$. Using the original units of the Hamiltonian (3), this formula reads

$$\omega_{a0} \leq \left\{-2\frac{\langle\mathbf{r}^2\rangle}{\partial\langle\mathbf{r}^2\rangle/\partial\Omega^2}\right\}^{1/2} . \tag{83}$$

Equation (83) has already been presented as a rigorous upper bound of the breathing frequency in the work of Menotti and Stringari [36]. However, aiming at the calculation of ω_{rel}, one should take into account that this statement is not necessarily true for all kinds of interaction. For example, in the case of dipole interaction, $\omega_{\mathrm{rel}} \geq \omega_{\mathrm{cm}}$ always holds. That means that the frequency of interest, ω_{rel}, does not correspond to the *first* excitation energy of $\hat{\mathbf{r}}^2$. In the case of Coulomb interaction, by contrast, $\omega_{\mathrm{rel}} \leq \omega_{\mathrm{cm}}$ is valid, i. e., it is assured that ω_{rel} is the lowest possible frequency. Furthermore, one can expect that the non-vanishing contribution of the center-of-mass system in the moments lowers the quality of the sum rule approximation. In the following, these ideas are expressed more formally. This will allow one to eliminate all center-of-mass contributions from the moments.

To start, the separable structure of the wave function is recalled, i. e., the set of eigenstates $\{|i\rangle\}$ can be expressed as $\{|i_{\mathrm{rel}}\rangle \otimes |k_{\mathrm{cm}}\rangle\}$. The corresponding eigenvalues are given by $E_{\mathrm{rel},i} + E_{\mathrm{cm},k}$. Further, introducing the notations

$$\hat{\mathbf{R}}^2_{\mathrm{cm}} := N\hat{\mathbf{R}}^2, \qquad \text{and} \qquad \hat{\mathbf{r}}^2_{\mathrm{rel}} := \frac{1}{N}\sum_{q<r}\hat{\mathbf{r}}^2_{qr} \,, \tag{84}$$

one can simply write

$$\hat{\mathbf{r}}^2 = \hat{\mathbf{R}}^2_{\mathrm{cm}} + \hat{\mathbf{r}}^2_{\mathrm{rel}} \,. \tag{85}$$

With this, the moments take the form

$$m_l = \sum_{i=1}^{\infty}\left(E_{\mathrm{rel},i} - E_{\mathrm{rel},0}\right)^l |\langle 0_{\mathrm{rel}}|\hat{\mathbf{r}}^2_{\mathrm{rel}}|i_{\mathrm{rel}}\rangle|^2 + \sum_{k=1}^{\infty}\left(E_{\mathrm{cm},k} - E_{\mathrm{cm},0}\right)^l |\langle 0_{\mathrm{cm}}|\hat{\mathbf{R}}^2_{\mathrm{cm}}|k_{\mathrm{cm}}\rangle|^2 \,. \tag{86}$$

This notation reveals the influence of the center-of-mass system, because all the terms in the second sum can be determined analytically. First, for all k with non-zero matrix elements $\langle 0_{\mathrm{cm}}|\hat{\mathbf{R}}^2_{\mathrm{cm}}|k_{\mathrm{cm}}\rangle$, the energy difference is $E_{\mathrm{cm},k} - E_{\mathrm{cm},0} = 2$. Second, one can show

$$\sum_{k=1}^{\infty}\left(E_{\mathrm{cm},k} - E_{\mathrm{cm},0}\right)^l |\langle 0_{\mathrm{cm}}|\hat{\mathbf{R}}^2_{\mathrm{cm}}|k_{\mathrm{cm}}\rangle|^2 = 2^{l-1}d \,, \tag{87}$$

where d is the dimension of the system. This equation can be derived, making use of the fact that the center-of-mass system has the potential energy $\langle 0|N\hat{\mathbf{R}}^2|0\rangle = d/4$, because it must be half the total energy $d/2$.

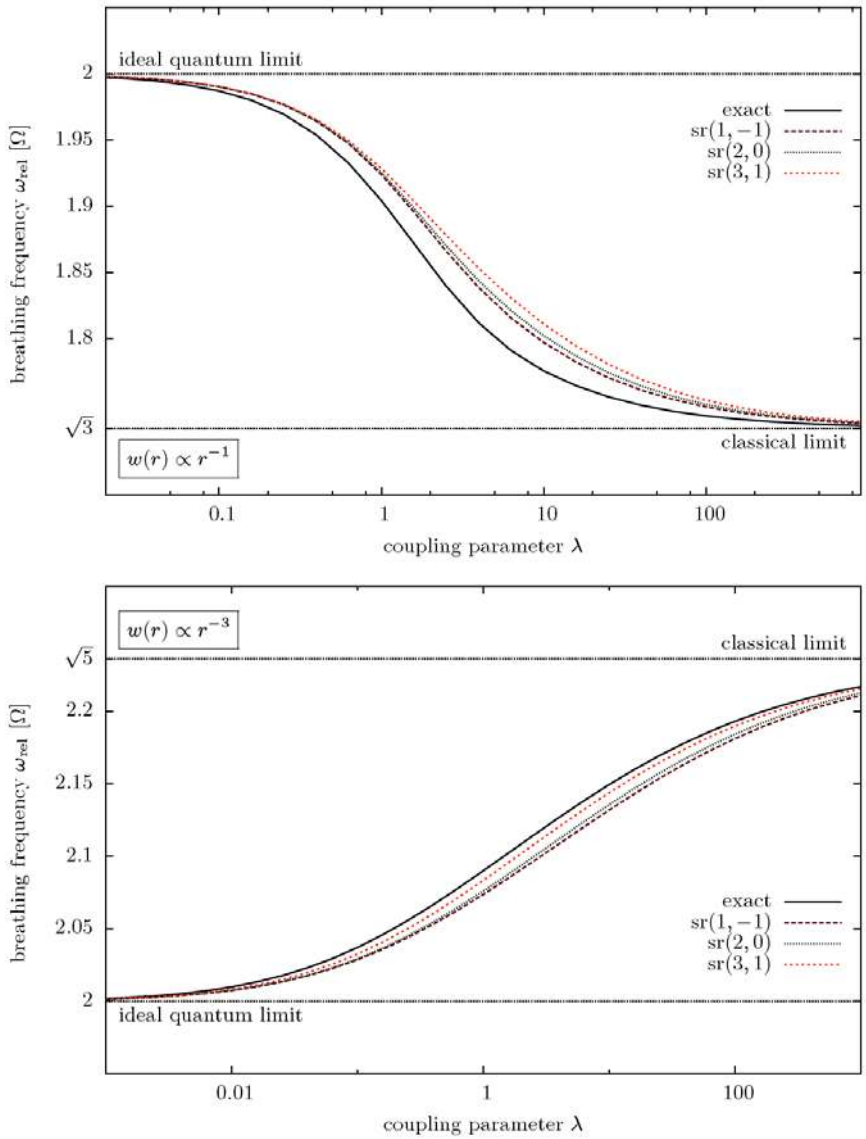

Fig. 11 Demonstration of the sum rule approximation for two particles with Coulomb interaction (top) and dipole interaction (bottom). For dipole interaction, the curves are not upper bounds. In this special case, the results for $\mathrm{sr}(3,1)$ are closer to the exact results than those for $\mathrm{sr}(1,-1)$.

The above derivations allow one to specify corrected moments m_l^* which do not contain any center-of-mass contributions,

$$m_l^* = m_l - 2^{l-1}d \; . \tag{88}$$

Using these moments, the following improved sum rule formulas,

$$\omega_{\mathrm{rel}} \leq \left(\frac{m_k^*}{m_{k-l}^*}\right)^{1/l} =: \mathrm{sr}^*(k, k-l) \; , \tag{89}$$

are valid for both Coulomb and dipole interaction. Especially the formula by Menotti and Stringari takes the form

$$\omega_{\mathrm{rel}} \leq \left\{ -\frac{2\langle \mathbf{r}^2 \rangle - d}{[\partial \langle \mathbf{r}^2 \rangle / \partial \gamma]_{\gamma=1} + d/4} \right\}^{1/2} . \tag{90}$$

Finally, to provide a visual impression of the sum rule formulas, Fig. 11 shows the calculated frequencies of a Coulomb interacting and a dipole interacting two-particle system. For this figure, the non-improved formulas have been used. For comparison, the corresponding formulas with the improved moments have been used for the results in Fig. 12. One can see that the results from the improved sum rule formulas have not only smaller errors, they also guarantee the bounding character in the case of dipole interaction.

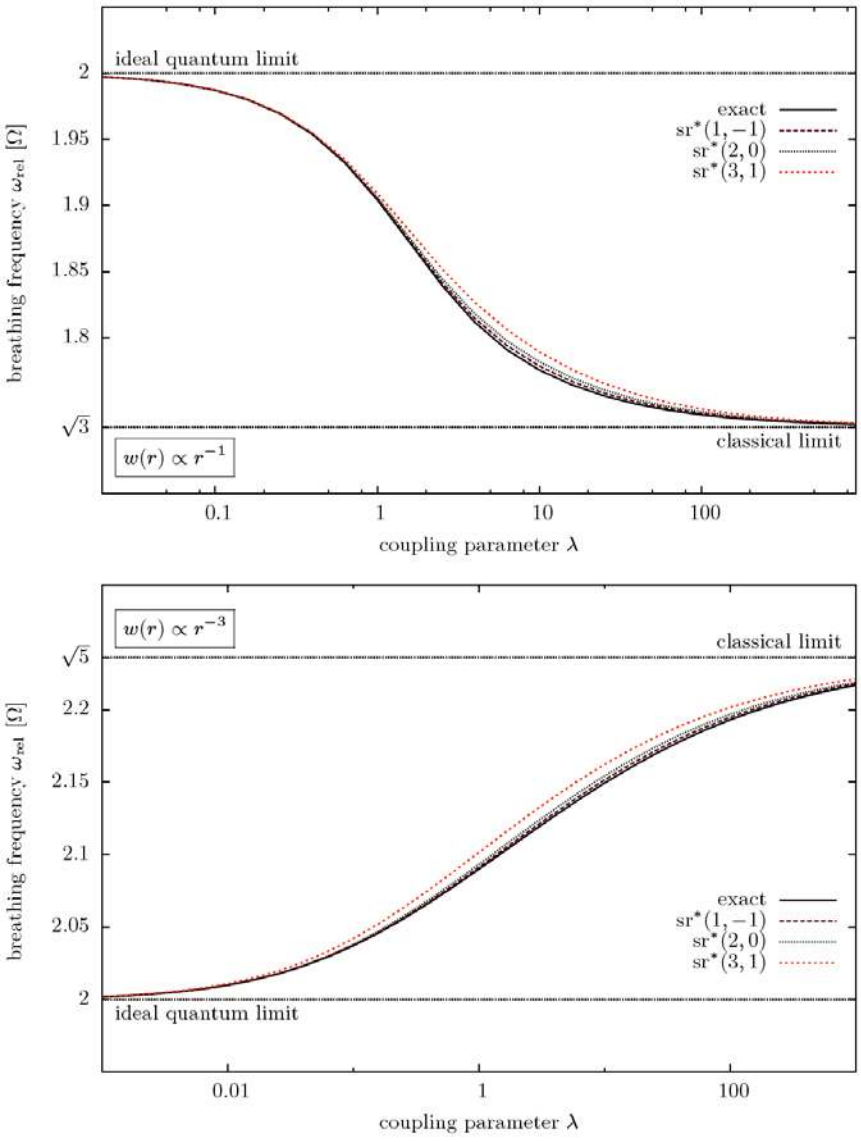

Fig. 12 Demonstration of the improved sum rule approximation for two particles with Coulomb interaction (top) and dipole interaction (bottom). The errors of the results for $\mathrm{sr}^*(1,-1)$ are nearly hidden by the resolution of the image.

The quality of the sum rule formulas strongly depends on the weights of the higher frequencies. For the breathing mode, their contribution is very small, which has already been shown for two particles in Fig. 8. As

will be seen later, this is still the case for larger particle numbers. All in all, the sum rules provide very accurate approximations to the relative frequency, and they demand only little computational effort.

3.2 Operator equation for the breathing mode

Another approach to the investigation of the quantum breathing mode is an approximate solution of the operator equation which was presented by Geller and Vignale [71]. In this section, the corresponding derivations are provided. A similar approach is presented in Ref. [37]. Following Ref. [71], the operator equation for the breathing oscillation reads

$$\frac{\mathrm{d}^2}{\mathrm{d}t^2}\hat{V} + (2+\alpha)\,\hat{V} = \alpha\hat{H}_0 + (2-\alpha)\,\hat{T}\;. \tag{91}$$

In the Heisenberg picture of quantum mechanics, the operators in this equation have an implicit time-dependence induced by the breathing motion. The goal is to simplify the equation to a basic harmonic oscillator equation which yields the breathing frequency. For that purpose, one can take the expectation value with respect to the ground state on both sides of the equation,

$$\frac{\mathrm{d}^2}{\mathrm{d}t^2}\langle\hat{V}\rangle + (2+\alpha)\,\langle\hat{V}\rangle = \alpha E_0 + (2-\alpha)\,\langle\hat{T}\rangle\;. \tag{92}$$

One important idea for the simplification of this equation is to make use of Eq. (20), which describes the basic structure of the time-dependent expectation values. To be precise, each quantity has small oscillations around its initial value. That means that the operator $\hat{A}$, representing $\hat{T}$, $\hat{V}$ or $\hat{W}$, has the form $\langle\hat{A}\rangle(t) = \langle\hat{A}\rangle(0) + \langle\Delta\hat{A}\rangle(t)$. Applying this to Eq. (92), one obtains

$$\frac{\mathrm{d}^2}{\mathrm{d}t^2}\langle\Delta\hat{V}\rangle(t) + (2+\alpha)\left(\langle\hat{V}\rangle(0) + \langle\Delta\hat{V}\rangle(t)\right) = \alpha E_0 + (2-\alpha)\left(\langle\hat{T}\rangle(0) + \langle\Delta\hat{T}\rangle(t)\right)\;. \tag{93}$$

Making use of $\langle\hat{T}\rangle(0) + \langle\hat{V}\rangle(0) + \langle\hat{W}\rangle(0) = E_0$, and of the virial theorem

$$2\langle\hat{T}\rangle(0) - 2\langle\hat{V}\rangle(0) + \alpha\langle\hat{W}\rangle(0) = 0\;,$$

Eq. (93) can be simplified to

$$\frac{\mathrm{d}^2}{\mathrm{d}t^2}\langle\Delta\hat{V}\rangle(t) + (2+\alpha)\,\langle\Delta\hat{V}\rangle(t) = (2-\alpha)\,\langle\Delta\hat{T}\rangle(t)\;. \tag{94}$$

The next idea is to separate the relative problem again, resulting in the equation

$$\frac{\mathrm{d}^2}{\mathrm{d}t^2}\langle\Delta\hat{V}_{\mathrm{rel}}\rangle(t) + (2+\alpha)\,\langle\Delta\hat{V}_{\mathrm{rel}}\rangle(t) = (2-\alpha)\,\langle\Delta\hat{T}_{\mathrm{rel}}\rangle(t)\;. \tag{95}$$

To eliminate $\langle\Delta\hat{T}_{\mathrm{rel}}\rangle(t)$, it is useful to write

$$\frac{\mathrm{d}^2}{\mathrm{d}t^2}\langle\Delta\hat{V}_{\mathrm{rel}}\rangle(t) + (2+\alpha)\,\langle\Delta\hat{V}_{\mathrm{rel}}\rangle(t) = (2-\alpha)\,\frac{\langle\Delta\hat{T}_{\mathrm{rel}}\rangle(t)}{\langle\Delta\hat{V}_{\mathrm{rel}}\rangle(t)}\langle\Delta\hat{V}_{\mathrm{rel}}\rangle(t)\;. \tag{96}$$

The goal is thus to find an expression for

$$K(t) := \frac{\langle\Delta\hat{T}_{\mathrm{rel}}\rangle(t)}{\langle\Delta\hat{V}_{\mathrm{rel}}\rangle(t)}\;. \tag{97}$$

Using again Eq. (20), one can write

$$K = \frac{\sum_{i=1}^{\infty}\langle 0_{\mathrm{rel}}|\hat{V}_{\mathrm{rel}}|i_{\mathrm{rel}}\rangle\langle i_{\mathrm{rel}}|\hat{T}_{\mathrm{rel}}|0_{\mathrm{rel}}\rangle\sin\left(\left[E_{\mathrm{rel},i} - E_{\mathrm{rel},0}\right]t\right)}{\sum_{i=1}^{\infty}\langle 0_{\mathrm{rel}}|\hat{V}_{\mathrm{rel}}|i_{\mathrm{rel}}\rangle\langle i_{\mathrm{rel}}|\hat{V}_{\mathrm{rel}}|0_{\mathrm{rel}}\rangle\sin\left(\left[E_{\mathrm{rel},i} - E_{\mathrm{rel},0}\right]t\right)}\;. \tag{98}$$

At this point, the only approximation is made: One assumes that in both sums, one can neglect all contributions except for one with the index a. Hence, the expression reduces to

$$K = \frac{\langle 0_{\rm rel}|\hat{V}_{\rm rel}|a_{\rm rel}\rangle\langle a_{\rm rel}|\hat{T}_{\rm rel}|0_{\rm rel}\rangle}{\langle 0_{\rm rel}|\hat{V}_{\rm rel}|a_{\rm rel}\rangle\langle a_{\rm rel}|\hat{V}_{\rm rel}|0_{\rm rel}\rangle} \,. \tag{99}$$

Using the sum rules for the potential energy and the kinetic energy—Eqs. (71) and (72)—and assuming again that the term with index a dominates, one arrives at

$$K = \frac{\langle 0_{\rm rel}|\hat{V}_{\rm rel}|a_{\rm rel}\rangle\langle a_{\rm rel}|\hat{T}_{\rm rel}|0_{\rm rel}\rangle\,(E_{{\rm rel},a} - E_{{\rm rel},0})}{\langle 0_{\rm rel}|\hat{V}_{\rm rel}|a_{\rm rel}\rangle\langle a_{\rm rel}|\hat{V}_{\rm rel}|0_{\rm rel}\rangle\,(E_{{\rm rel},a} - E_{{\rm rel},0})} = \frac{-\langle \hat{T}_{\rm rel}\rangle}{\langle \hat{V}_{\rm rel}\rangle} = \text{const.} \tag{100}$$

With this time-independent expression, one can finally reduce Eq. (96) to a simple oscillator equation that yields the breathing frequency

$$\omega_{\rm rel} = \left\{ (2+\alpha) + (2-\alpha)\,\frac{\langle \hat{T}_{\rm rel}\rangle}{\langle \hat{V}_{\rm rel}\rangle} \right\}^{1/2} \,. \tag{101}$$

Of course, this formula is also just an approximation. Similarly to the sum rules, the quality of this approximation depends on the contribution of higher excitation energies. From the analysis of the two-particle system, one can expect that it is reasonable to neglect these energies. Later in this work, there will also be some tests for higher particle numbers.

An interesting property of formula (101) is that it exactly includes both, the quantum limit, with $\langle \hat{T}_{\rm rel}\rangle/\langle \hat{V}_{\rm rel}\rangle = 1$, and the classical limit, with $\langle \hat{T}_{\rm rel}\rangle/\langle \hat{V}_{\rm rel}\rangle = 0$. Furthermore, for arbitrary intermediate couplings, this formula gives rise to a very intuitive interpretation of the breathing frequency in terms of energy ratios[6].

Comparison with classical formulas. Equation (101) resembles a formula by Olivetti *et al*. [28, 78] for the breathing frequency of classical systems,

$$\omega = \sqrt{(2+\alpha) + (2-\alpha)p} \,, \tag{102}$$

where p is the ratio of the thermal energy ($\propto k_{\rm B}T$) and the potential energy due to the trap. That means that in classical systems, only finite temperatures can induce deviations from the frequency $\sqrt{2+\alpha}\,\Omega$. In quantum systems, however, the kinetic energy may be non-zero even for zero temperature. Hence, the thermal fluctuations in the classical expression are replaced by quantum fluctuations in Eq. (101).

Other analytical representations. For the application of Eq. (101) in practical computations, it is often easier to calculate the energies of the full system instead of just the relative energies. To do so, one has to subtract the center-of-mass contributions from the full energies,

$$\omega_{\rm rel} = \left\{ (2+\alpha) + (2-\alpha)\,\frac{\langle \hat{T}\rangle - d/4}{\langle \hat{V}\rangle - d/4} \right\}^{1/2} \,. \tag{103}$$

With the help of the virial theorem, one can find various other representations of this formula, for example

$$\omega_{\rm rel} = \left\{ (2+\alpha) + (2-\alpha)\left(1 - \frac{\alpha\langle \hat{W}\rangle}{2\langle \hat{V}\rangle - d/2}\right) \right\}^{1/2} \,. \tag{104}$$

One might prefer this notation for the demonstration of the ideal quantum limit which is recovered by simply setting $\langle \hat{W}\rangle = 0$.

[6] The idea to characterize the breathing mode of quantum systems with ratios of relevant contributions to the total energy was already presented in Ref. [41], although Eq. (101) was still unknown at the time of publication.

Finally, it is emphasized that the above considerations are only strictly valid for pure power-law potentials, i. e., screened potentials or wake potentials in nonequilibrium plasmas, e.g. [79, 80] are not covered. For those potentials, for example, the virial theorem is not as simple as it is stated here. In Ref. [37], an attempt was made to incorporate the effect of static screening into the final formula which is discussed in Sec. 7.1.4

3.3 Using the breathing mode for diagnostics of correlated trapped systems

In Section 1.3 the idea was outlined that the normal modes of strongly correlated trapped systems may be used as a diagnostic of the system properties. We are now in the position to outline a possible realization of this concept which was presented in Ref. [37]. To this end, we first establish a direct relation between the formula (101) and the sum rules and then express the different energy contributions of a trapped system as a function of the breathing frequency.

Relation to the sum rules. In fact, there is a direct connection between formula (101) and the sum rules. To realize this, one must evaluate the commutator for the moment m_3 which, in general, is given by [1]

$$m_3 = \frac{1}{2}\langle 0|\,[[\hat{Q},\hat{H}_0],[\hat{H}_0,[\hat{H}_0,\hat{Q}]]]\,|0\rangle\ . \tag{105}$$

Since the calculation for the operator $\hat{Q} = \hat{\mathbf{r}}^2$ is a bit tedious only the result is given here,

$$m_3 = 8\langle\hat{T}\rangle + 8\langle\hat{V}\rangle + 2\alpha^2\langle\hat{W}\rangle\ . \tag{106}$$

The derivation which is straightforward can be found in Appendix A.2. A similar result for contact interaction was derived in Ref. [49]. Recalling that $m_1 = 4\langle\hat{V}\rangle$, and computing the ratio

$$\left\{\frac{m_3^*}{m_1^*}\right\}^{1/2} = \left\{\frac{8\langle\hat{T}_{\rm rel}\rangle + 8\langle\hat{V}_{\rm rel}\rangle + 2\alpha^2\langle\hat{W}\rangle}{4\langle\hat{V}_{\rm rel}\rangle}\right\}^{1/2}\ , \tag{107}$$

with the improved moments, one immediately recovers formula (101). Hence, one can conclude that Eq. (101) yields another upper bound which, however, is slightly less accurate than the improved formula (90). Nevertheless, Eq. (101) is well suited for physical interpretations, and it can easily be evaluated numerically.[7]

From Eq. (107), we can now establish relations of the breathing frequency to many-particle observables of the system. In particular, it is straightforward to deduce how the breathing frequency is related to the kinetic energy, the trap energy and the interaction energy. Making use of the virial theorem, one can even go further and rewrite the contributions to the total energy, where the breathing frequency is the only independent quantity [37],

$$\frac{\langle\hat{W}\rangle}{E_{\rm rel}} = \frac{2(4-\omega_{\rm rel}^2)}{(2-\alpha)(2\alpha+4-\omega_{\rm rel}^2)}, \tag{108}$$

$$\frac{\langle\hat{T}_{\rm rel}\rangle}{E_{\rm rel}} = \frac{\alpha(\omega_{\rm rel}^2-\alpha-2)}{(2-\alpha)(2\alpha+4-\omega_{\rm rel}^2)}, \tag{109}$$

$$\frac{\langle\hat{V}_{\rm rel}\rangle}{E_{\rm rel}} = \frac{\alpha}{2\alpha+4-\omega_{\rm rel}^2}\ . \tag{110}$$

We underline that all energy contributions depend in a complicated way on the nature of the system—the type of particles and their spin, the type of pair interaction and the system dimensionality, as well as on the system parameters, including particle number N and the coupling strength λ. The same properties and parameters determine the breathing frequency. The power of the above relations is that they show that, via a single measurement (or computation) of the breathing frequency, one can determine the kinetic, trap and interaction energy. While these relations have been derived for a quantum system in the ground state, they are straightforwardly extended to excited states or to systems at finite temperature. Then standard thermodynamic relations can be used to obtain e.g. the free energy and other quantities.

This discussion underlines again the central importance of the breathing frequency for trapped strongly correlated quantum systems and the need for its accurate computation to which we now proceed.

[7] Although the operator approach is redundant due to the derivation of Eq. (107), it is interesting an reassuring to see that the different approaches lead to the same result.

4 Exact and Approximate Many-body Methods for the Breathing Mode

After having derived a number of important relations for the quantum breathing mode in terms of equilibrium expactation values we now turn to the computation of theses expectation values. To this end many-body theory provides a broad arsenal of exact and approximate tools. Our choice is by no means complete or general but is dictated solely by the suitability of the methods for computing the required expectation values for strongly correlated trapped quantum systems. Several methods and details of their implementations will be presented.

The focus of the present work is on large quantum systems which can only be treated approximately. Here, the methods of choice are the Hartree-Fock approximation and the Thomas-Fermi approximation that will be discussed in detail in sections 5, 6 below. Nevertheless, it is important to benchmark these approximate methods. Here we take advantage of existing exact resutls for some systems which will also be presented. These are exact diagonalization (CI) solutions of the Schrödinger equation and quantum Monte Carlo simulations. This section briefly introduces these exact methods. Beforehand, some notational conventions and the single-particle basis sets for the implementations of the configuration interaction method and the Hartree-Fock method are presented.

4.1 Notational conventions

For some of the following derivations, there are important peculiarities of the notation. These are briefly mentioned hereinafter. The product state $|\phi_a\rangle|\phi_b\rangle$ is often abbreviated by $|\phi_a\phi_b\rangle$. For the adjoint state, the notation

$$|\phi_a\phi_b\rangle^\dagger = \langle\phi_b|\langle\phi_a| = \langle\phi_a\phi_b| \tag{111}$$

is used. A representation of the product state $|\phi_a\rangle|\phi_b\rangle$ in the coordinates $1, 2$ is obtained via

$$\phi_a(1)\phi_b(2) = \langle 2|\langle 1|\phi_a\rangle|\phi_b\rangle = \langle 1\ 2|\phi_a\phi_b\rangle\ . \tag{112}$$

The operator of the binary interactions $\hat{w}$ has the property

$$\langle \mathbf{r}_1\mathbf{r}_2|\hat{w}|\mathbf{r}_1'\mathbf{r}_2'\rangle = \delta(\mathbf{r}_1-\mathbf{r}_1')\delta(\mathbf{r}_2-\mathbf{r}_2')\frac{\lambda}{|\mathbf{r}_1-\mathbf{r}_2|^\alpha}\ . \tag{113}$$

Using the above basis states the matrix elements become

$$\begin{aligned}\langle\phi_a\phi_b|\hat{w}|\phi_c\phi_d\rangle &= \int \mathrm{d}\mathbf{r}_1 \int \mathrm{d}\mathbf{r}_2 \int \mathrm{d}\mathbf{r}_1' \int \mathrm{d}\mathbf{r}_2'\, \delta(\mathbf{r}_1-\mathbf{r}_1')\delta(\mathbf{r}_2-\mathbf{r}_2') \\ &\quad\times \langle\phi_a\phi_b|\mathbf{r}_1\mathbf{r}_2\rangle\langle\mathbf{r}_1\mathbf{r}_2|\hat{w}|\mathbf{r}_1'\mathbf{r}_2'\rangle\langle\mathbf{r}_1'\mathbf{r}_2'|\phi_c\phi_d\rangle \\ &= \int \mathrm{d}\mathbf{r}_1 \int \mathrm{d}\mathbf{r}_2\, \phi_a^*(\mathbf{r}_1)\phi_b^*(\mathbf{r}_2)\frac{\lambda}{|\mathbf{r}_1-\mathbf{r}_2|^\alpha}\phi_c(\mathbf{r}_1)\phi_d(\mathbf{r}_2).\end{aligned} \tag{114}$$

Below we will use the following notations for the matrix elements of the single-particle and two-particle operators

$$h_{ab} := \langle\phi_a|\hat{h}|\phi_b\rangle, \qquad \text{and} \qquad w_{ac,bd} := \langle\phi_a\phi_b|\hat{w}|\phi_c\phi_d\rangle, \tag{115}$$

where the latter indicates that the indices a and c (b and d) refer to the first (second) particle.

4.2 Single-particle basis sets

It is a common idea in many-body theories to expand certain quantities in terms of a basis. This allows one to reformulate abstract wave functions and operators with vectors and matrices. Thus, the problems are transferred to the level of discrete linear algebra. The configuration interaction method and the Hartree-Fock method need data from single-particle basis sets as an input. To be more precise, the matrix representations of the Hamiltonian and all other quantities of interest are needed. In the following, the used basis sets are briefly documented. Details of the implementation are skipped, but the necessary references are provided.

4.2.1 Harmonic oscillator basis

If the interaction terms of the considered problem of particles in a trap were absent, the Schrödinger equation could be reduced to a single-particle harmonic oscillator equation. Therefore, a reasonable choice for the single-particle basis are the eigenfunctions of the harmonic oscillator Hamiltonian

$$h(\mathbf{r}) = -\frac{1}{2}\frac{\mathrm{d}^2}{\mathrm{d}\mathbf{r}^2} + \frac{1}{2}\mathbf{r}^2 \ . \tag{116}$$

In the following, 1D and 2D systems are considered.

One-dimensional systems. In 1D, the eigenfunctions of $h(r)$ are given by the Hermite functions [81]

$$\psi_n(r) = \pi^{-1/4}\frac{1}{\sqrt{2^n n!}}H_n(r)\exp\left(-\frac{1}{2}r^2\right) \ , \tag{117}$$

where $H_n(r)$ is the n-th Hermite polynomial. The eigenfunction $|\psi_n\rangle$ corresponds to the eigenvalue

$$\epsilon_n = n + \frac{1}{2} \ . \tag{118}$$

The matrix elements for the kinetic energy and the trap energy

$$t_{nm} = \frac{1}{2}\langle\psi_n|\hat{p}^2|\psi_m\rangle \ , \qquad \text{and} \qquad v_{nm} = \frac{1}{2}\langle\psi_n|\hat{r}^2|\psi_m\rangle \ , \tag{119}$$

are listed in Refs. [68, 82]. For all required two-body operators $\hat{u}$—especially the operator of the screened Coulomb/dipole interaction—the matrix elements $u_{ij,kl}$ are precalculated on a grid. For 1D systems, this can be done in an acceptable amount of time. The 1D harmonic oscillator basis was used for all of the following configuration interaction results in one dimension.

Two-dimensional systems. For 2D systems, one may choose between basis functions in Cartesian coordinates and spherical coordinates. The presented results in this work were obtained with the single-particle basis functions in the latter coordinates. The eigenfunctions read

$$\psi_{nm}(r,\theta) = (-1)^n\left\{\frac{2n!}{(n+|m|)!}\right\}^{1/2}\exp(\mathrm{i}m\theta)r^{|m|}L_n^{|m|}(r^2)\exp(-r^2/2) \ , \tag{120}$$

where $L_n^{|m|}$ is the generalized Laguerre polynomial. The eigenfunction $|\psi_{nm}\rangle$ corresponds to the eigenvalue

$$\epsilon_{nm} = 2n + |m| + 1 \ . \tag{121}$$

The representation in spherical coordinates has the advantage that the matrix elements of the Coulomb interaction can efficiently be evaluated. Furthermore, the potential does not have to be screened. The calculation of the matrix elements is based on implementations by Hochstuhl [83] and Kvaal [84]. The 2D harmonic oscillator basis in spherical coordinates was used for all 2D Hartree-Fock calculations.

4.2.2 FEDVR basis

The acronym FEDVR stands for "finite-element discrete variable representation". The underlying idea of the basis is to split a finite interval $[r_a, r_b]$ into n_d divisions (finite elements), each of which contains n_e weighted Lobatto shape functions (element functions). Further, neighboring finite elements are connected via bridge functions which ensure the continuity of the wave function at the boundary points. In Fig. 13, the FEDVR basis functions are illustrated. Typically for finite-element methods, an important property of the basis is that it restricts the wave function to a finite interval. The size of this interval has to be chosen carefully.

The mathematical details of the basis are left out here, as they can be found in numerous references [83, 85–87]. Nevertheless, it shall be emphasized that the FEDVR basis has the important numerical advantage that the interaction energy matrix is highly sparse due to the diagonality in several indices. Hence, with the total number of basis functions n_b, one only has to store n_b^2 matrix elements instead of n_b^4 in the general case. Another advantage of the FEDVR basis is its flexible applicability to various physical situations. In this work, the FEDVR basis was used for the 1D Hartree-Fock calculations and the exact solutions of the two-particle problems in Sec. 2.4.

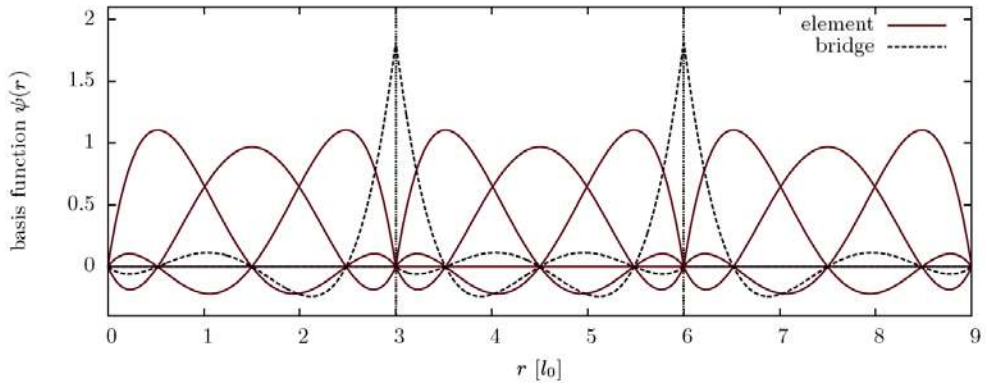

Fig. 13 Exemplary FEDVR basis functions on the grid $[0, 9]$ with $n_\mathrm{d} = 3$ divisions. Each division has $n_\mathrm{e} = 3$ element functions.

4.3 Exact solution of the Schrödinger equation: configuration interaction

With the configuration interaction (CI) method, one can obtain exact stationary and time-dependent solutions of the TDSE

$$\mathrm{i}\frac{\mathrm{d}}{\mathrm{d}t}|\Psi(t)\rangle = \hat{H}(t)|\Psi(t)\rangle \ . \tag{122}$$

In this section, the main ideas are outlined. Further details of this standard method can be found in Refs. [83, 88, 89]. Configuration interaction can be applied to both bosonic and fermionic systems. This explanation, however, refers to fermions. The fundamental idea is to expand the many-body wave function in Slater determinants,

$$|\Psi(t)\rangle = \sum_I C_I(t)|\phi_{i_1} \dots \phi_{i_N}\rangle \ . \tag{123}$$

The multi-index $I = (i_1, \dots, i_N)$ represents the indices of the single-particle orbitals ϕ_{i_j} that form the Slater determinants. Analogously to the derivation in Sec. 5, these orbitals are constructed as products of a spatial part and a spin part. If n_b is the number of single-particle orbitals, a total number of

$$n_\mathrm{s} = \binom{n_\mathrm{b}}{N} \tag{124}$$

different determinants can be formed. Inserting the expansion (123) into the TDSE and multiplying with $\langle\phi_{j_1} \dots \phi_{j_N}|$ from the left, one obtains

$$\mathrm{i}\sum_I S_{JI}\frac{\mathrm{d}}{\mathrm{d}t}C_I(t) = \sum_I H_{JI}(t)C_I(t) \tag{125}$$

with the matrix elements

$$H_{JI}(t) = \langle\phi_{j_1} \dots \phi_{j_N}|\hat{H}(t)|\phi_{i_1} \dots \phi_{i_N}\rangle \qquad \text{and} \qquad S_{JI}(t) = \langle\phi_{j_1} \dots \phi_{j_N}|\phi_{i_1} \dots \phi_{i_N}\rangle \ . \tag{126}$$

As it is the case for the basis sets introduced above, in the following

$$S_{JI} = \delta_{JI} = \delta_{j_1 i_1} \dots \delta_{j_N i_N} \tag{127}$$

is assumed. Defining the matrix H, containing the elements H_{JI}, and the coefficient vector C, containing the coefficients C_I, Eq. (125) can also be written as the matrix equation

$$\mathrm{i}\frac{\mathrm{d}}{\mathrm{d}t}C(t) = H(t)C(t) \ . \tag{128}$$

To obtain the exact breathing frequencies, it is sufficient to solve the stationary problem

$$HC = EC \; . \tag{129}$$

More precisely, one has to diagonalize the matrix H to obtain its eigenvalues E_K. Then, one can calculate the breathing frequencies $E_K - E_0$ for all K with a non-vanishing matrix element

$$\langle \Psi_K | \hat{\mathbf{r}}^2 | \Psi_0 \rangle \; . \tag{130}$$

Here, $|\Psi_K\rangle$ is an abstract eigenfunction of $\hat{H}$, which can be expressed with the K-th coefficient eigenvector of H.

The CI method was used for the results of small 1D systems with $N \leq 8$. For 2D, it could only be applied to the two-particle system, for which the methods from Sec. 2.4 already provide satisfactory results. The limited applicability of the method is due to the strong increases of required basis sizes n_s for larger particle numbers and higher dimensions. Hence, the number of determinants can become a problem for the memory as well as for the CPU, noting that modern linear algebra libraries perform diagonalizations with run times of the order $\mathcal{O}(n_\mathrm{s}^3)$.

4.3.1 Implementation of time-independent perturbation theory

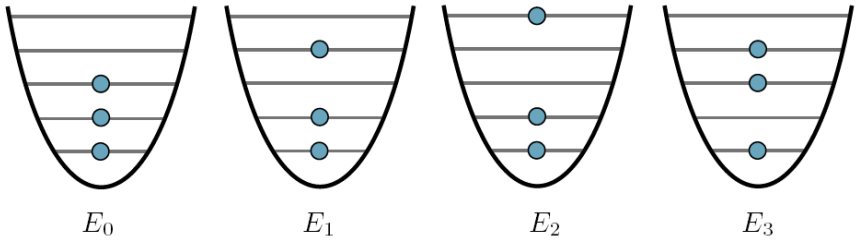

Fig. 14 Formation of the first four Slater determinants in a non-interacting 1D oscillator system with three spin-polarized particles. The horizontal lines indicate the orbital energies with the equal spacing $\hbar\Omega$. The energies E_2 and E_3 correspond to the monopole oscillation with the degenerate frequency $2\,\Omega$.

With only very little programming effort, a CI program can be modified to perform calculations in the framework of time-independent perturbation theory (PT). In Appendix A.1.1, the theory is explained. The Slater determinants $|\Psi_I\rangle$ of the non-interacting system are constructed with the harmonic oscillator single-particle basis functions. The indices I are assumed to be sorted according to the corresponding energy eigenvalues, starting with the lowest energy E_0 for $I = 0$. In fact, one does not need any other input quantity than the matrix elements of the interaction energy, W_{IJ}. For a clear notation, the W_{IJ} are defined without the prefactor λ. Furthermore, only 1D systems of fermions with spin polarization, i. e., with equal spin projections, are considered. The formation of the Slater determinants with the lowest energies is illustrated in Fig. 14. Recalling that the oscillator orbitals have the energies $\epsilon_i = i + 1/2$, one finds that the ground-state energies of the non-interacting systems are given by $E_0(N) = 1/2N^2$. For small coupling parameters, one can use first-order perturbation theory to obtain the energy of the interacting system,

$$E_0^\mathrm{PT} = E_0 + \lambda W_{00} \; . \tag{131}$$

The lowest states for the breathing excitation are $|\Psi_2\rangle$ and $|\Psi_3\rangle$ with the degenerate eigenvalues $E_{2/3} = E_0 + 2$. For the interacting system, the corrections are

$$E_{2/3}^\mathrm{PT} = E_{2/3} + \lambda \tilde{E}_{2/3} \; , \tag{132}$$

where $\tilde{E}_{2/3}$ are the eigenvalues of the matrix

$$\begin{pmatrix} W_{22} & W_{23} \\ W_{32} & W_{33} \end{pmatrix} \; . \tag{133}$$

Hence, $\omega_{20} = E_2^\mathrm{PT} - E_0^\mathrm{PT}$ and $\omega_{30} = E_3^\mathrm{PT} - E_0^\mathrm{PT}$ are easily obtainable estimators for the two lowest breathing frequencies. According to the theory, one of those frequencies must have the value 2.

4.4 Path integral Monte Carlo

This work contains results for dipolar zero-spin bosons, which were obtained with the *ab initio* path integral Monte Carlo (PIMC) method in continuous space. The idea of the method is to express the partition function of a quantum-statistical ensemble in Feynman's path integral picture. Based on first principles, PIMC is considered exact within some statistical errors. Differing relatively strong from the other methods in this work, a complete understanding of PIMC cannot be provided here, instead we refer to the extensive literature, for example, Ref. [90]. The main idea of PIMC consists in generating successive randomly sampled particle configurations with the fixed conditions that are imposed by the selected statistical ensemble. More precisely, the samples form a Markov chain [90]. To ensure that the sampling reproduces the correct probability distribution, a generalized Metropolis algorithm [91] is employed. After a sufficient number of Monte Carlo steps, the quantities of interest can be calculated as thermodynamic averages over the samples.

A peculiarity of the PIMC method[8] is—in contrast to the implicit zero-temperature assumptions of the other methods—that the temperature has to be finite. The lower is the temperature, the higher is the computational effort because of the increasing role of spin statistics. The results in this work were obtained with an implementation of the worm algorithm by Alexey Filinov [19,92]. As these PIMC simulations are performed in the grand canonical ensemble, the system is embedded in a heat reservoir with fixed temperature T and chemical potential μ. The central quantity for the description of such a system is the grand canonical partition function

$$Z = \mathrm{Tr}\left\{\exp\left(-\beta\left(\hat{H}_0 - \mu\hat{N}\right)\right)\right\} \ , \tag{134}$$

where $\beta = 1/T$, and the Boltzmann constant k_B has been set equal to 1. Using dimensionless oscillator units the temperature is measured in units of $\hbar\Omega$. In the simulations, the parameter $\beta = 30$ has been used to obtain low temperature results (essentially ground state results) at an acceptable numerical cost. Since the particle number may fluctuate in the simulations, the chemical potential must be chosen in a way that the particle numbers of interest have a high sampling probability.

5 The Hartree-Fock Approximation

The Hartree-Fock (HF) approximation is one of the main tools with which the numerical results in this work were obtained. It can be used for both time-independent and time-dependent considerations. This section deals with the derivation of the time-independent and time-dependent Hartree-Fock equations as well as their application to perturbed systems. The derivations are intended to be on a rather general level. The necessary restrictions for the breathing mode are explicitly mentioned.

5.1 Time-independent Hartree-Fock

The time-independent Hartree-Fock approximation is used to determine the fermionic ground state of the N-particle stationary Schrödinger equation. It is a standard method for the numerical treatment of atoms and molecules in quantum chemistry, see, e. g., Refs. [93, 94]. Further, it is often the starting point of more sophisticated methods which handle correlation effects [68,95]. This section contains a review of the Hartree-Fock equations. The purpose is to show the basic ideas of the method. Complete introductions are given in the literature, for example, see Refs. [89, 96]. Details on the implementation can also be found in Refs. [68, 97].

5.1.1 Hartree-Fock equations

The following considerations refer to fermions with spin 1/2, e. g., electrons. The goal of the Hartree-Fock method is to get an approximate ground-state solution of the stationary Schrödinger equation

$$\hat{H}_0|\Psi\rangle = E|\Psi\rangle \ . \tag{135}$$

[8] Here we do not discuss the corresponding zero temperature methods such as diffusion Monte Carlo.

Just for this introduction, it is assumed that $\hat{H}_0$ is a general Hamiltonian of the form

$$\hat{H}_0 = \sum_{i=1}^{N} \hat{h}(\hat{\mathbf{p}}_i, \hat{\mathbf{r}}_i) + \sum_{i<j} \hat{w}(\hat{\mathbf{r}}_i, \hat{\mathbf{r}}_j) \ , \tag{136}$$

where $\hat{h}$ represents all the single-particle terms, i. e., the kinetic energy operator $\hat{t}$ and maybe an additional external potential operator $\hat{v}$, and $\hat{w}$ is—just for simplicity—assumed to represent the Coulomb interaction.

The basic idea of the Hartree-Fock approximation is to assume that the desired fermionic wave function is a single Slater determinant

$$|\Psi\rangle \equiv |\phi_1 \dots \phi_N\rangle \ , \tag{137}$$

where the particles are represented by the spin orbitals ϕ_i. This assumption is exact for a non-interacting system, which is described by single-particle operators only. It will be shown that the Hartree-Fock equations are used to describe the system solely with single-particle operators that effectively contain the binary interactions. According to the Ritz variational principle [98], the desired Slater determinant has to minimize the total energy, for which one finds the expression

$$E = \langle\Psi|\hat{H}_0|\Psi\rangle = \sum_{i=1}^{N}\langle\phi_i|\hat{h}|\phi_i\rangle + \frac{1}{2}\sum_{i=1}^{N}\sum_{j=1}^{N}\langle\phi_i\phi_j|\hat{w}|\phi_i\phi_j\rangle - \langle\phi_i\phi_j|\hat{w}|\phi_j\phi_i\rangle \ . \tag{138}$$

Defining the Coulomb and the exchange operator by their action

$$\hat{J}_i|\phi_k\rangle = \langle\phi_i|\hat{w}|\phi_i\rangle|\phi_k\rangle \qquad \text{and} \qquad \hat{K}_i|\phi_k\rangle = \langle\phi_i|\hat{w}|\phi_k\rangle|\phi_i\rangle \ , \tag{139}$$

respectively, Eq. (138) can also be written as

$$E = \sum_{i=1}^{N}\langle\phi_i|\hat{h}|\phi_i\rangle + \frac{1}{2}\sum_{i=1}^{N}\sum_{j=1}^{N}\langle\phi_j|\hat{J}_i|\phi_j\rangle - \langle\phi_j|\hat{K}_i|\phi_j\rangle \ . \tag{140}$$

The interaction energy has two contributions. The one due to the Coulomb operator is usually called “Hartree” term, and the other one due to the exchange operator is usually called “Fock” term.

A systematic variation of the spin orbitals with the orthonormality constraint $\langle\phi_i|\phi_j\rangle = \delta_{ij}$ yields the Hartree-Fock equations [89]

$$\hat{F}|\phi_k\rangle = \epsilon_k|\phi_k\rangle \tag{141}$$

for $k = 1, \dots, N$. Equation (141) resembles a stationary Schrödinger equation with the Hamiltonian replaced by the so-called Fock operator

$$\hat{F} := \hat{h} + \sum_{i=1}^{N} \hat{J}_i - \hat{K}_i \ . \tag{142}$$

The Hartree-Fock method aims at finding the spin orbitals that solve Eq. (141). Since the Fock operator itself depends on the spin orbitals ϕ_k, the problem is nonlinear. Hence, it requires a self-consistent solution.

Going more into detail, one has to make an a priori decision for the treatment of the spins. For that purpose, one first factorizes the wave function into a spatial part $|\varphi_k\rangle$ and a spin part $|\chi_k\rangle$,

$$|\phi_k\rangle = |\varphi_k\rangle|\chi_k\rangle \ . \tag{143}$$

As a first restriction, one allows the $|\chi_k\rangle$ to be only one of the orthonormal eigenfunctions $|+\rangle$ or $|-\rangle$ of the spin operator $\hat{s}_z$. This assumption is made, because the Hamiltonian is spin-independent. In the following, two different treatments of the spins are outlined.

Hartree-Fock for spin polarization. Several systems investigated in this work are assumed to be *spin-polarized*. That means that all N particles have the same spin projection. In this simplest case, one can assume without loss of generality that the spin orbitals have the form

$$|\varphi_1\rangle|+\rangle, |\varphi_2\rangle|+\rangle, \ldots, |\varphi_N\rangle|+\rangle \; . \tag{144}$$

Calculating

$$\begin{pmatrix} \langle +|\hat{F}|+\rangle & \langle +|\hat{F}|-\rangle \\ \langle -|\hat{F}|+\rangle & \langle -|\hat{F}|-\rangle \end{pmatrix} = \begin{pmatrix} \hat{F}^+ & 0 \\ 0 & 0 \end{pmatrix} \; , \tag{145}$$

one obtains a set of N Hartree-Fock equations for the spatial orbitals,

$$\hat{F}^+|\varphi_k\rangle = \epsilon_k|\varphi_k\rangle \; . \tag{146}$$

Here, the Fock operator $\hat{F}^+$ is defined by its action

$$\hat{F}^+|\varphi_k\rangle = \hat{h}|\varphi_k\rangle + \sum_{i=1}^{N}\langle\varphi_i|\hat{w}|\varphi_i\rangle|\varphi_k\rangle - \sum_{i=1}^{N}\langle\varphi_i|\hat{w}|\varphi_k\rangle|\varphi_i\rangle \; . \tag{147}$$

In the literature, one usually finds an analogous derivation for systems in which each pair of particles with anti-parallel spins share the same spatial orbital. For such a configuration, requiring even particle numbers, one speaks of *restricted closed-shell Hartree-Fock*. The more general approach, respecting the different spin projections and allowing each particle to have its own spatial orbital, is presented in the following.

Unrestricted Hartree-Fock. As a starting point, one divides the particles into one fraction of N^+ particles with the spin orbitals

$$|\varphi_1^+\rangle|+\rangle, |\varphi_2^+\rangle|+\rangle, \ldots, |\varphi_{N^+}^+\rangle|+\rangle \tag{148}$$

and another fraction of N^- particles with the spin orbitals

$$|\varphi_1^-\rangle|-\rangle, |\varphi_2^-\rangle|-\rangle, \ldots, |\varphi_{N^-}^-\rangle|-\rangle \; . \tag{149}$$

With these orbitals, one calculates

$$\begin{pmatrix} \langle +|\hat{F}|+\rangle & \langle +|\hat{F}|-\rangle \\ \langle -|\hat{F}|+\rangle & \langle -|\hat{F}|-\rangle \end{pmatrix} = \begin{pmatrix} \hat{F}^+ & 0 \\ 0 & \hat{F}^- \end{pmatrix} \; , \tag{150}$$

yielding two coupled sets of Hartree-Fock equations for each spin projection,

$$\hat{F}^+|\varphi_k^+\rangle = \epsilon_k^+|\varphi_k^+\rangle \qquad \text{and} \qquad \hat{F}^-|\varphi_k^-\rangle = \epsilon_k^-|\varphi_k^-\rangle \; . \tag{151}$$

The actions of $\hat{F}^+$ and $\hat{F}^-$ are given by

$$\hat{F}^+|\varphi_k^+\rangle = \hat{h}|\varphi_k^+\rangle + \sum_{i=1}^{N^+}\langle\varphi_i^+|\hat{w}|\varphi_i^+\rangle|\varphi_k^+\rangle + \sum_{i=1}^{N^-}\langle\varphi_i^-|\hat{w}|\varphi_i^-\rangle|\varphi_k^+\rangle - \sum_{i=1}^{N^+}\langle\varphi_i^+|\hat{w}|\varphi_k^+\rangle|\varphi_i^+\rangle \tag{152}$$

and

$$\hat{F}^-|\varphi_k^-\rangle = \hat{h}|\varphi_k^-\rangle + \sum_{i=1}^{N^-}\langle\varphi_i^-|\hat{w}|\varphi_i^-\rangle|\varphi_k^-\rangle + \sum_{i=1}^{N^+}\langle\varphi_i^+|\hat{w}|\varphi_i^+\rangle|\varphi_k^-\rangle - \sum_{i=1}^{N^-}\langle\varphi_i^-|\hat{w}|\varphi_k^-\rangle|\varphi_i^-\rangle \; . \tag{153}$$

5.1.2 Basis expansion

So far, the presented Hartree-Fock equations do not allow for an easy computational solution. Aiming at the application of standard linear algebra techniques, it is useful to expand the spatial orbitals in a single-particle basis, according to

$$|\varphi_k^\sigma\rangle = \sum_i^{\mathrm{basis}_\sigma} c_{ik}^\sigma |\psi_i\rangle \ . \tag{154}$$

The index σ represents both spin sorts, $+$ and $-$. The special choice of the ψ_i is determined by numerical convenience and physical motivations. The notation of the sum is meant to suggest that the summation is performed over all possible basis functions. In many cases, the dimension of the basis is infinity. Following a standard numerical technique, the basis is therefore restricted to a finite number of basis functions n_b. For this derivation, it is required that the ψ_i form a complete orthonormal[9] system. Concentrating on the unrestricted case, the next step is to insert the expanded orbitals into the Hartree-Fock equations,

$$\sum_i c_{ik}^\sigma \hat{F}^\sigma |\psi_i\rangle = \sum_i c_{ik}^\sigma \epsilon_k^\sigma |\psi_i\rangle \ . \tag{155}$$

Multiplying these equations with $\langle\psi_j|$ from the left, the matrix equations

$$F^\sigma C^\sigma = \epsilon^\sigma C^\sigma \tag{156}$$

can be obtained for both $\sigma = +$ and $\sigma = -$. These equations can be identified as two coupled Roothaan-Hall equations [99, 100]. In the literature, they are also referred to as Pople-Nesbet equations [89, 101]. The matrix C^σ has the matrix elements c_{ik}^σ, representing the i-th expansion coefficient of the k-th spatial orbital. The matrix ϵ^σ only has the diagonal entries ϵ_k^σ. The matrix elements of the Fock operators are given by

$$F_{ab}^+ = \langle\psi_a|\hat{F}^+|\psi_b\rangle = h_{ab} + \sum_{ij}^{\mathrm{basis}_+} D_{ji}^+ \left(w_{ab,ij} - w_{aj,ib}\right) + \sum_{ij}^{\mathrm{basis}_-} D_{ji}^- w_{ab,ij} \tag{157}$$

and

$$F_{ab}^- = \langle\psi_a|\hat{F}^-|\psi_b\rangle = h_{ab} + \sum_{ij}^{\mathrm{basis}_-} D_{ji}^- \left(w_{ab,ij} - w_{aj,ib}\right) + \sum_{ij}^{\mathrm{basis}_+} D_{ji}^+ w_{ab,ij} \ . \tag{158}$$

Here, the single-particle density matrix

$$D_{ij}^\sigma = \sum_{k=1}^{N^\sigma} c_{ik}^\sigma \left(c_{jk}^\sigma\right)^* \tag{159}$$

has been defined. In the Hartree-Fock approximation, it contains the full information of the system.

5.1.3 Solution of the Pople-Nesbet equations

To solve the problem in Hartree-Fock approximation, one has to find the coefficient matrices C^σ and the corresponding eigenvalue matrices ϵ^σ that solve the Pople-Nesbet equations. As the Fock matrix F^σ itself depends on the coefficients, the following iterative scheme is applied.

1. Precalculation of the matrix elements h_{ij} and $w_{ij,kl}$.
2. Initialization of the density matrices D^σ with random or physically motivated values.
3. Calculation of the Fock matrices F^σ with the density matrices as an input.

[9] In general, orthogonality is not required, but since all basis sets used in this work are orthogonal, this simplification is appropriate.

4. Diagonalization of the Fock matrices.

5. Calculation of the new density matrices with the eigenvectors of the Fock matrix.

6. Procession with step 3 until a stopping criterion is fulfilled. (For the stopping criterion, one typically measures the difference between the previous and the current density matrix, and claims that the algorithm stops when the difference is in the range of a predefined accuracy.)

After step 6, one can output all interesting quantities, for example, the kinetic energy and the energy of the external potential

$$\langle \hat{T} \rangle = \sum_{\sigma} \sum_{ab}^{\mathrm{basis}_\sigma} t_{ab} D^{\sigma}_{ba} \ , \qquad \text{and} \qquad \langle \hat{V} \rangle = \sum_{\sigma} \sum_{ab}^{\mathrm{basis}_\sigma} v_{ab} D^{\sigma}_{ba}, \tag{160}$$

respectively, and the interaction energy

$$\langle \hat{W} \rangle = \frac{1}{2} \sum_{\sigma\tau} \sum_{ab}^{\mathrm{basis}_\sigma} \sum_{cd}^{\mathrm{basis}_\tau} D^{\sigma}_{ab} D^{\tau}_{cd} w_{ba,dc} - \frac{1}{2} \sum_{\sigma} \sum_{abcd}^{\mathrm{basis}_\sigma} D^{\sigma}_{cb} D^{\sigma}_{da} w_{ac,bd} \ . \tag{161}$$

Another quantity of interest is the diagonal element of the single-particle density operator in spatial coordinates,

$$n(\mathbf{r}) = \langle \mathbf{r} | \hat{D} | \mathbf{r} \rangle \ . \tag{162}$$

This quantity is often suitable to provide insight into the basic physical behavior of the system. For example, in Fig. 15, one can track the crystallization process of charged particles in a trap.

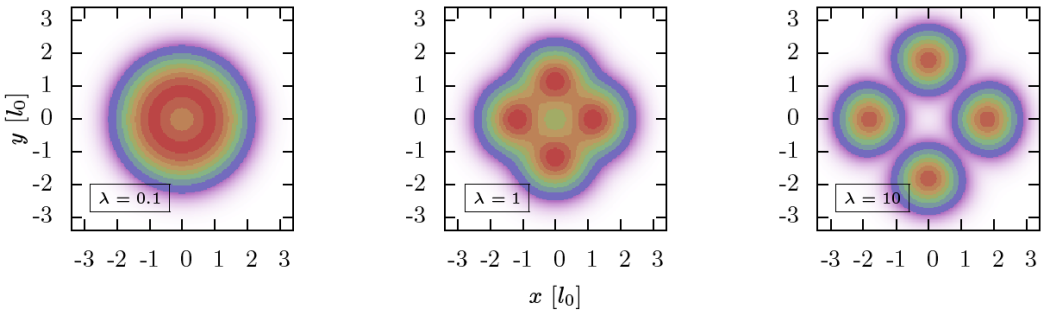

Fig. 15 Schematic densities $n(\mathbf{r})$ in Hartree-Fock approximation (2D, $N = 4$, spin polarization, Coulomb interaction) for different coupling parameters λ. Although the Hartree-Fock approximation is usually inaccurate for $\lambda \geq 1$, the trend of crystallization can be reproduced.

5.2 Time-dependent Hartree-Fock

The extension of the static Hartree-Fock equations to nonequilibrium leads to the well-known time-dependent Hartree-Fock (TDHF) equations. As well as the TDSE, they can be derived from the time-dependent variational principle [102], which states that the action functional

$$S[\Psi] = \int_{t_0}^{t_1} \mathrm{d}t \, \langle \Psi | \hat{H}(t) - \mathrm{i}\partial_t | \Psi \rangle, \tag{163}$$

must be stationary under arbitrary variations of Ψ. In the general case, this leads to the time-dependent Schrödinger equation. However, the Hartree-Fock approximation makes the assumption that the wave function is a single determinant, i. e., $|\Psi\rangle \equiv |\phi_1 \dots \phi_N\rangle$. In this case, the stationarity condition $\delta S = 0$ refers to variations of the orbitals ϕ_i at times t_0 and t_1 [103]. The resulting time-dependent Hartree-Fock equations were already derived

by Dirac [104] and Frenkel [105] in the 1930s. Using a time-dependent Fock operator $\hat{F}$, they can be written in the simple form

$$\mathrm{i}\frac{\mathrm{d}}{\mathrm{d}t}|\phi_i\rangle = \hat{F}(t)|\phi_i\rangle, \qquad i = 1, \ldots, N. \tag{164}$$

These equations are the time-dependent counterpart of Eqs. (141), which resembles the relation between the stationary and the time-dependent Schrödinger equation. The time-dependence of the Fock operator depends on the terms in the time-dependent Hamiltonian $\hat{H}(t)$. Henceforth, it is assumed that the Fock operator has the form

$$\hat{F}(t) = \hat{h} + \hat{\Lambda}(t) + \sum_{i=1}^{N} \hat{J}_i + \hat{K}_i \ , \tag{165}$$

i. e., the time-dependence is incorporated by an additional single-particle operator $\hat{\Lambda}$. For the excitation of the breathing mode, it has the form

$$\hat{\Lambda}(t) = \eta\delta(t)\hat{\mathbf{r}}^2 \ . \tag{166}$$

Nevertheless, the following derivations are valid for arbitrary operators. It is convenient to express Eqs. (164) in an equivalent equation of motion for the single-particle density operator. The resulting equation is

$$\mathrm{i}\frac{\mathrm{d}}{\mathrm{d}t}\hat{D} = [\hat{F}, \hat{D}] \ , \tag{167}$$

which is also known as the first-order equation of the quantum mechanical BBGKY in HF approximation [95, 106–109].

There are several ways to resolve the time-dependence of the density matrix. A calculation usually starts with the determination of the initial density matrix. For example, this can be done as explained in the last section. But there are also other methods, e. g., imaginary time stepping [83]. Knowing the initial density matrix, one can start the propagation, according to Eq. (167). Without explicitly writing out the spin, the basis representation of the equation reads

$$\begin{aligned} \mathrm{i}\frac{\mathrm{d}}{\mathrm{d}t}D_{ab} = &\sum_{k}^{\text{basis}} \left(h_{ak} + \Lambda_{ak}\right) D_{kb} + \sum_{kij}^{\text{basis}} D_{kb}D_{ji}\left(w_{ij,ak} - w_{ik,aj}\right) \\ &- \sum_{k}^{\text{basis}} \left(h_{kb} + \Lambda_{kb}\right) D_{ak} - \sum_{kij}^{\text{basis}} D_{ak}D_{ji}\left(w_{ij,kb} - w_{ib,kj}\right) \ . \end{aligned} \tag{168}$$

These equations can be solved with arbitrary integrators for the numerical solution of differential equations. The main problem to handle is the fact that the matrix D can be very large, resulting in a large system of equations. In the FEDVR matrix, for example, typical matrix sizes for the problems considered in this work were between 120×120 and 700×700.

To overcome the problem of large matrices, one can also perform the time propagation in the Hartree-Fock basis, i. e., in the basis formed by the eigenfunctions of the Fock operator. Especially for small particle numbers, this is very useful, as basis sizes of $n_\mathrm{b} = N + n_\mathrm{add}$ with $n_\mathrm{add} \approx 15$ are usually sufficient to capture the time-dependent breathing oscillation. In order to perform the calculations in the HF basis, one starts the calculation of the ground state in an arbitrary basis and afterwards transforms all necessary matrix elements into the obtained HF basis. The transformation into the Hartree-Fock basis does not only allow to speed up calculations. It also gives rise to another approach to solve Eq. (167) perturbatively which is illustrated in the next subsection.

5.2.1 Perturbative solution of the TDHF equations

In the theory part of this work, it was shown how to calculate the collective modes with time-dependent perturbation theory by applying a monopole-type perturbation to the initial Hamiltonian $\hat{H}_0$. Another idea is to make

the HF approximation first and to treat the resulting equations with perturbation theory. In the following, this procedure is elaborated in detail.

The starting point is the basis representation of the equation for the time-dependence of the density matrix, Eq. (167). Writing $\eta\hat{\Lambda}$ with the small parameter η instead of $\hat{\Lambda}$ from now on, it is intended to assure that the system is exposed to a weak perturbation. Furthermore, all quantities are expanded in the basis of the initial HF states. As the perturbation is weak, one can make an ansatz for the density matrix,

$$D = D^{(0)} + \eta D^{(1)}(t) + \mathcal{O}(\eta^2) \; . \tag{169}$$

In this ansatz, $D^{(0)}$ is the time-independent density matrix of the unperturbed system. It is given by $D^{(0)}_{ab} = \delta_{ab} n_a$ with

$$n_a = \begin{cases} 1 & 1 \leq a \leq N \\ 0 & \text{else} \; . \end{cases} \tag{170}$$

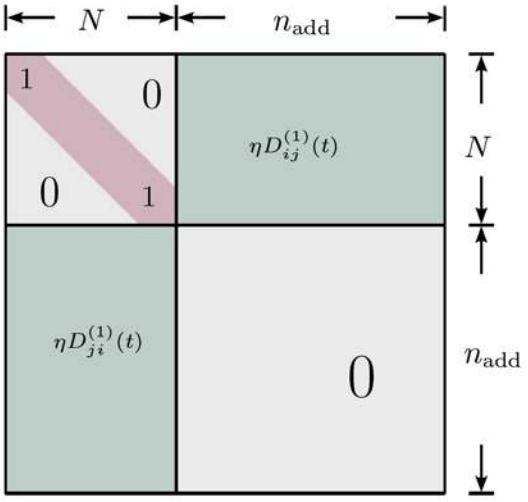

Fig. 16 Structure of the density matrix $D(t) = D^{(0)} + \eta D^{(1)}(t)$, according to the perturbative solution of the Hartree-Fock equations.

Furthermore, the unperturbed Fock operator has the eigenvalues ϵ_k. Inserting the ansatz for D with all terms up to the first order into Eq. (168), one obtains

$$\begin{aligned} \mathrm{i}\frac{\mathrm{d}}{\mathrm{d}t}\left(D^{(0)}_{ab} + \eta D^{(1)}_{ab}(t)\right) = &\sum_{k}^{\text{basis}} \left(h_{ak} + \eta\Lambda_{ak}(t)\right)\left(D^{(0)}_{kb} + \eta D^{(1)}_{kb}(t)\right) \\ &+ \sum_{kij}^{\text{basis}} \left(D^{(0)}_{kb} + \eta D^{(1)}_{kb}(t)\right)\left(D^{(0)}_{ji} + \eta D^{(1)}_{ji}(t)\right)\left(w_{ij,ak} - w_{ik,aj}\right) \\ &- \sum_{k}^{\text{basis}} \left(h_{kb} + \eta\Lambda_{kb}(t)\right)\left(D^{(0)}_{ak} + \eta D^{(1)}_{ak}(t)\right) \\ &- \sum_{kij}^{\text{basis}} \left(D^{(0)}_{ak} + \eta D^{(1)}_{ak}(t)\right)\left(D^{(0)}_{ji} + \eta D^{(1)}_{ji}(t)\right)\left(w_{ij,kb} - w_{ib,kj}\right) \; . \end{aligned} \tag{171}$$

This equation can be reduced to

$$\left\{\mathrm{i}\frac{\mathrm{d}}{\mathrm{d}t} - \epsilon_a + \epsilon_b\right\} D^{(1)}_{ab}(t) = \left(n_b - n_a\right)\left\{\Lambda_{ab}(t) + \sum_{ij}^{\text{basis}} D^{(1)}_{ji}(t)\left(w_{ij,ab} - w_{ib,aj}\right)\right\} \; . \tag{172}$$

The prefactor $n_b - n_a$ on the right side of this equation is responsible for the fact that the matrix $D^{(1)}$ only has entries for the pairs of indices $(b > N, a < N)$ and $(a > N, b < N)$. That means that for all $a, b \leq N$ the matrix D has the "frozen core" $D_{ab} = D^{(0)}_{ab} = \delta_{ab}$. Furthermore, for all $a, b > N$, D_{ab} remains zero. The overall structure of the matrix D is illustrated in Fig. 16.

With the assumption of a weak perturbation, one has derived the simplified equation (172). Hence, instead of solving the full system as in Eq. (168), one can also numerically solve Eq. (172) for the remaining $2Nn_{\mathrm{add}}$ indices α, β with the property $n_\beta - n_\alpha \neq 0$. However, one can even go further, making use of the structure of Eq. (172). In the following, this is explained in detail.

One starts by defining the multi-index $I = (\alpha, \beta)$ for the $2Nn_{\mathrm{add}}$ relevant combinations of α and β. Further, the inverse functions $\alpha(I)$ and $\beta(I)$ shall be given. With the additional definitions

$$A_{IK} = \left(n_{\beta(I)} - n_{\alpha(I)}\right)\left(w_{j(K)i(K),\alpha(I)\beta(I)} - w_{j(K)\beta(I),\alpha(I)i(K)}\right) + \left(\epsilon_{\alpha(I)} - \epsilon_{\beta(I)}\right)\delta_{KI} \tag{173}$$

and $g_I = \left(n_{\beta(I)} - n_{\alpha(I)}\right)\Lambda_I$, one can write

$$\mathrm{i}\frac{\mathrm{d}}{\mathrm{d}t}D^{(1)}_I = \sum_K A_{IK} D^{(1)}_K + g_I \tag{174}$$

instead of Eq. (172). Further, defining the vectors $\mathbf{d}$ with the elements $-\mathrm{i}D^{(1)}_I$ and $\mathbf{g}$ with the elements $-\mathrm{i}g_I$, one obtains the simple form

$$\frac{\mathrm{d}}{\mathrm{d}t}\mathbf{d}(t) = A\mathbf{d}(t) + \mathbf{g}(t) \; . \tag{175}$$

This is an inhomogeneous system of linear differential equations with constant coefficients. To find a general solution of this system, one first has to solve the corresponding homogeneous problem

$$\frac{\mathrm{d}}{\mathrm{d}t}\mathbf{d}_{\mathrm{h}}(t) = A\mathbf{d}_{\mathrm{h}}(t) \; . \tag{176}$$

A fundamental system for this differential equation is given by the matrix exponential $F(t) = \exp(tA)$. Instead of this, however, in practical situations, one calculates the fundamental system

$$F'(t) = S\exp(tJ) \; , \tag{177}$$

where $J = S^{-1}AS$ is the Jordan normal form. According to the variation of parameters, a solution to the inhomogeneous system is given by

$$\mathbf{d}_{\mathrm{p}}(t) = F(t)\int F^{-1}(t)\mathbf{g}(t)\,\mathrm{d}t \; . \tag{178}$$

Restricting the inhomogeneity to be of the type $\mathbf{g}(t) = \delta(t)\mathbf{q}$, the particular solution is simply given by $\mathbf{d}_{\mathrm{p}} = \mathbf{q}$. As a consequence, one can finally formulate the general solution

$$\mathbf{d}(t) = \sum_{I=1}^{2Nn_{\mathrm{add}}} \left(F'(t)\right)^{(I)} c_I + \mathbf{q} \; , \tag{179}$$

where $\left(F'(t)\right)^{(I)}$ is the I-th column of the fundamental system. The c_I are determined with respect to the initial condition $\mathbf{d}(t=0) = \mathbf{0}$, i. e., one has to solve the system of equations

$$\sum_{I=1}^{2Nn_{\mathrm{add}}} (S)^{(I)} c_I = -\mathbf{q} \; . \tag{180}$$

As for the systems in this work, the matrix A is diagonalizable, the Jordan normal form J is a diagonal matrix, which contains the eigenvalues of A. Consequently, all possible mode frequencies are

$$\omega_I = \Re(J_{II}) \; . \tag{181}$$

The frequencies corresponding to a specific mode are given for all indices I with the property $c_I \neq 0$.

In summary, a semi-analytical solution of the time-dependent Hartree-Fock problem has been found. With this solution, one can exactly reproduce the time-dependent behavior that one would obtain with a time propagation for a weak and rapid excitation process. The advantage of the method is that it can be applied to arbitrary excitation operators. Furthermore, it reveals *all* frequencies of a mode. Hence, it can be a valuable alternative to the sum rules. For the breathing mode, one specifies the inhomogeneity with $q_I = q_{ab} = \langle\phi_a|\hat{\mathbf{r}}^2|\phi_b\rangle$. The dipole mode (sloshing mode)—just as another example—is reproduced for $q_{ab} = \langle\phi_a|\hat{\mathbf{R}}|\phi_b\rangle$. In Sec. 7.1.1, this method is used for a supportive analysis of the results from time-dependent calculations. In principle, with this perturbative approach, time-dependent HF calculations become unnecessary unless one is interested in higher-order processes or the sizes of the involved matrices $2Nn_{\mathrm{add}} \times 2Nn_{\mathrm{add}}$ are too large for a diagonalization. However, in the latter case, one can expect that the time-dependent calculations are also quite costly.

6 Thomas-Fermi Theory

Although this work focuses on small systems, it is interesting to get an estimation for the behavior of larger systems. An appropriate tool for the investigation of large systems is the Thomas-Fermi (TF) approximation—a theory which was independently formulated by Thomas [110] and Fermi [111] to approximate the electronic density in an atom. Comprehensive overviews of the theory are given in Refs. [112, 113]. In Refs. [114, 115], it is shown that the approximation becomes exact for large atomic systems. Further, a systematic analysis on the effect of neglected correlations is found in Ref. [116]. Being a very simple theory, the Thomas-Fermi approximation enables one to quickly get a rough overview of some basic physical properties. In this section, an introduction to the theory is given for fermions in arbitrary dimensions. After that, some different applications for Coulomb interacting particles in one- and two-dimensional systems are explained.

6.1 Energy functional and Thomas-Fermi equation

In the following, N fermionic particles, e. g., electrons, are considered in a d-dimensional space. The extension of the whole system is restricted to a volume V. The goal is to describe all properties of the system with the particle density $n(\mathbf{r})$.

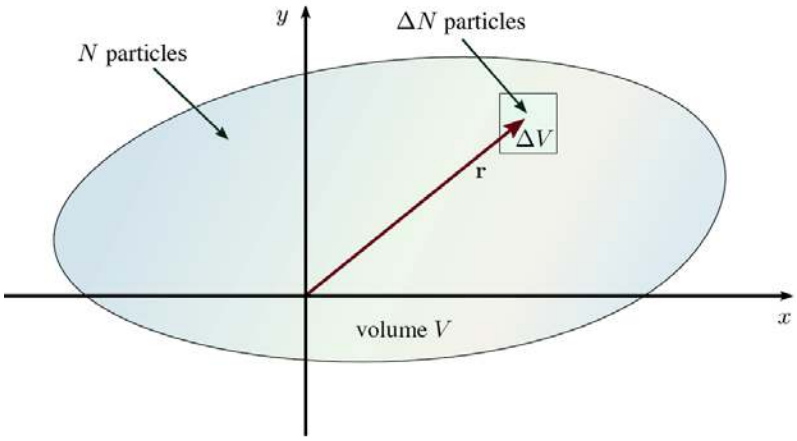

Fig. 17 Setting for the Thomas-Fermi approximation. A system of N particles extends over a volume V. In a small volume element ΔV, the particles have a uniform distribution. On the global scale, the density $n(\mathbf{r})$ may vary.

One starts with the concentration on a small volume element ΔV at the point $\mathbf{r}$, containing ΔN particles (see Fig. 17). Although the density $n(\mathbf{r})$ may vary in space, one approximates the local density by that of a homogeneous gas. This is a classical idea, requiring that the de Broglie wavelength has only a weak dependence on the spatial coordinate. It is assumed that the particles in ΔV have an energy E that is below the Fermi energy

$$E \leq E_{\mathrm{F}} = \frac{p_{\mathrm{F}}^2}{2} \,, \tag{182}$$

where p_F is the Fermi momentum, which may be different for each coordinate $\mathbf{r}$ outside the volume ΔV. This idea corresponds to the picture of a hypersphere in momentum space with the radius p_F, where the momenta of the particles must be within the hypersphere (see Fig. 18). The volume of such a hypersphere is given by

$$\Delta\tilde{V} = V_d p_\mathrm{F}^d \,, \tag{183}$$

where V_d is the volume of a d-dimensional unit hypersphere. The explicit values for V_d and the corresponding surfaces A_d are listed for $d = 1$, 2 and 3 in Table 6.1. With the phase space volume $\Delta\tilde{V}\Delta V$, one finds

$$\Delta N = \frac{2s+1}{(2\pi)^d}\Delta\tilde{V}\Delta V \,. \tag{184}$$

Here, one has made use of the quantum mechanical idea that the unit volume in the phase space is occupied by $(2s+1)$ particles[10]. In the limit of infinitely small volumes ΔV, one obtains the density

$$n(\mathbf{r}) = \frac{\Delta N}{\Delta V} = \frac{2s+1}{(2\pi)^d} V_d p_\mathrm{F}^d(\mathbf{r}) \,. \tag{185}$$

With this expression, one can calculate the kinetic energy density

$$t(\mathbf{r}) = \int_0^{p_\mathrm{F}} n(\mathbf{r})\frac{p^2}{2}\frac{A_d p^{d-1}}{V_d p_\mathrm{F}^d(\mathbf{r})}\,\mathrm{d}p = C_\mathrm{k}(d,s)n(\mathbf{r})^{(d+2)/d},$$

with the constant

$$C_\mathrm{k}(d,s) = \frac{2s+1}{(2\pi)^d}\frac{A_d}{2(d+2)}\left(\frac{1}{2s+1}\frac{(2\pi)^d}{V_d}\right)^{(d+2)/d} \,.$$

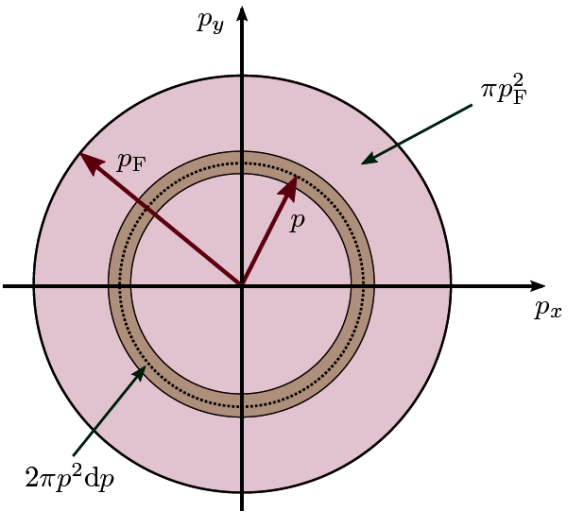

Fig. 18 Fermi hypersphere in two dimensions with the volume πp_F^2 and a Fermi surface of equal energy, with the corresponding momentum p.

Table 1 Volumes V_d and surfaces A_d of d-dimensional unit hyperspheres.

d	V_d	A_d
1	2	2
2	π	2π
3	$4\pi/3$	4π

[10] In SI units, the unit volume is $(2\pi\hbar)^d$.

For probably the most prominent example of electrons in 3D with $s = 1/2$, the constant is

$$C_{\rm k}(3, 1/2) = \frac{6\pi^2}{5}\left(\frac{3}{8\pi}\right)^{2/3} .$$

Hence, for the mean kinetic energy and mean potential (trap) energies in Thomas-Fermi approximation we have

$$\langle\hat{T}\rangle = C_{\rm k}(d, s)\int n(\mathbf{r})^{(d+2)/d}\,{\rm d}\mathbf{r} , \qquad \text{and} \qquad \langle\hat{V}\rangle = \int v(\mathbf{r})n(\mathbf{r})\,{\rm d}\mathbf{r} .$$

The mean interaction energy is taken into account on the Hartree level,

$$\langle\hat{W}\rangle = \frac{\lambda}{2}\int\int \frac{n(\mathbf{r})n(\mathbf{r}')}{|\mathbf{r}-\mathbf{r}'|^{\alpha}}\,{\rm d}\mathbf{r}\,{\rm d}\mathbf{r}' .$$

This is even simpler than the interaction term in Hartree-Fock approximation, where also exchange effects are respected. Further, obviously, the interaction in Hartree approximation lacks all correlation effects. The goal of the approximation is to find the density $n(\mathbf{r})$ which minimizes the energy functional

$$E[n] = \langle\hat{T}\rangle + \langle\hat{V}\rangle + \langle\hat{W}\rangle \tag{186}$$

under the normalization constraint, $\int n(\mathbf{r}){\rm d}\mathbf{r} = N$. In principle, one can try to find the density directly by inserting trial densities into the energy functional. In fact below, for 2D systems, we will proceed this way However, another systematic way to find the density is to introduce a Lagrange multiplier μ and set the variational condition

$$\delta(E - \mu N) = 0 . \tag{187}$$

Then, one arrives at the Thomas-Fermi equation

$$\frac{d+2}{d}C_{\rm k}(d, s)n(\mathbf{r})^{2/d} + v(\mathbf{r}) + \lambda\int \frac{n(\mathbf{r}')}{|\mathbf{r}-\mathbf{r}'|^{\alpha}}\,{\rm d}\mathbf{r}' = \mu . \tag{188}$$

With Eq. (187), one recognizes

$$\frac{\partial E}{\partial N} = \mu , \tag{189}$$

that is, μ can be interpreted as the chemical potential of the system. Compared to Eq. (186), this equation has the advantage that due to the variation, one integral was canceled in each term. But still, one has to search for a pair of the density and a corresponding chemical potential. This can be a difficult task, because Eq. (188) is an integral equation. For 3D systems with Coulomb interaction, it is therefore a typical procedure to transform Eq. (188) into a differential equation. For that purpose, one introduces the potential

$$u(\mathbf{r}) = \lambda\int \frac{n(\mathbf{r}')}{|\mathbf{r}-\mathbf{r}'|}\,{\rm d}\mathbf{r}', \tag{190}$$

which has to satisfy Poisson's equation $\Delta u(\mathbf{r}) = -4\pi\lambda n(\mathbf{r})$. For other dimensions and interactions, such a transformation can be impossible. A discussion on the treatment of the dimensionality is to be found in Ref. [112]. In the following sections, the specific methods for the problems in this work are presented.

6.2 Solution for one-dimensional systems

For a 1D system with spin-polarized Coulomb-interacting particles, the Thomas-Fermi equation (188) is solved on a spatial grid. This requires again that the interaction potential is screened. Hence, the equation to be solved reads

$$3C_{\rm k}(1, 0)n(r)^2 + \frac{1}{2}r^2 + \lambda\int \frac{n(r')}{\left((r-r')^2+\kappa^2\right)^{1/2}}{\rm d}r' = \mu . \tag{191}$$

The following scheme is applied to solve this equation self-consistently:

1. Initial guess of the density $n(r)$ with respect to the normalization condition.
2. Calculation of the Hartree terms with the current density $n(r)$,

$$w(r) = \lambda \int \frac{n(r')}{[(r-r')^2+\kappa^2]^{1/2}} \mathrm{d}r', \quad \text{on the whole grid.}$$

3. Determination of the new chemical potential μ and a new density $\tilde{n}(r)$, according to

$$\tilde{n}(r) = \frac{1}{\sqrt{3C_{\mathrm{k}}(1,0)}} \left\{ \mu - \frac{1}{2}r^2 - w(r) \right\}^{1/2} , \tag{192}$$

   where μ ensures that the density is normalized. Further, one must take into account that the density $\tilde{n}(r)$ is only non-zero for $\mu - \frac{1}{2}r^2 - w(r) > 0$.
4. Return to step 2 with $n(r) = \tilde{n}(r)$ until a given stopping criterion is fulfilled.
5. Calculation of all necessary observables.

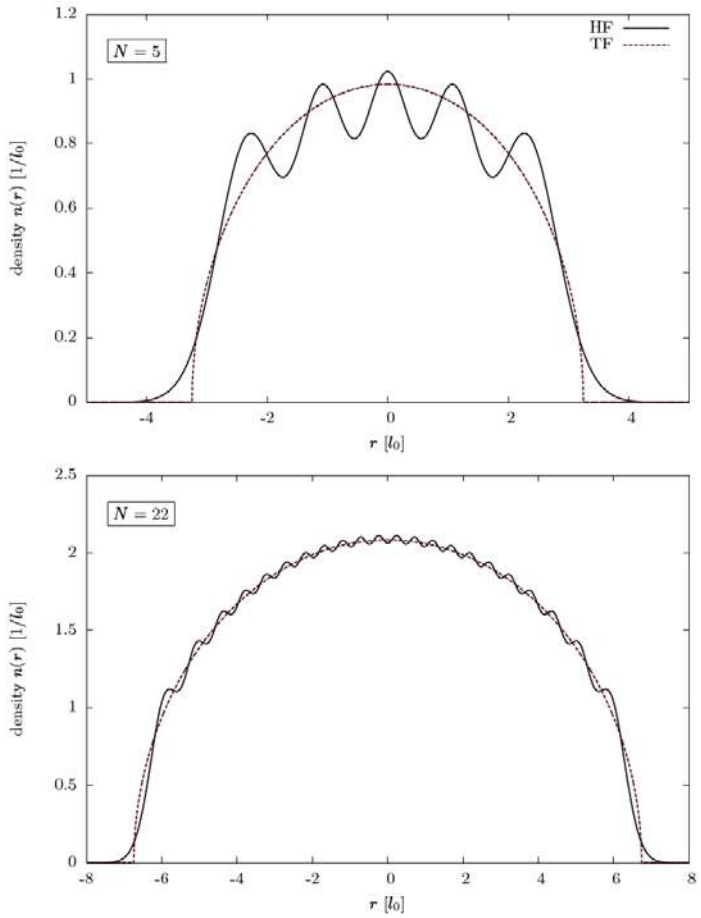

Fig. 19 Comparison of the densities in Hartree-Fock and Thomas-Fermi approximation for 1D systems with Coulomb interaction, at $\lambda = 0.1$ with the particle numbers $N = 5$ (top) and $N = 22$ (bottom). The oscillations of the HF density (and the exact density) are reduced with increasing particle number.

Of course, it cannot be guaranteed that the density converges. A proper choice of the initial density is crucial for the convergence. For the results in this work, the following scheme was applied:

- Choice of a particle number N and definition of a series $\lambda_1 < \lambda_2 < \ldots$, starting with a very small initial value λ_1. The difference between the successive values λ_i and λ_{i+1} should be small.
- First calculation with λ_1. The initial guess for the density is that of a non-interacting system,

$$n(r) = \frac{1}{\sqrt{3C_{\mathrm{k}}(1,0)}} \left\{ \mu - \frac{1}{2} r^2 \right\}^{1/2} ,$$

  with $\mu = N$ [117]. This density has the shape of a semicircle.
- For the subsequent calculations with λ_i, one starts with the final densities from the calculations with λ_{i-1}.

In this work, the calculations were restricted to the positive coordinate axis, as the problem is symmetric. Typically, satisfactory results were obtained with a grid size around $3\sqrt{N}$ and 5000 grid points.

Figure 19 provides a first visual impression of the density in TF approximation in comparison with the corresponding Hartree-Fock result. One can see that the oscillations are not reproduced in the TF model. However, for large particle numbers, these oscillations tend to vanish. This is one reason why TF is expected to become more accurate with increasing N.

6.3 Solution for two-dimensional systems

In Ref. [118], the Thomas-Fermi equation is exactly solved for fermions in a 2D trap with logarithmic interaction. In this work, maintaining the Coulomb interaction, the energy functional (186) is minimized directly. The spin is set to $s = 1/2$. According to Ref. [119], it is assumed that the density is radial-symmetric and has the shape of an inverted parabola,

$$n(\mathbf{r}) = n(r) = \frac{1}{2\pi\gamma}(r_0^2 - r^2) \tag{193}$$

with the variational parameter γ. For the non-interacting system, this yields the exact density profile. The ansatz has the advantage that the interaction energy can be calculated analytically [119],

$$\langle \hat{W} \rangle = \lambda \frac{512}{315} \frac{\sqrt{2}}{\pi\gamma^{1/4}} N^{7/4} . \tag{194}$$

For the mean kinetic an potential (trap) energy, one obtains, respectively,

$$\langle \hat{T} \rangle = \frac{1}{3} N^{3/2} \frac{1}{\gamma^{1/2}} , \qquad \langle \hat{V} \rangle = \frac{1}{3} N^{3/2} \gamma^{1/2} .$$

Hence, in order to minimize the functional $E[n]$, one only has to find the parameter γ. This is a very easy task, which, for example, can be accomplished with the golden section search [120]. Finally, we mention recent attempts to further improve the Thomas-Fermi model [121] that might be helpful for obtaining more accurate results for the breathing frequency of large Fermi systems in the future.

7 Results for the Breathing Frequency of 1D Systems

The first many-body results shown in this work are for 1D systems. Although the real space is always three-dimensional, there are some physical situations that can be treated as effective 1D systems, see, e. g., Refs. [35, 36, 122, 123]. Offering a drastic computational simplification, the 1D system is also interesting from a theoretical point of view, as it can be used to quickly test diverse numerical methods. In this section, the results from both time-dependent and time-independent methods are applied. A major goal is to show that the presented equilibrium methods can be used for an accurate description of the collective monopole mode. The focus will

be on an overview on results for Coulomb-interacting fermions that have been presented in Ref. [41]. Beyond that, some results for dipolar fermions are presented. However, quite unlike Coulomb systems, the numerical treatment of the 1D dipole system turns out to be a difficult problem, where the standard Hartree-Fock procedure fails.

Before presenting the results, some numerical details are mentioned. To treat the singularity in the Coulomb/dipole potential, the potential is screened, according to

$$w(|\mathbf{r}_i - \mathbf{r}_j|) = \frac{\lambda}{\left\{(\mathbf{r}_i - \mathbf{r}_j)^2 + \kappa^2\right\}^{\alpha/2}} \ . \tag{195}$$

If not stated otherwise, the parameter κ is set to 0.1. Since only spin-polarized particles are considered, one does not have to expect a non-monotonic λ-dependence as described in Sec. 2.4.1. The main methods used for the results in this section are the Hartree-Fock (HF) method and its time-dependent extension (TDHF). The single-particle basis for the HF ground-state calculations is always the FEDVR basis with sizes in the range between $n_\mathrm{b} \approx 120$ and 2500. Time-dependent calculations of the single-particle density matrix were performed in the FEDVR basis as well as in the Hartree-Fock basis. In order to estimate the error of the HF approximation, results from the configuration interaction (CI) method are also shown. The breathing frequencies were determined with an exact diagonalization of the ground-state Hamiltonian, followed by an evaluation of the eigenvalue spectrum. Furthermore, several time-dependent CI calculations were performed, allowing to compare the TDHF spectra to exact ones. The single-particle basis for the CI calculations is always the 1D harmonic oscillator basis. For two particles with Coulomb interaction, usually $n_\mathrm{b} \approx 15$ basis functions are sufficient. For larger particle numbers, the size of the single-particle basis is chosen in a way that the total number of N-particle basis functions, n_s, does not exceed 10000.

7.1 Fermions with Coulomb interaction

We start with spin-polarized Coulomb-interacting fermions, e. g., electrons. This system is used as a test for most methods described in the following and we, therefore, present a broad overview of the relevant characteristics. We first present results from time-dependent calculations which will serve to test and verify the equilibrium methods that will be used in the following.

7.1.1 Time-dependent results

Extensive computations for up to 20 particles with coupling parameters $\lambda = 0.1$, 0.3, and 1 were performed to study the time-dependent reaction to a monopole-type excitation [41]. In time-dependent calculations, one cannot use the idealized instantaneous excitation with a δ-like perturbation. Instead, the excitation is turned on at $t = 0$ and turned off again at $t_\mathrm{exc} > 0$. This time interval is chosen very short, usually on the order of the time step of the integrator. To guarantee a monopole-type excitation we employ a short reduction of the trap frequency [56]. Then the Hamiltonian takes the form

$$\hat{H}(t) = \hat{H}_0 - \eta f(t) \hat{V} \ , \quad \text{where} \quad f(t) := \begin{cases} 1, & 0 \le t \le t_\mathrm{exc} \\ 0, & \text{else} \end{cases}$$

has been defined. For the excitation strength, η, we use very small positive values on the order of 0.01. A typical time series of the potential trap energy $\langle \hat{V}(t) \rangle$ is shown in Fig. 20. As expected, the beating of two sinusoids with the frequencies ω_rel and ω_cm is observed. The small value of η guarantees that there are only weak oscillations around the initial value and no higher harmonics are being excited.

In order to determine the breathing frequencies, the spectra of the time-dependent quantities $\langle \hat{V} \rangle$ are evaluated for each parameter set. To uncover peaks with small spectral weights, the spectra are calculated, by multiplying the time-dependent quantities with a Blackman function. Further, to achieve a high resolution in frequency space, large propagation times t_prop are required. Performing the computations in the Hartree-Fock basis on one CPU, one can achieve propagation times $t_\mathrm{prop} \approx 5000\,\Omega^{-1}$ in several hours, which usually leads to a sufficiently high accuracy.

To provide a first visual impression, Fig. 21 shows the relevant parts of the monopole spectra from TDHF calculations for different coupling strengths and particle numbers. As expected, each spectrum shows one peak, representing the relative frequency $\omega_{\rm rel}$, and another one, representing the center-of-mass frequency $\omega_{\rm cm}$. Further, the weights of the $\omega_{\rm cm}$ peaks do not depend on the particle number, in agreement with our theory, cf. Sec. 2. However, for $\lambda = 0.3$, one can already notice that this analytical fact is slightly violated in the Hartree-Fock approximation, and the effect increases with growing coupling parameter. For $\lambda = 1$, for example, the $\omega_{\rm cm}$ peak already shows up around $2.04\,\Omega$ in the case of two particles. However, another small peak appears close to the expected value $2\,\Omega$, which can be seen in Fig. 22. Despite the fact that the small peak has the wrong spectral weight, one can also vary η and observe how the peak heights change. As the figure shows, only the leftmost and the rightmost peaks scale down linearly with η. The peaks close to $2\,\Omega$, by contrast, scale down quadratically with η. However, in the sense of time-dependent perturbation theory, described in Sec. 2.1.3, only the linear terms are relevant for the breathing mode. This example should demonstrate that the spectra have to be analyzed carefully and that the excitation strength must be very weak.

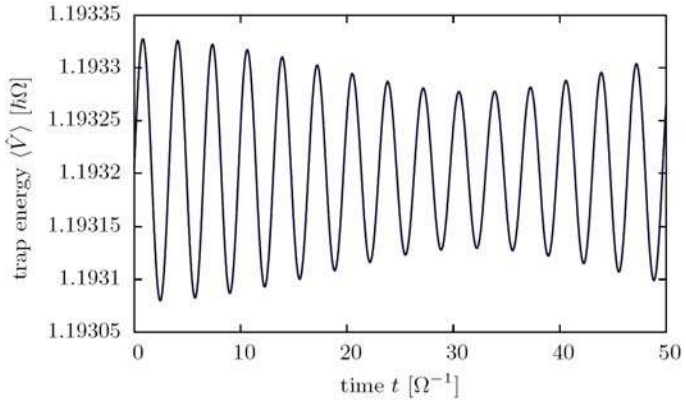

Fig. 20 Exemplary time series of the potential (trap) energy for two particles with Coulomb interaction and coupling strength $\lambda = 1$. The waveform clearly shows a superposition of two sinusoids, resulting from the breathing frequencies $\omega_{\rm rel}$ and $\omega_{\rm cm}$, respectively. The excitation time for this calculation, $t_{\rm exc} = 0.01$, is much smaller than the relevant oscillation periods assuring excitation of a broad spectrum.

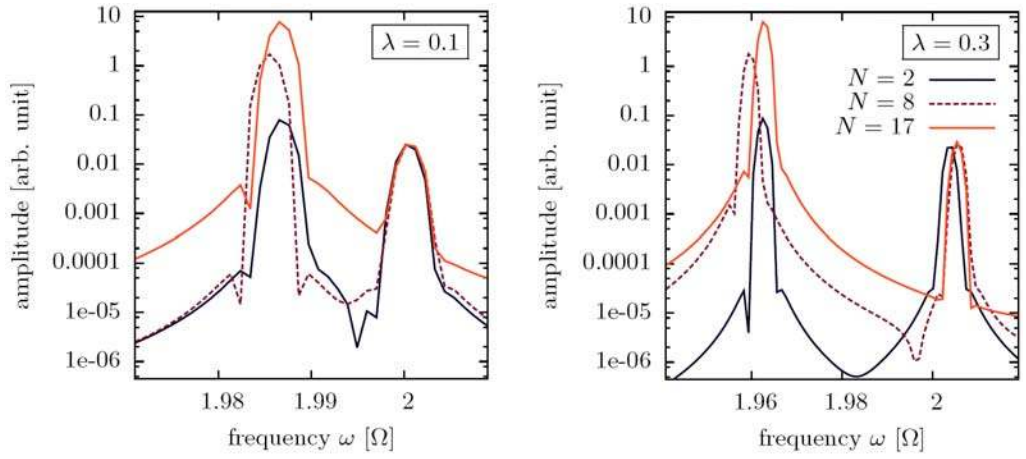

Fig. 21 Monopole excitation spectra for 2, 8 and 17 particles for the coupling strengths $\lambda = 0.1$ (left) and $\lambda = 0.3$ (right) [41]. The spectra show the expected peaks for the breathing frequencies $\omega_{\rm rel}$ (left peaks) and $\omega_{\rm cm} = 2\,\Omega$ (right peaks). The data is taken from TDHF calculations in the HF basis with $t_{\rm prop} = 6000\,\Omega^{-1}$ and $\eta = 0.001$.

To fully understand the spectra, one should also note the higher frequencies. For two particles, their occurrence has already been predicted quantitatively in Sec. 2.4.1. In Fig. 23, the spectrum is shown around the breathing

frequencies and the nearest higher spectral features. The figure shows both the spectra of TDHF and time-dependent CI (TDCI) calculations with the same parameter sets ($N = 2$, $\lambda = 1$) and a very small excitation strength. As expected, the CI calculations exactly represent the breathing frequencies, in good agreement with the predictions in Sec. 2.4.1. Especially the center-of-mass peak appears on the right position $2\,\Omega$. Regarding the leftmost peaks, one notices that TDHF produces the frequency ω_{rel} quite accurately. Similarly like the value for ω_{cm}, the first possible higher TDHF frequency deviates from the exact value by $\sim 0.05\,\Omega$. Further, TDHF even produces a peak around $4.05\,\Omega$ in first order of η. This peak probably represents a higher harmonic of the center-of-mass mode. However, it can be shown analytically that in first-order perturbation theory, the center-of-mass subsystem only produces one frequency $2\,\Omega$. This analytical fact is also confirmed by the exact TDCI results, which do not show an equivalent peak. One can conclude that weak excitations do not produce completely the same physics in TDHF and exact methods. Just for comparison, the figure also shows the corresponding spectrum obtained by Bauch *et al.* [56] with an exact solution of the TDSE. On the one hand, this is to show the progress in the spectral accuracy. On the other hand, this curve shows once more—as it was produced with the excitation strength $(\eta = 1)$— that processes of higher order can occur: The peak at $4\,\Omega$ represents a two-fold transition in the center-of-mass system, and the peak near $3.9\,\Omega$ represents an addition of the transition $2\,\Omega$ in the center-of-mass system and the frequency $\omega_{\mathrm{rel}} \approx 1.9\,\Omega$ in the relative system. Loosely speaking, this is explained by the fact that in second-order perturbation theory, it is allowed to add up the transitions from the first order.

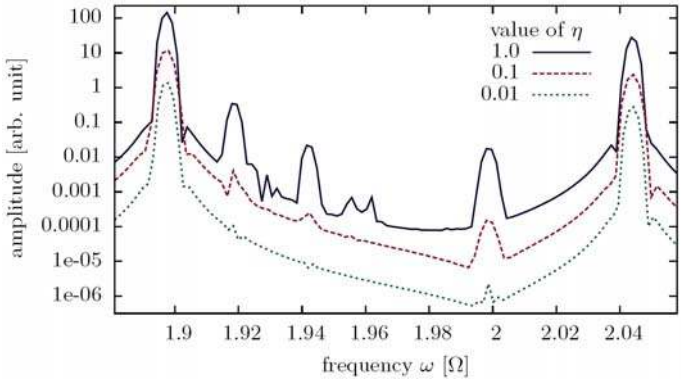

Fig. 22 Vanishing of higher-order peaks in the spectrum with decreasing excitation strength η [41]. The peaks close to $2\,\Omega$ do not represent the center-of-mass frequency ω_{cm}, because they can be suppressed with η. The data were obtained by TDHF calculations in the HF basis with the parameters $N = 2$, $\lambda = 1$.

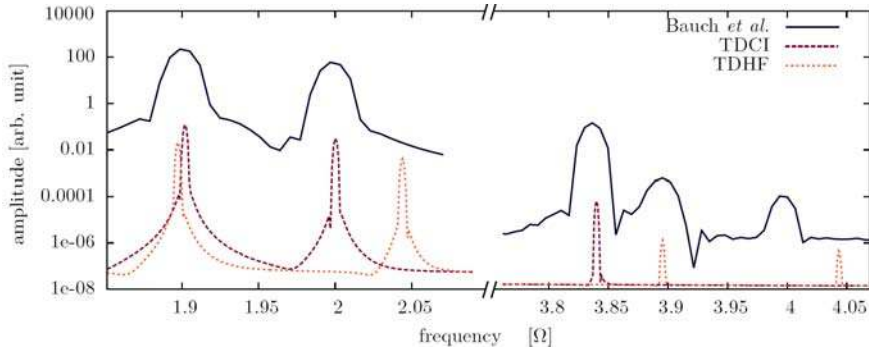

Fig. 23 Comparison of the spectra from different time-dependent methods around the breathing frequencies ω_{rel} and ω_{cm} (left), and the first occurrence of higher frequencies (right) [41]. The relevant parameters are $N = 2$, $\lambda = 1$ and $\eta = 0.0001$. The emphasis is on the difference between the TDCI and the TDHF results. The curve by Bauch *et al.* [56] is just for further comparison, as it was obtained with the large excitation strength $\eta = 1$ and a relatively short propagation time.

In Sec. 5.2.1, it was shown how to solve the time-dependent Hartree-Fock equations with perturbation theory (TDHF+PT). As the excitation strength has been kept weak in the TDHF calculations, it should be possible to

compare with the frequencies obtained by the perturbative solution. To do so, Fig. 24 shows the λ-dependent monopole frequencies occurring in the first order of TDHF+PT. Further, as the TDHF+PT solution is not limited to monopole excitations, the figure also shows the frequency of the sloshing mode, ω_{slosh}, which is known to have the universal value $1\,\Omega$ (see Sec. 2.2.2). The reason to plot this frequency is the following: On the one hand, it is a good test for the correctness of the implementation and the applicability of the theory. On the other hand, one can observe that the numerical accuracy gets lower, the higher the excitation energies are. This is expressed in false increases of the frequencies, starting in certain coupling regimes. The calculations have been performed with 13 Hartree-Fock basis functions. For coupling parameters up to $\lambda \sim 5$, this is sufficient for an accurate description of the sloshing frequency and the relative monopole frequency ω_{rel}. The next frequency, ω_{cm}, is already visibly inaccurate at the coupling $\lambda = 1$. To be precise, it attains the value $2.04\,\Omega$, as has also been observed in the time-dependent calculations. As this frequency can be traced back to the correct value $2\,\Omega$ with decreasing λ, another hint is given that the problematic peaks close to $2.04\,\Omega$ in the TDHF examples actually represent the center-of-mass mode.

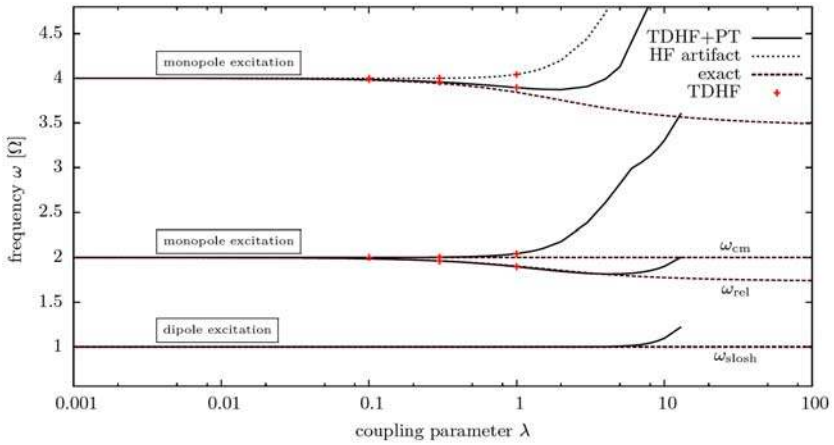

Fig. 24 λ-dependent prediction of the first monopole-allowed frequencies for two particles. The frequencies were obtained with a perturbative solution of the TDHF equations (TDHF+PT). To show the capabilities of the method, the sloshing frequency ω_{slosh} with the theoretical value $1\,\Omega$ is also plotted. The exact values calculated in Secs. 2.4.1 and 2.2 are shown for comparison.

Having analyzed the various features of the spectra, one can finally concentrate on the investigation of the relative frequency ω_{rel}. In Fig. 25, a more detailed view on the N-dependence is provided for the selected coupling strength $\lambda = 1$. First, one notices again the qualitatively wrong behavior of the ω_{cm} peaks. Not only is the frequency too large, the peaks also exhibit an unphysical N-dependence. Second, the peaks of the relative frequencies are clearly dependent on the particle number. This dependence is expressed in a monotonic decrease of the breathing frequency from two up to five particles, followed by a monotonic increase for larger particle numbers. Hence, the breathing frequency attains a minimum for five particles. Contrary to the unphysical N-dependence of the frequency ω_{cm}, this behavior is not caused by numerical problems that arise with a growing coupling parameter. As Fig. 26 shows, the same characteristic N-dependence shows up for the different coupling strengths $\lambda = 0.1$, 0.3 and 1. For comparison, the results from exact diagonalizations (CI) are also plotted in the figure. For small coupling parameters like $\lambda = 0.1$, one notices that the overall agreement between CI and TDHF is quite good. Nevertheless, the CI frequencies have their minimum for six instead of five particles, but the difference between the frequencies for both particle numbers is very small. For further comparison, the results from TDHF+PT are also plotted in the case $\lambda = 0.1$. These frequencies attain a minimum for six particles, just like the CI values. Since the TDHF+PT calculations do not demand as much computational effort as the corresponding time propagations they could be obtained with a relatively large single-particle-basis. Furthermore, the accuracy of the results is not limited by the resolution in the frequency space. As the TDHF+PT results agree well with the exact CI solutions, one can assume that the exact position of the minimum actually occurs for six particles. Nevertheless, despite the small numerical errors, one can state that the TDHF solutions are capable to reproduce the correct trend of the N-dependence.

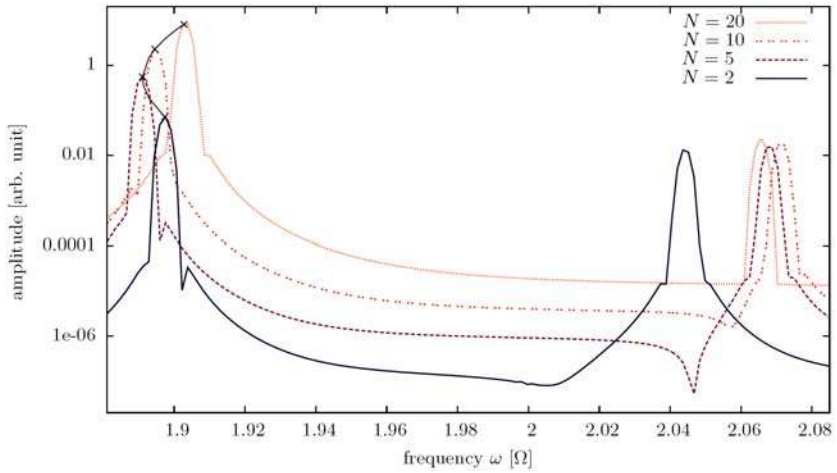

Fig. 25 Dependence of the TDHF spectrum on the particle number N [41]. The coupling strength is $\lambda = 1$. The relative mode (left peaks) has a characteristic N-dependence, which is trustworthy, as it is also apparent for very weak couplings. As a guide for the eye, the peak positions for all particle numbers $N \leq 20$ are highlighted by a bold line (with crosses for $N = 2$, 5, 10, 20). The center-of-mass mode frequency (right peaks), however, deviates from the analytical prediction $\omega_{\rm cm} = 2\,\Omega$.

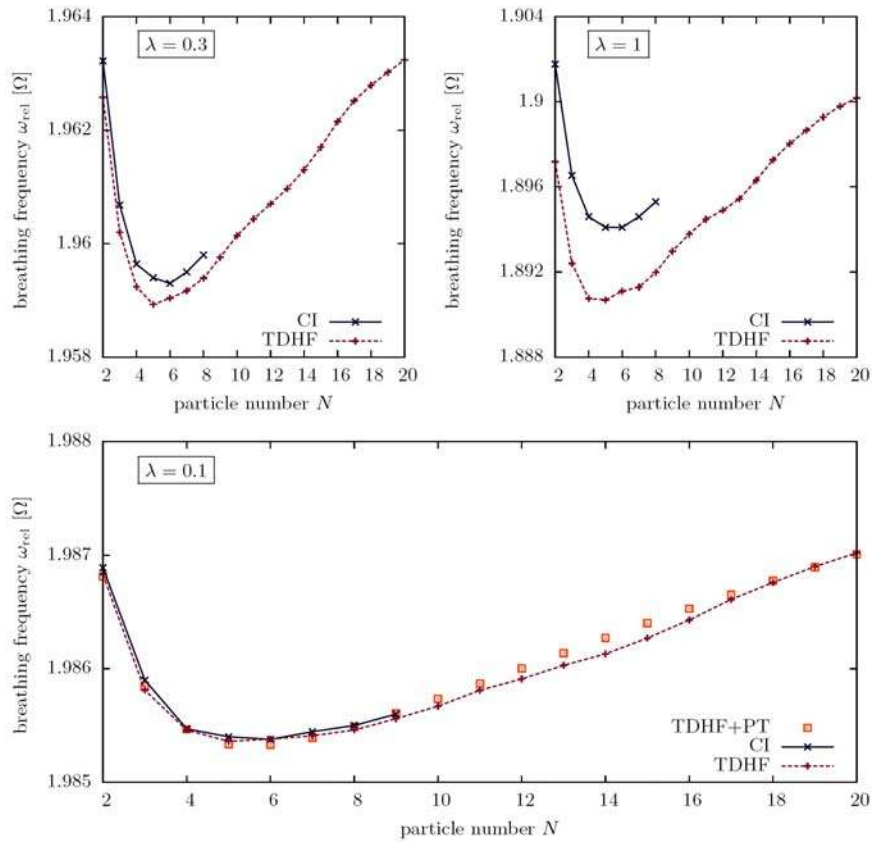

Fig. 26 N-dependence of the breathing frequencies for the selected coupling parameters $\lambda = 0.1$, 0.3 and 1. The results from TDHF calculations (in the FEDVR basis) are compared with the results from exact diagonalizations (CI). For $\lambda = 0.1$, the perturbative solution of the TDHF equations is also shown (TDHF+PT). While the TDHF frequencies attain a minimum for five particles, in the CI and TDHF+PT calculations, the minima show up for six particles.

All in all, it has been shown that time-dependent Hartree-Fock calculations allow for a relatively accurate determination of the breathing frequencies for coupling strengths up to $\lambda = 1$ and particle numbers up to $N = 20$. The various features of the spectra could be identified. Further, the TDHF equations need not be solved with a propagation. The solution based on time-dependent perturbation theory yields the same or—due to the possibility to increase the basis sets—even more accurate results. The calculations reveal the unexpected result that for each coupling parameter, the frequency $\omega_{\rm rel}$ has a minimum for six particles. In the following, equilibrium methods are used to check the position of the minimum and to investigate the trend of increasing frequencies for larger particle numbers.

7.1.2 Application of equilibrium methods to the breathing fequency

For a further analysis, the formulas presented in Sec. 3 are applied. First of all, it is of interest to see how the sum rule formulas are able to reproduce the N-dependence of the breathing frequencies. In Fig. 27, the results for the improved sum rule formula $\mathrm{sr}^*(1,-1)$ are compared to the CI and TDHF results. The input data for the sum rules is taken from static Hartree-Fock calculations. One notices that the results with the sum rules are always closer to the exact CI results than the TDHF results. This can be explained by the large single-particle basis that could be used for the sum rule calculations. Furthermore, the minimum coincides with the CI results for $N = 6$ particles. All in all, the exact results and the sum rules are in good agreement. The most important error in the sum rule results is due to the Hartree-Fock approximation. This error, which increases with λ, is also responsible for the fact that the frequencies are not necessarily above the exact CI values.

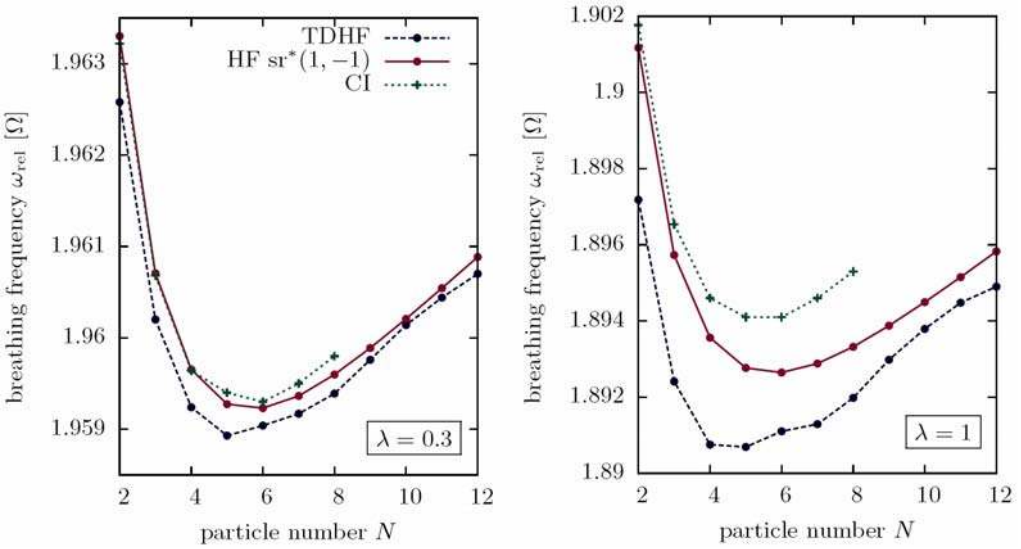

Fig. 27 Results for the N-dependence of the breathing frequencies for the coupling strengths $\lambda = 0.3$ and 1. The results with the sum rule formulas perform better than those from the TDHF calculations. With the sum rules, one can reproduce the minimum for six particles.

For a further comparison, Fig. 28 shows the N-dependent breathing frequencies for different sum rule formulas. As expected, the frequencies for $\mathrm{sr}^*(3,1)$ are always above the values for $\mathrm{sr}^*(1,-1)$. Moreover, the curves reveal that the correct behavior for small systems is only captured by the improved formulas. With the formula $\mathrm{sr}(3,1)$, the minimum occurs for seven particles instead of six. Already for 25 particles, however, the differences between sr and sr* are nearly vanished.

Finally, to provide an overview of the dependence on the coupling parameter, the λ-dependent breathing frequencies are plotted for selected particle numbers in Fig. 29. As expected, the frequencies start at the ideal value $2\,\Omega$, followed by a monotonic decrease with λ. Furthermore, the curves $\omega_{\rm rel}(\lambda, N)$ do not intersect. Comparing to the exact curve for $N = 2$, and noticing the non-monotonic behavior for coupling parameters $\lambda \geq 3$, the figure also demonstrates the limitations of the Hartree-Fock method. To go beyond those intermediate coupling regimes, more sophisticated methods are required to incorporate correlation effects.

Figure 29 shows first results for relatively large particle numbers. It turns out that the breathing frequencies become more ideal with growing N. In the next subsection, a more detailed analysis of this phenomenon is provided.

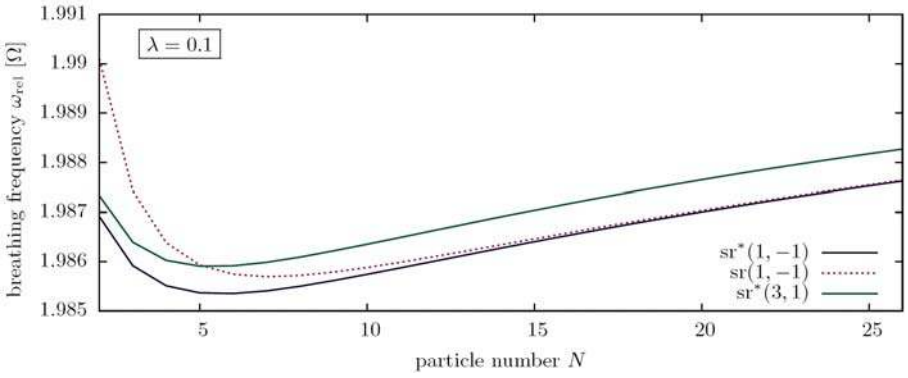

Fig. 28 Comparison of different sum rule formulas. For small particle numbers, the improved sum rule formula $\mathrm{sr}^*(1,-1)$ captures the correct behavior, while the original formula $\mathrm{sr}(1,-1)$ fails to do so. The results were obtained with HF calculations.

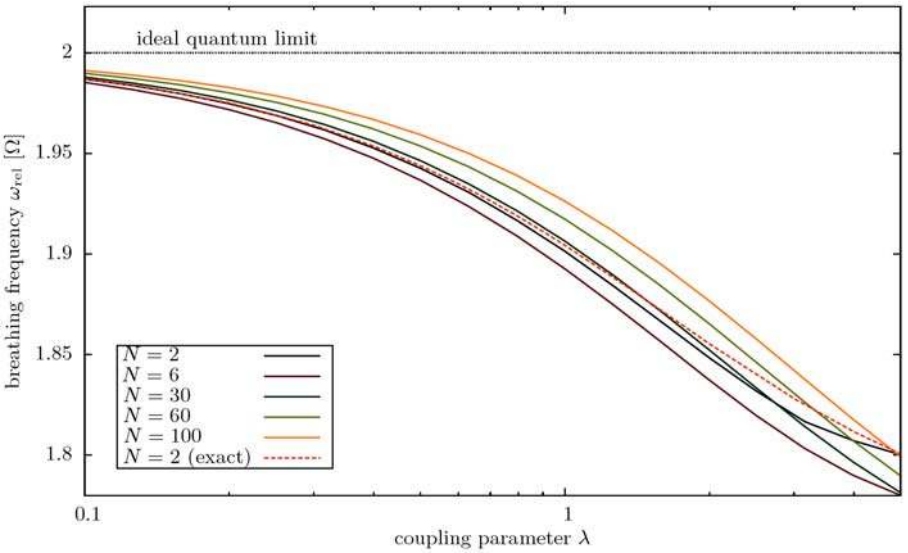

Fig. 29 Dependence of the breathing frequency on the coupling parameter for different particle numbers. The results were obtained in HF calculations with the estimator $\mathrm{sr}^*(1,-1)$. Around $\lambda \sim 3$, the results become inaccurate due to an increase of neglected correlation effects.

7.1.3 Large systems

So far, the results have been restricted to rather small systems. It could be observed that beyond the minimum, the breathing frequencies increase with the particle number. To answer the question, how this trend carries on for larger systems, extensive Hartree-Fock and Thomas-Fermi calculations were performed. Figure 30 shows the breathing frequencies for up to 620 particles with the selected coupling strength $\lambda = 0.1$. Both the Hartree-Fock and the Thomas-Fermi ground-state calculations were connected with the sum rule formulas. For computational convenience, the Thomas-Fermi results were used in combination with the formula $\mathrm{sr}^*(3,1)$ instead of $\mathrm{sr}^*(1,-1)$. The figure confirms the trend that the frequencies increase monotonically with N, but it is still impossible to see the limiting behavior. As a test for the theories, it is also important to compare HF and TF. It turns out that it

takes several hundred particles until the difference between both theories is veiled by the resolution of the image. Especially the non-monotonic behavior for small systems cannot be reproduced by the TF theory.

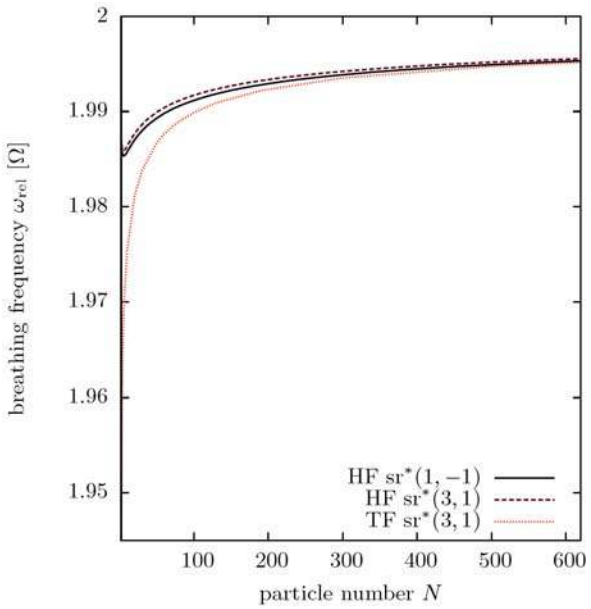

Fig. 30 Investigation of the breathing frequency for up to 620 particles with the coupling strength $\lambda = 0.1$. The values were obtained with the time-independent Hartree-Fock and Thomas-Fermi methods combined with the sum rules. In the limit of large particle numbers, both methods yield the same results.

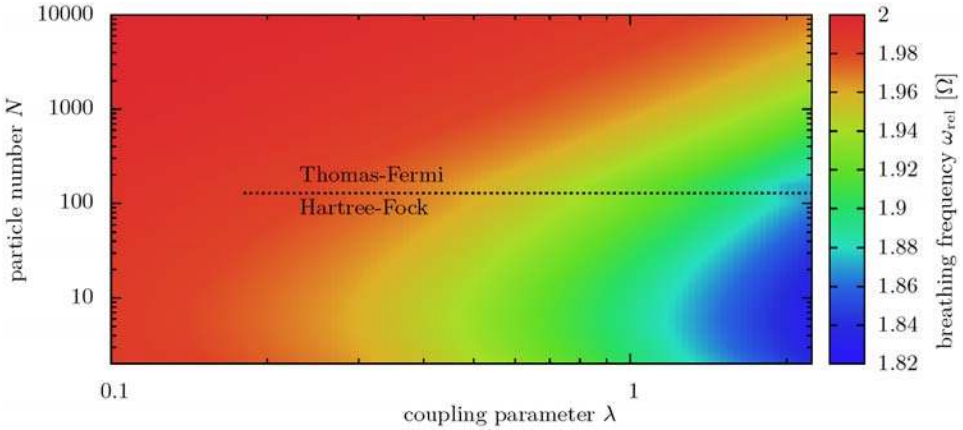

Fig. 31 Dependence of the breathing frequencies on the coupling parameter and the particle number [125]. The results were obtained in HF calculations for $N \leq 100$ (with sr$^*(1,-1)$) and TF calculations for larger particle numbers (with sr$^*(3,1)$). The transition between both results is relatively smooth, but it is still visible. To achieve a smooth color gradient, the frequency data were post-processed with an interpolation in the (λ, N)-plane.

For a schematic overview of the breathing frequency, Fig. 31 pictures $\omega_{\rm rel}$ in the (λ, N)-plane. In the figure, the results from HF and TF are joint, which explains a small step around 100 particles. However, both results provide a clear picture of the physical situation. Whenever one fixes an arbitrary coupling parameter, one can increase the particle number to reach the ideal quantum limit. At the same time, if one fixes the particle number, one reaches the classical limit by increasing λ. Furthermore, as indicated by equal colors in the figure, there exist characterizing lines with equal breathing frequencies in the (λ, N)-plane. At last, it is mentioned that one can give a proof for the large-N behavior in terms of the Thomas-Fermi approximation. According to Sec. 6.2, one has to find a self-consistent solution for the density

$$n(r) = \frac{1}{\sqrt{3C_{\rm k}(1,0)}} \left\{ \mu - \frac{1}{2} r^2 - w(r) \right\}^{1/2} . \tag{196}$$

Inserting the semicircle-shaped density of the non-interacting system, one finds that for each coupling parameter, one can always increase N to a very large value to ensure that the density-dependent expression $w(r)$ can be neglected. Hence, the system becomes effectively non-interacting, and the breathing frequency attains the ideal value $\omega_{\mathrm{rel}} = 2\,\Omega$.

7.1.4 Influence of the screening parameter

It is still an unanswered question how important the influence of the screening parameter κ is for the observed phenomena. To answer that question, the screening was varied in Hartree-Fock calculations with different system parameters. The results for the coupling parameter $\lambda = 0.1$ and screening parameters from $\kappa = 0.6$ to 0.001 are shown in Fig. 32. One finds that the breathing frequencies are nearly converged for $\kappa = 0.1$. Furthermore, the described non-monotonic behavior does not change for smaller values of κ. Especially the minimum for six particles attains the fixed position $N = 6$. Although there are still some small differences between the results for $\kappa = 0.1$ and the results for $\kappa = 0.01$, the value $\kappa = 0.1$ was preferred for numerical reasons and a better comparability with the results from previous publications.

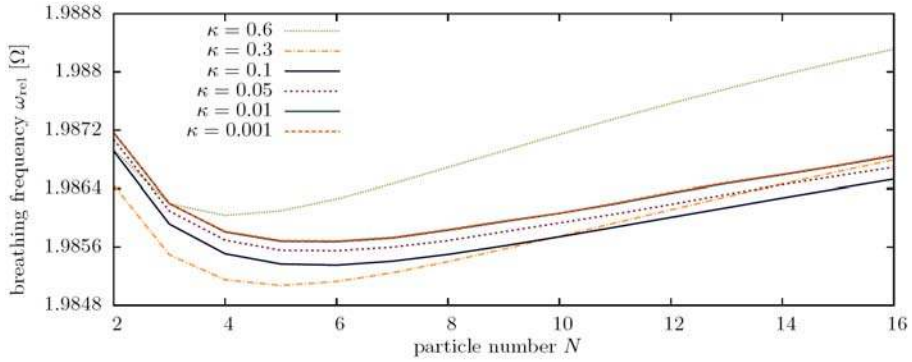

Fig. 32 Dependence of the breathing frequencies on the screening parameter κ for the coupling parameter $\lambda = 0.1$. The results were obtained with the Hartree-Fock method combined with the sum rule formulas $\mathrm{sr}^*(1,-1)$. The results are nearly converged for $\kappa \leq 0.1$. Especially the position of the frequency minimum ($N = 6$) does not change for smaller values.

In the derivation of formula (101) based on the operator equation,

$$\omega_{\mathrm{rel}} \leq \left\{ (2+\alpha) + (2-\alpha)\,\frac{\langle \hat{T}_{\mathrm{rel}} \rangle}{\langle \hat{V}_{\mathrm{rel}} \rangle} \right\}^{1/2} = \mathrm{sr}^*(3,1)\;, \tag{197}$$

it was required that the interaction potential is a pure power law. So far, it has always been assumed that there is no need for a correction due to the small screening parameter. In Ref. [37], a correction is proposed for systems with a screened potential. The derivation is based on the above operator equation with the result

$$\omega_{\mathrm{rel}} = \left\{ 4 - \frac{\langle \hat{U}^{\alpha} \rangle}{2\langle \hat{V}_{\mathrm{rel}} \rangle} \right\}^{1/2} \quad \text{with the two-body operator} \quad \hat{U}^{\alpha} := \sum_{i<j} \hat{\mathbf{F}}^{\alpha}_{ij} \cdot \hat{\mathbf{r}}_{ij}, \tag{198}$$

$$\text{and} \quad \mathbf{F}^{\alpha}_{ij}(\mathbf{r}) := \sum_{i<j} \left[2 - \alpha - \frac{(\alpha+2)\kappa^2}{\mathbf{r}_{ij}^2 + \kappa^2} \right] \frac{\alpha \lambda \mathbf{r}_{ij}}{\left(\mathbf{r}_{ij}^2 + \kappa^2\right)^{\alpha/2+1}}\;. \tag{199}$$

In Fig. 33, formula (198) is plotted together with the original formula (101) for three and five particles. The results were obtained in CI calculations, i. e., the input quantities for the formulas are exact. From the figure and several other numerical tests (not shown) one can conclude that the application of the corrections is not necessary. In fact, the figure shows that the frequencies even become slightly more inaccurate.

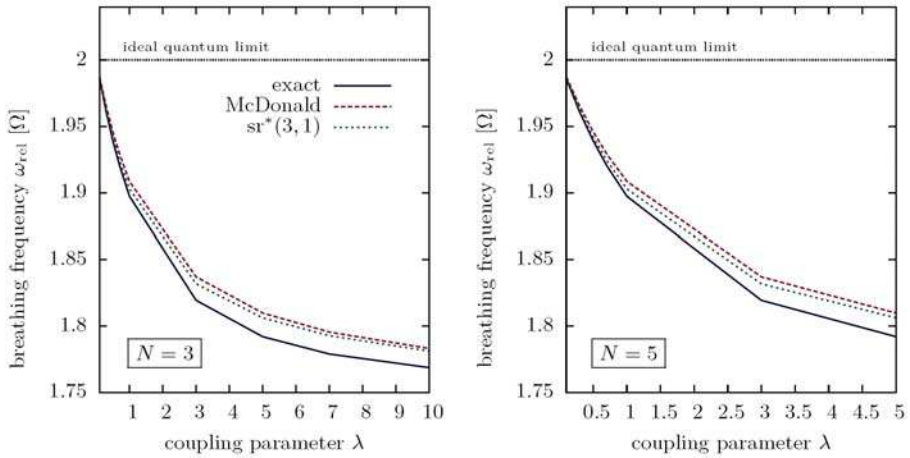

Fig. 33 Configuration interaction results for three and five particles with Coulomb interaction ($\alpha = 1$), concerning the necessity to use the corrected formula in Eq. (198) (obtained by McDonald *et al.* [37]) instead of formula (197). In all numerical tests, the corrections suggested by Eq. (198) even lead to slightly more inaccurate results.

7.1.5 Time-independent perturbation theory

As mentioned in Sec. 4.3.1, the extension of the working CI code to an implementation of time-independent perturbation theory (PT) was immediately possible. To finish the presentation for the charged particles, one last graph with PT results is shown in Fig. 34. The figure confirms again the non-monotonic behavior for a very small coupling parameter. The quantitative frequency values are justified by Hartree-Fock results. A new insight from this picture is the fact that PT can be used to exactly recover the center-of-mass frequency $\omega_{\rm cm}$. However, the main reason to apply perturbation theory is the following: As has been stated, the only input for the calculations are the matrix elements W_{IJ} of the interaction operator, constructed by the many-particle states of the non-interacting oscillator system. Hence, it is possible to locate the numerical origin of the observed phenomena in basic quantities which can be analyzed without extensive computations.

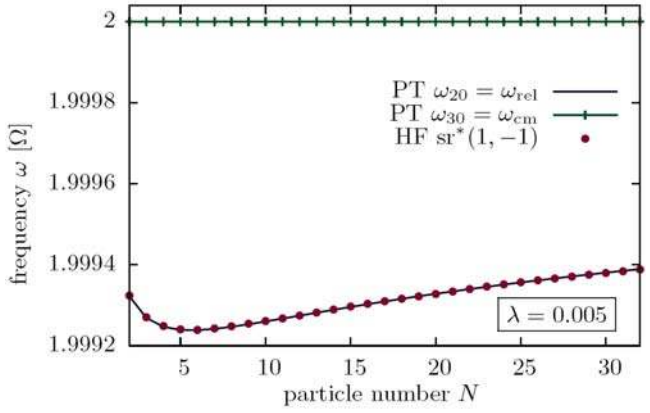

Fig. 34 Breathing frequencies as obtained with time-independent perturbation theory (PT) in comparison with the Hartree-Fock values.

7.2 Fermions with dipole interaction

The breathing mode of two dipolar fermions in 1D was investigated with a time-dependent solution of the Schrödinger equation in Ref. [42]. The authors mentioned that the steepness of the dipole potential $w(r) \sim r^{-3}$ imposes big numerical challenges. Using the equilibrium methods, the numerical handling of the dipole system is significantly simplified. But still it turns out that the numerical description is only satisfying for very small coupling parameters. In Fig. 35, the λ-dependent Hartree-Fock results are shown in comparison with the exact results from Sec. 2.4.1 and the corresponding frequencies from time-independent perturbation theory. Although

the numerical treatment of a two-particle system should not pose any problems, one notices that already for small couplings, the HF and PT results strongly deviate from the exact results. The results were obtained with large single-particle basis sets and seem to be converged. In contrast to Coulomb interaction, here screening has a major influence. This can be seen in Fig. 36, where the N-dependent breathing frequencies are plotted for several different screening parameters κ. For large κ, one can see a similar non-monotonic behavior as in Coulomb systems. For $\kappa = 0.1$, the frequencies have a maximum for $N = 4$ particles. However, the behavior changes drastically for smaller κ. At the same time, a higher numerical effort is required to describe the steep potential. In summary, one can state that the present methods are not well suited to describe finite dipole systems in 1D. A promising alternative is to perform quantum Monte Carlo simulations. For example, path integral Monte Carlo simulations in continuous space will allow one to perform the calculations with the pure (unscreened) dipole potential. Furthermore, one can make use of the Bose-Fermi mapping to overcome the fermion sign problem [124]. Beyond that, sufficiently large systems have successfully been described, using the local density approximation and reptation quantum Monte Carlo techniques [118].

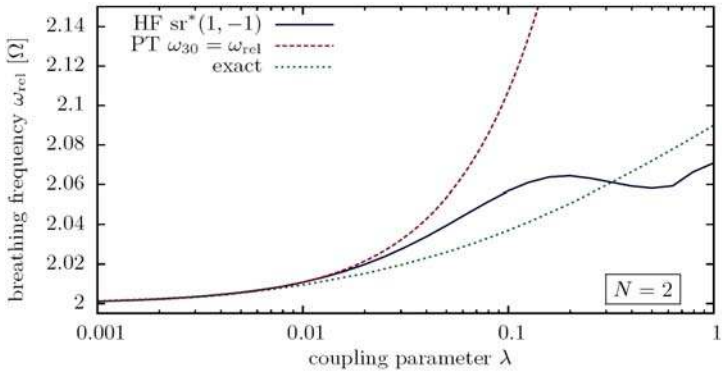

Fig. 35 Different estimators for the λ-dependent breathing frequencies of two spin-polarized dipoles ($\kappa = 0.01$). Already for small couplings $0.01 \leq \lambda \leq 0.1$, Hartree-Fock (HF) and time-independent perturbation theory (PT) fail to describe the frequencies accurately.

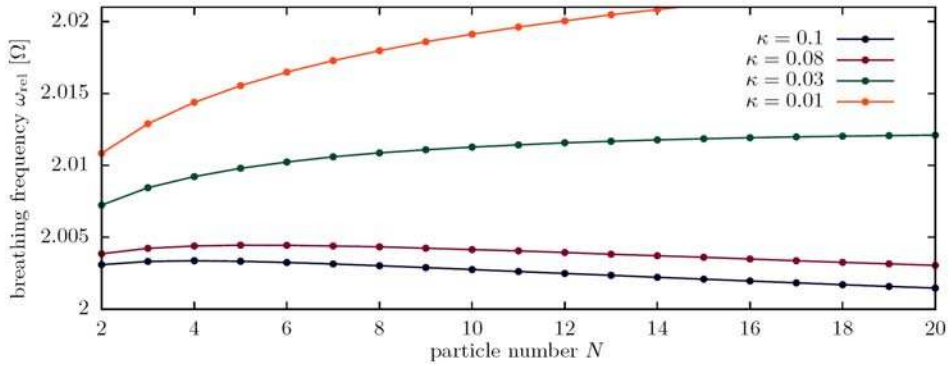

Fig. 36 N-dependent breathing frequencies of dipolar fermions ($\lambda = 0.01$) for different screening parameters. The results were obtained with the Hartree-Fock approximation by computing the sum rule $\mathrm{sr}^*(1, -1)$, using up to $n_\mathrm{b} \sim 2500$ FEDVR basis functions.

7.3 Discussion of the 1D results

Above we presented results for 1D fermionic systems, and we give now some conclusions for Coulomb systems[11]. First of all, we confirmed that the breathing mode can be accurately described with equilibrium methods. After several numerical tests with independent methods, we can draw the following conclusions [125]:

[11] Dipole systems are numerically more challenging and, therefore, yet less thoroughly investigated.

1. The breathing frequency attains a minimum for six particles if the coupling parameter λ is fixed. This is an effect of the finite size of the system. The minimum is unexpected, since in 1D systems, there is no particular "shell" geometry ("magic" configurations) as in 2D or 3D that could be responsible, So far, no simple physical reason for the special particle number $N = 6$ is known.

2. In the limit $N \to \infty$, at fixed λ, the breathing frequency approaches the ideal quantum value $2\,\Omega$.

3. In the limit $\lambda \to \infty$, at fixed N, the classical breathing frequency, $\sqrt{3}\,\Omega$, is obtained. While this has been obtained from Hartree-Fock simulations which are restricted to intermediate coupling parameters, $\lambda \leq 2$, we expect this trend to hold also for larger values of λ.

For the physical interpretation of these trends, we can employ the sum rule formula

$$\omega_{\rm rel} \leq \left\{ 3 + \frac{\langle \hat{T}_{\rm rel} \rangle}{\langle \hat{V}_{\rm rel} \rangle} \right\}^{1/2}, \tag{200}$$

which shows that the breathing frequency depends on the ratio of the mean kinetic and mean (relative) potential energy. In the classical limit, kinetic energy vanishes (in the ground state), and the frequency approaches $\sqrt{3}\,\Omega$. On the other hand, in the ideal quantum limit, kinetic and potential energy approach one another and the frequency equals $2\,\Omega$. Hence, the breathing frequency is a sensitive measure of the nonideality of the system.

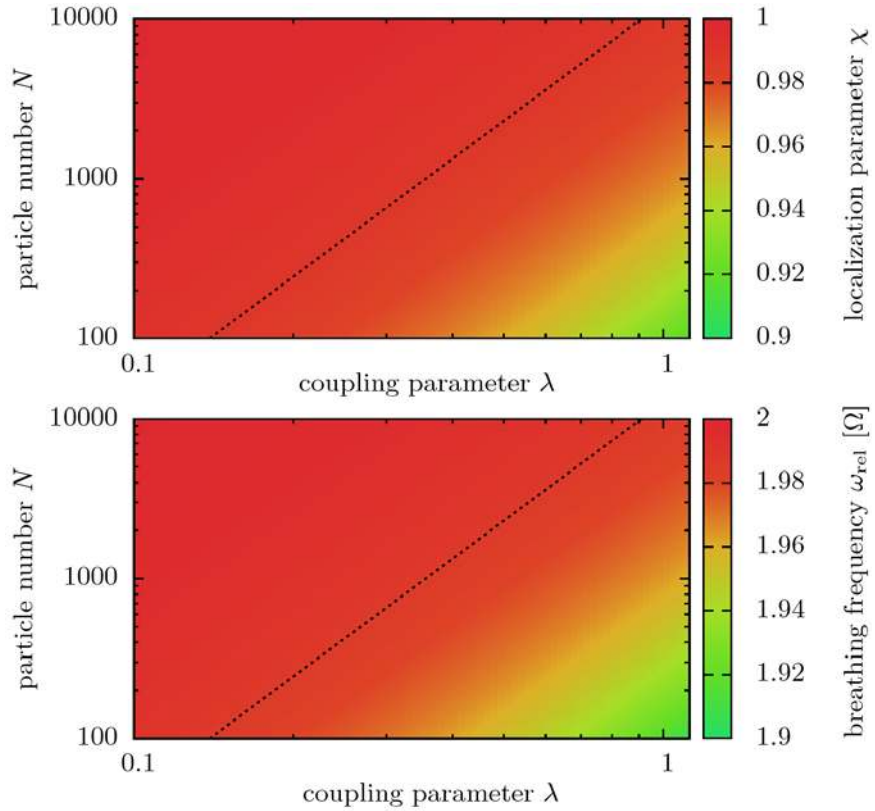

Fig. 37 Comparison of the localization parameter and the breathing frequency for trapped Coulomb systems in one dimension [125]. The values were obtained with the Thomas-Fermi approximation. The dotted lines (with the same definition) represent equal values of χ and $\omega_{\rm rel}$.

Another important consequence from the investigation of the ground state is the fact that the sole knowledge of the coupling parameter λ is not sufficient to decide whether quantum or classical effects dominate. Instead, the particle number has be taken into account as well. For a summarizing characterization of the ground-state

properties, one can introduce a localization parameter for the trap. This is inspired by the degeneracy parameter χ of a macroscopic homogeneous electron gas, see Sec. 2.1.1. It turned out that the characteristics of the system can be described in terms of the mean extension of the system which is estimated from

$$\sigma = \left\{ \int n(r) r^2 \mathrm{d}r \right\}^{1/2} = \left\{ 2\langle \hat{V} \rangle \right\}^{1/2} , \tag{201}$$

which, for a non-interaction system, has the value $\sigma_{\mathrm{ideal}} = \left\{ \frac{1}{2} N^2 \right\}^{1/2}$. With this, one can define the localization parameter

$$\chi = \frac{\sigma_{\mathrm{ideal}}}{\sigma} , \tag{202}$$

which measures how much the extension of the system deviates from that of an ideal non-interacting system which has the value $\chi_{\mathrm{ideal}} = 1$. In the transition to classical systems, χ decreases to zero. In Fig. 37, the values of the breathing frequency and the localization parameter are compared for large systems in the (λ, N)-plane. Apparently, both quantities show the same behavior. To illustrate this, straight lines indicating equal values of each quantity are plotted additionally. These lines have the same definitions

$$N = (1.3 \times 10^4) \lambda^{2.45} . \tag{203}$$

Interestingly, χ characterizes not only the behavior of large systems, but it also qualitatively captures the observed finite-size effects. In Fig. 38, χ is shown for small systems with selected coupling strengths. In all cases, χ attains a minimum for $N = 7$ particles, indicating a maximum of classical effects. The position of the minimum slightly differs from the minimum $N = 6$ for the breathing frequency. A similar effect has already been observed for the non-improved sum rule formulas, where the inclusion of the center-of-mass contributions shifted the minimum to seven particles.

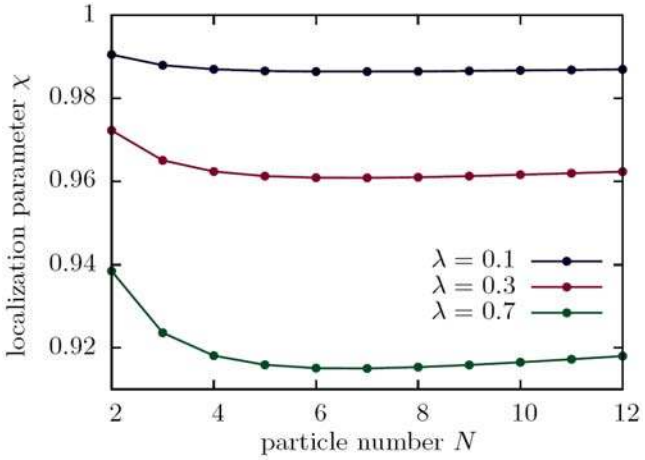

Fig. 38 Localization parameter χ for small systems. For all coupling parameters λ, a minimum occurs for seven particles.

Quantum-classical crossover. Another simple explanation of the observed characteristics can be attempted as follows. Let us compare an ideal (spin-polarized) quantum system to a classicl Wigner-crystallized Coulomb system. Thomas-Fermi theory predicts that the total energy of such a classical system is [117]

$$E_{\mathrm{c}} = \frac{3}{10} N \left(3\lambda N \ln N \right)^{2/3} . \tag{204}$$

Here, both the classical and the quantum equations are expressed in oscillator units. To justify the formula, a comparison with the results from exact classical Monte Carlo simulations[12] is provided in Fig. 39. Since the

[12] The results were kindly provided by Hauke Thomsen [126]. The simulations were performed with the Metropolis algorithm and parallel tempering. An explanation of the method can be found in Ref. [127].

results are in good agreement, Eq. (204) is assumed to be sufficiently accurate for the classical description in the following. For comparison, the total energy of a non-interacting quantum system is

$$E_{\mathrm{q}} = \frac{1}{2}N^2 \, . \tag{205}$$

As discussed in Ref. [117], both quantities can be used as estimators for the total energies in strongly and weakly coupled systems. For a fixed particle number, it is expected that the systems demand a full quantum mechanical description in the coupling regime, where both estimators are equal. Defining $\tilde{\lambda}(N)$ as the coupling parameter with $E_{\mathrm{q}} = E_{\mathrm{c}}$, one can estimate that $\tilde{\lambda}$ roughly marks the transition between quantum-like and classical behavior. It is given by

$$\tilde{\lambda} = \frac{1}{3}\left(\frac{5}{3}\right)^{3/2} \frac{N^{1/2}}{\ln N} \, . \tag{206}$$

In Fig. 7.3, this function is shown revealing that $\tilde{\lambda}$ reaches a minimum for $N = 7$ particles. Moreover, with increasing particle number, the value $\tilde{\lambda}$ is shifted to larger values. Agreeing with the findings from the previous discussion, even this simple theory explains the trend of increasing quantum-like behavior in large systems.

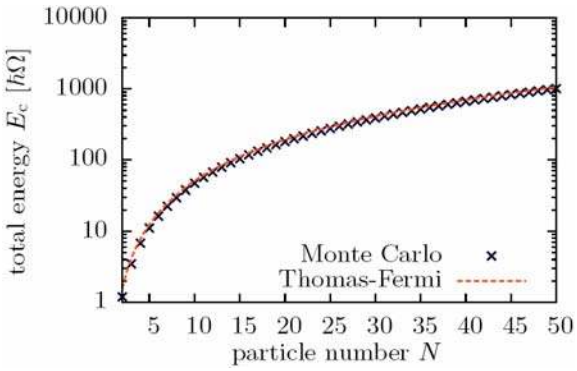

Fig. 39 N-dependent total energy E_{c} of a classical system with $\lambda = 1$. The results from classical Monte Carlo simulations are in good agreement with the Thomas-Fermi prediction in Eq. (204).

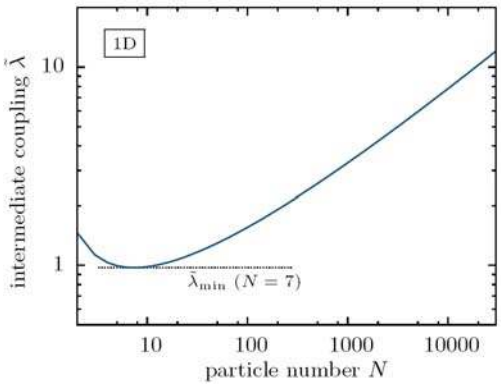

Fig. 40 N-dependent coupling parameters $\tilde{\lambda}$, for which the ideal quantum estimator E_{q} and the classical estimator E_{c} are equal. The minimum occurs for $N = 7$.

8 Results for the Breathing Brequency of 2D Systems

Having investigated 1D systems in detail, the analysis will now be extended to 2D. Especially for quantum dots, this is a more realistic setting [14]. However, the computational demands of 2D systems drastically increase. Roughly estimating, a 2D calculation requires n_{b}^2 single-particle basis functions if a corresponding 1D problem requires n_{b} basis functions. This is due to the fact that a basis function in 2D usually has two quantum numbers for each spatial direction. As is reported in Ref. [37], accurate time-dependent calculations can take several days for just a single frequency. Aside from that, one is usually restricted to particle numbers $N < 10$.

With the sum rules at hand, the problems of time-dependent calculations can be circumvented. This section is devoted to the presentation of equilibrium results for Fermi particles with Coulomb interaction and Bose particles with dipole interaction.

8.1 Fermions with Coulomb interaction

For the Coulomb-interacting fermions, time-independent Hartree-Fock calculations were performed. Utilizing the spherical harmonic oscillator functions as a single-particle basis, a pure Coulomb potential could be employed. The calculations were performed with at least $n_{\mathrm{b}} = 78$ single-particle basis functions. Further, it is

remarked that the 2D oscillator basis is only suitable for coupling parameters $\lambda \leq 1$. This problem even occurred in some numerical tests with exact CI for two particles. To access larger coupling parameters, a possible alternative is the numerical solution on a 2D grid.

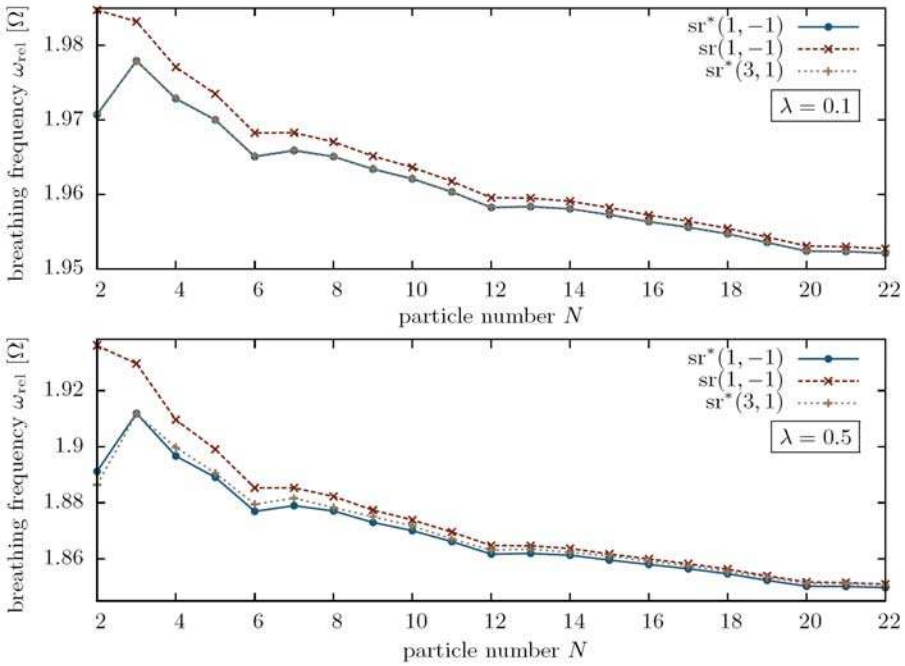

Fig. 41 N-dependent breathing frequencies for two-dimensional systems with Coulomb interaction [125]. The spin configurations follow Hund's rules. The minima for $N = 2, 6, 12, 20$ correspond to configurations with closed shells.

Table 2 Occupation of the first single-particle orbitals, according to Hund's rules. N^+ and N^- are the numbers of particles with "spin up" and "spin down". Closed shells are indicated by boxes.

N	N^+	N^-	configuration	N	N^+	N^-	configuration
1	1	0	$\uparrow$	7	4	3	$\boxed{\uparrow\downarrow}\ \boxed{\uparrow\downarrow\uparrow\downarrow}\ \uparrow$
2	1	1	$\boxed{\uparrow\downarrow}$	8	5	3	$\boxed{\uparrow\downarrow}\ \boxed{\uparrow\downarrow\uparrow\downarrow}\ \uparrow\ \uparrow$
3	2	1	$\boxed{\uparrow\downarrow}\ \uparrow$	9	6	3	$\boxed{\uparrow\downarrow}\ \boxed{\uparrow\downarrow\uparrow\downarrow}\ \uparrow\ \uparrow\ \uparrow$
4	3	1	$\boxed{\uparrow\downarrow}\ \uparrow\ \uparrow$	10	6	4	$\boxed{\uparrow\downarrow}\ \boxed{\uparrow\downarrow\uparrow\downarrow}\ \uparrow\downarrow\uparrow\ \uparrow$
5	3	2	$\boxed{\uparrow\downarrow}\ \uparrow\downarrow\uparrow$	11	6	5	$\boxed{\uparrow\downarrow}\ \boxed{\uparrow\downarrow\uparrow\downarrow}\ \uparrow\downarrow\uparrow\downarrow\uparrow$
6	3	3	$\boxed{\uparrow\downarrow}\ \boxed{\uparrow\downarrow\uparrow\downarrow}$	12	6	6	$\boxed{\uparrow\downarrow}\ \boxed{\uparrow\downarrow\uparrow\downarrow}\ \boxed{\uparrow\downarrow\uparrow\downarrow\uparrow\downarrow}$

In Fig. 41, the N-dependent breathing frequencies are shown for the selected coupling parameters $\lambda = 0.1$ and 0.5. For the Hartree-Fock calculation, it was assumed that the energy shells are filled according to Hund's rules [128]. A detailed listing of the configurations is given in Table 2. Other than in 1D systems, the breathing frequencies are strongly non-monotonic. This can be explained by the successive filling of the energy shells. Similarly to atomic systems, configurations with completely filled shells are more stable than configurations with open shells. A configuration with closed shells is characterized by a relatively strong contribution of the interaction energy. The energy eigenvalues of the 2D single-particle harmonic oscillator are given by 1, 2, 2, 3, 3, 3, ... Each corresponding orbital can be occupied by two particles. With the sum rule formulas, it is immediately clear that the frequency has local minima for 2, 6, 12 and 20 particles. These numbers are also known as "magic numbers". From the numerical point of view, one can see again how the improved sum rule formulas provide a qualitatively different picture for very small particle numbers than the original formulas. Especially the minimum

for two particles is not captured by the non-improved formulas. For $N = 2$ and $\lambda = 0.5$, the estimator $\mathrm{sr}^*(3,1)$—calculated with the sum rules in Eq. (107)—gives a smaller value than $\mathrm{sr}^*(1,-1)$. This contradicts the theory, and it seems to be a numerical issue. So far, however, the problem could not be resolved. For all larger particle numbers, $\mathrm{sr}^*(1,-1) \leq \mathrm{sr}^*(3,1)$ is fulfilled, agreeing with the theoretical prediction.

For comparison, spin-polarized systems have also been investigated. Results for the coupling parameter $\lambda = 0.3$ and up to 15 particles are shown in Fig. 42. Due to the spin polarization, the single-particle orbitals can only be occupied once. Since the i-th shell is closed if it is occupied by i particles, the minima appear for $N = 3$, 6 and 10 particles.

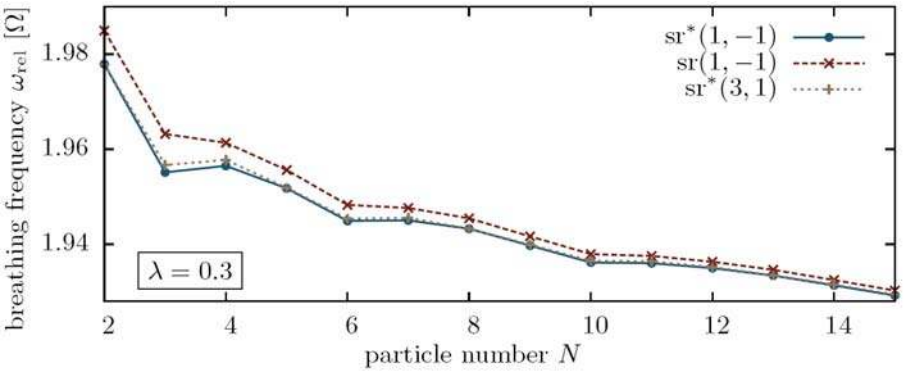

Fig. 42 N-dependent breathing frequencies for two-dimensional spin-polarized systems with Coulomb interaction. The minima appear for $N = 3, 6, 10$ particles.

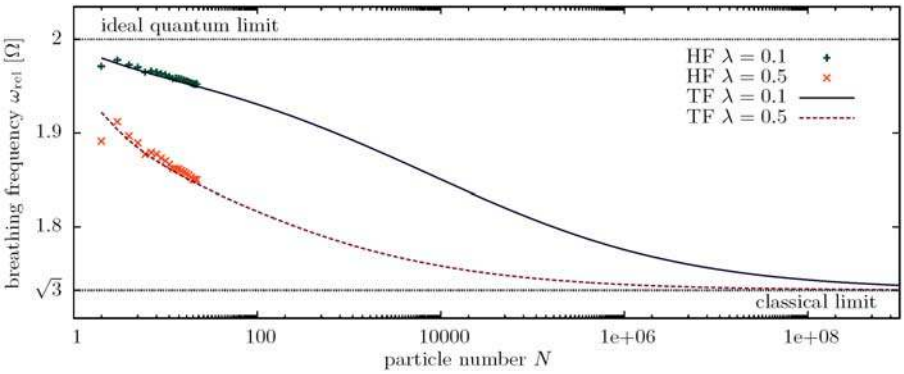

Fig. 43 N-dependent breathing frequencies for different coupling parameters in Thomas-Fermi approximation (with $\mathrm{sr}^*(3,1)$) and Hartree-Fock approximation (with $\mathrm{sr}^*(1,-1)$) [125]. For large N, the classical value $\sqrt{3}\,\Omega$ is reached.

Just like for 1D systems, it is again of interest to consider the transition to large systems. For that purpose, Thomas-Fermi calculations were performed, according to the explanation in Sec. 6.3. The frequencies were estimated with the formula $\mathrm{sr}^*(3,1)$. The Hartree-Fock results are compared to the Thomas-Fermi results in Fig. 43. First, it can be noted that the TF results follow the trend of the HF results, but the non-monotonic behavior is not captured. Nevertheless, the deviations between both results are on small scales. Second, the figure reveals a limiting behavior that is contrary to that of 1D systems. For both plotted coupling strengths, the frequencies reach the classical value $\sqrt{3}\,\Omega$ in the limit of very large particle numbers. As the variational procedure for the 2D case is exceptionally simple, the whole (λ, N)-plane can be covered numerically within just a few seconds of computing time. An overview of $\omega_{\mathrm{rel}}(\lambda, N)$ is provided in Fig. 44. The figure reveals that for a fixed coupling parameter λ, the frequencies always transition into the classical values with increasing particle numbers. This is a fundamental difference to the 1D case.

Finally, the ansatz for the density in the TF approximation shall be justified. It is known that the ansatz is correct for a non-interacting system. The good agreement between the breathing frequencies in HF and TF

approximation (Fig. 43) confirms that the ansatz is also well suited for weakly interacting systems. To show that the correct energies of the classical limit can be captured with the ansatz, the λ-dependent total energies are shown for different particle numbers in Fig. 45. The corresponding values of the non-interacting system and the classical[13] system are indicated by straight lines. These lines represent rough approximations for the energies of weakly and strongly interacting systems, respectively. A similar illustration for 1D systems can be found in Ref. [117]. The figure reveals that both the ideal quantum limit and the classical limit are correctly included in the TF approximation. However, as the TF density is continuous, the density of the classical point charges can only be approximated with sufficient accuracy if the particle number is large.

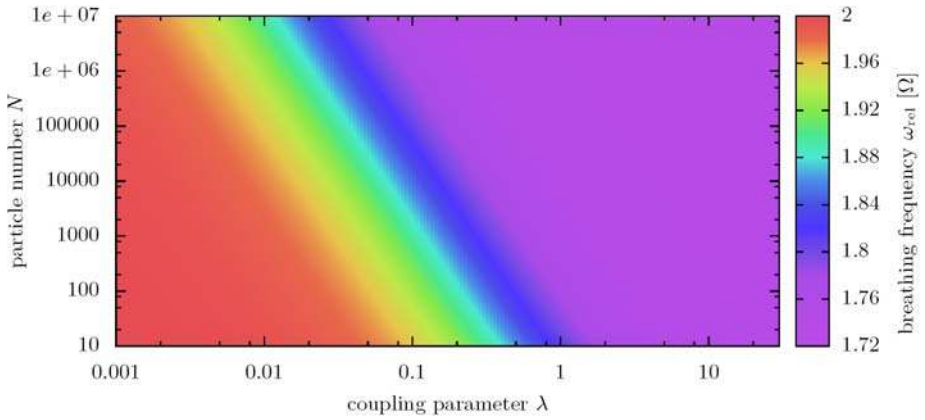

Fig. 44 Dependence of the breathing frequencies on the coupling parameter and the particle number in two-dimensional systems with Coulomb interaction [125]. The results were obtained in TF calculations with the sum rule formula $\mathrm{sr}^*(3,1)$.

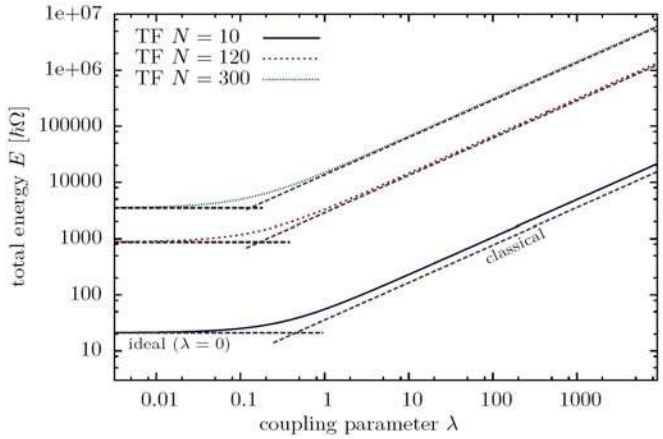

Fig. 45 Total energies of a 2D Coulomb system, depending on N and λ [125]. The Thomas-Fermi (TF) results are compared to the results from classical Monte Carlo simulations and the analytical values of an ideal Fermi gas.

8.2 Bosons with dipole interaction

The exact description of bosonic systems is a major strength of quantum Monte Carlo methods. As collective oscillations are also relevant for Bose gases, this section is devoted to the investigation of dipolar bosons with the path integral Monte Carlo (PIMC) method. Especially for strongly coupled systems, the PIMC calculations have good statistics. The dipole potential is chosen, because Coulomb interacting bosons are quite rare in nature.

In Fig. 46, the frequencies $\omega_{\rm rel}$ are shown for up to 95 particles. The estimator for the breathing frequencies is $\mathrm{sr}^*(3,1)$, as this quantity has the best statistics in the simulations. For all investigated coupling parameters, the overall trend is an increase of the frequency with the particle number. It can be expected that the classical frequency, $5\,\Omega$, will be reached in the limit $N \to \infty$.

[13] Just like for the 1D systems, these values were produced with Metropolis Monte Carlo simulations.

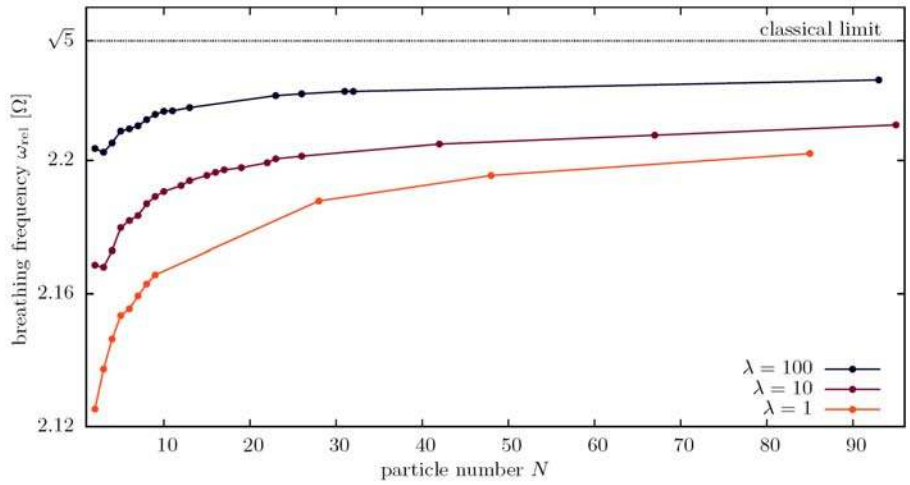

Fig. 46 N-dependent breathing frequencies for two-dimensional dipolar bosons, as obtained in path integral Monte Carlo simulations with different coupling parameters. The results were obtained with the inverse temperature $\beta = 30$.

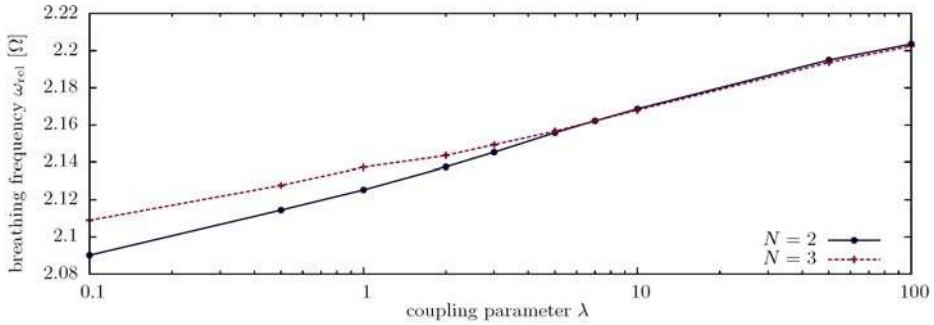

Fig. 47 λ-dependent breathing frequencies for two and three two-dimensional dipolar bosons. The curves intersect near $\lambda = 7$.

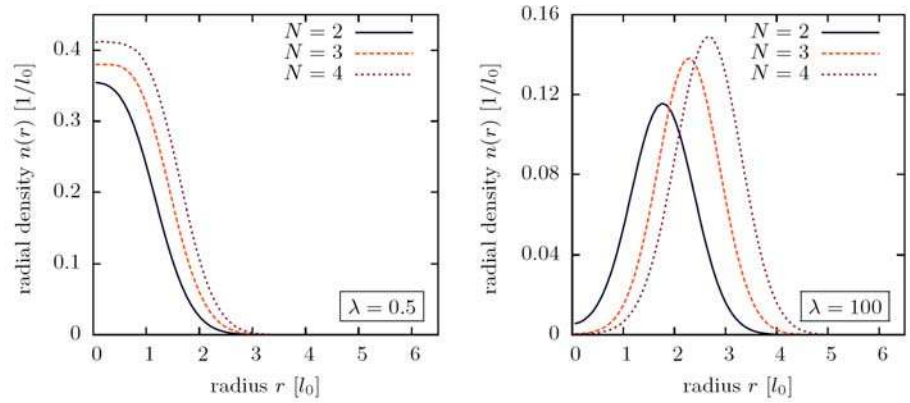

Fig. 48 Radial densities for weakly (left) and strongly coupled (right) dipolar bosons. With increasing coupling parameter, the densities are not centered at the origin anymore, and they represent the shell structures of crystallized systems.

Covering a broad range of coupling parameters, it is observed that with increasing λ, a non-monotonic behavior of the frequency evolves. The most noticeable example is the step from two to three particles: While the frequencies always increase for small λ, the frequencies decrease for large λ. This behavior can also be seen in Fig. 47, showing the λ-dependent frequencies for two and three particles. Around $\lambda = 7$, the frequencies for

$N = 2$ reach those for $N = 3$. However, the difference between the curves becomes small. Nevertheless, since there are no deviations from this trend, it is unlikely that the behavior is due to statistical errors. In the limit $\lambda \to \infty$, the curves for all particle numbers will of course converge to the joint limit $\sqrt{5}\,\Omega$. The λ-dependent increase of the non-monotonic behavior is associated with a crystallization of the system. For weak couplings, bosonic systems at low temperatures are characterized by high occupation numbers of the lowest single-particle orbital. It is not expected that certain particle numbers are outstanding. In the transition to the strongly coupled regime, however, the densities start to obtain the discrete shapes of classical point masses. Apparently, this process is mapped to the behavior of the breathing frequency. For further illustration, in Fig. 48, the radial densities of strongly coupled ($\lambda = 100$) systems can be compared to those of weakly coupled ($\lambda = 0.5$) systems. It is demonstrated for small particle numbers, how the system abandons its origin-centered density and obtains a shell configuration.

8.3 Discussion of the 2D results

In this section we have presented results for two-dimensional systems. On the one hand, for weakly interacting fermions with Coulomb interaction, it could be observed how the orbital structure of the non-interacting system manifests itself in the breathing frequencies ("magic numbers"). On the other hand, for strongly coupled dipolar bosons, the behavior of the breathing frequency was associated with crystallization.

The important result of this section is that the limiting behavior of the breathing frequency differs radically from that of 1D systems. In both cases, $\lambda \to \infty$ and $N \to \infty$, the frequency converges to its classical limit. So far, this could only be shown for the fermionic system, but the results for the bosonic case confirm this trend.

To explain the observed behavior, we use again the localization parameter $\chi = \sigma_{\mathrm{ideal}}/\sigma$. Defining the extension σ, as in Sec. 7.3

$$\sigma = \left\{ \int n(\mathbf{r}) \mathbf{r}^2 \mathrm{d}\mathbf{r} \right\}^{1/2} , \tag{207}$$

we obtain the value of for an ideal system in 2D

$$\sigma_{\mathrm{ideal}} = \left\{ \frac{2}{3} N^{3/2} \right\}^{1/2} , \tag{208}$$

which differs from the 1D case ($\sigma_{\mathrm{ideal}} = N/\sqrt{2}$). In Fig. 49, the breathing frequency and the localization parameter χ are compared for a system of fermions with Coulomb interaction. Both quantities have a similar behavior, which is shown again by two straight lines with the same definition,

$$N = 100\lambda^{-4} . \tag{209}$$

Quantum-classical crossover. To complete this analysis, an estimator for intermediate couplings is determined for the 2D system. The energy of a non-interacting quantum systems is given by $E_{\mathrm{q}} = \frac{2}{3} N^{3/2}$, whereas, for a purely classical system, one finds $E_{\mathrm{c}} = K \lambda^{2/3} N^{5/3}$. This value can be obtained if one sets the kinetic energy to zero and minimizes the remaining terms in Eq. (186). The constant K is given by

$$K = \left(\frac{256\sqrt{2}}{315\pi} \right)^{2/3} + \frac{512\sqrt{2}}{315\pi} \left(\frac{256\sqrt{2}}{105\pi} \right)^{-1/3} .$$

Consequently, the estimator for intermediate couplings which we define from equal values of the quantum kinetic and classical interaction energy, i.e. $E_{\mathrm{c}} = E_{\mathrm{q}}$, is given by

$$\tilde{\lambda} = \left(\frac{2}{3K} \right)^{3/2} N^{-1/4} .$$

It is reasonable to use the parameter $\tilde{\lambda}$ to subdivide 2D systems into ones with dominantly quantum behavior ($\lambda < \tilde{\lambda}$) and ones with dominantly classical behavior ($\lambda > \tilde{\lambda}$). In contrast to 1D systems, $\tilde{\lambda}$ indicates that, in

2D, the classical regime is shifted to smaller coupling parameters if the particle number N is increased. Hence, by means of this simple estimator, it is confirmed that the breathing frequencies tend to the classical value in the limit $N \to \infty$.

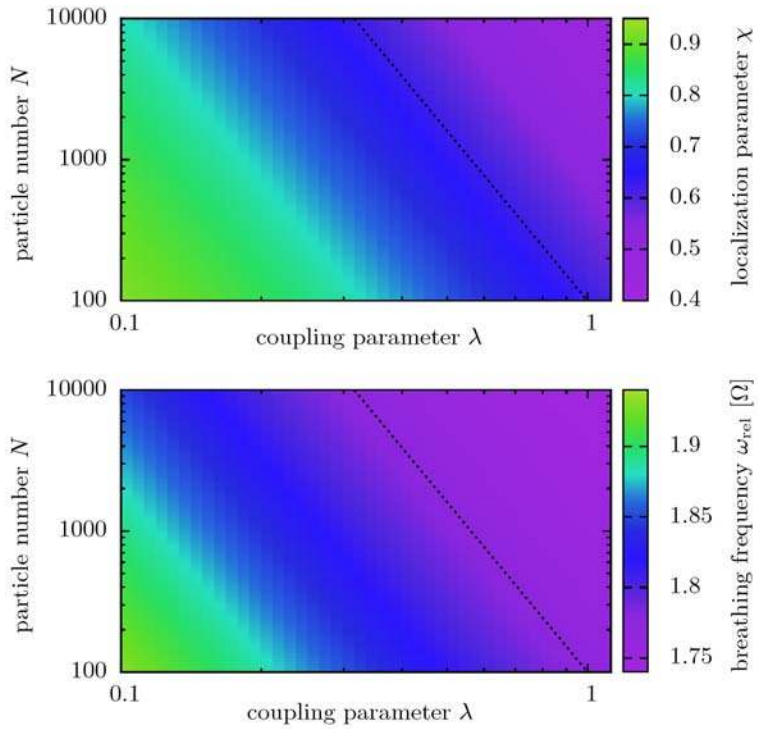

Fig. 49 Localization parameter and the breathing frequency for trapped Coulomb systems in two dimensions [125]. The values were obtained with the Thomas-Fermi approximation. The dotted lines (with the same definition) represent equal values of χ and $\omega_{\rm rel}$.

9 Summary and Outlook

The present work gave an overview on recents results for the quantum breathing mode of trapped systems. While the breathing mode has been studied in great detail for classical systems, the corresponding understanding for quantum systems is far less complete. Recent theoretical advances have brought important physical insight.

The first surprising results is that, in contrast to strongly correlated classical systems, an interacting quantum system in a harmonic trap possesses two breathing frequencies, $\omega_{\rm rel}$ and $\omega_{\rm cm}$. The former is related to the relative collective "breathing" motion of all particles and is similar to its classical counterpart, but the frequencies are essentially modified due to quantum effects. The latter mode is a pure quantum effect which was observed by Bauch *et al.* [56] and exists already in the absence of interactions and even for a single quantum particle in a harmonic trap. This motion is a consequence of the finite extension of the wave function of a quantum particle and is associated with the radial expansion and contraction of this wave function. In an N-particle system all particles exhibit this "individual" radial "breathing". This purely quantum mode has the universal frequency $2\,\Omega$, i.e., it is independent of the coupling strength, spin, interaction potential and the number of particles. The relative amplitude (oscillator strength) of this mode, compared to the relative breathing mode, decreases with N.

Our second result was to demonstrate how previous time-dependent simulation results that are computationally very expensive and, thus, limited to small particle numbers, can be extended to large systems by application of time-dependent perturbation theory. This theory allows for a systematic description of the normal modes, and especially an approximation of the breathing frequency $\omega_{\rm rel}$ with the help of quantum mechanical sum rules. A thorough study of the two-particle system gave insight into the quality of approximate methods. Especially the

improvement of the conventional sum rule formulas for $\omega_{\rm rel}$ by correcting for the center of mass mode is a simple, but important achievement for the accurate description of the breathing frequency of small systems.

Third, for the investigation of many-body systems, different physical settings were chosen. The focus was mainly on 1D fermions with Coulomb interaction. For this system, the results from time-dependent Hartree-Fock calculations could be reproduced with various time-independent approaches. It was shown that the breathing frequencies have a minimum for six particles, which is independent of the coupling parameter. Further, Thomas-Fermi theory was employed to show that the breathing frequency converges to its ideal value $2\,\Omega$ if one fixes the coupling parameter λ and performs the limit $N \to \infty$. To compare with other types of interaction, 1D dipolar fermions were considered afterwards. It turned out that the numerical handling of the dipole potential is quite more challenging than the treatment of the Coulomb potential. The dependence on the screening parameter in the dipole case is to be clarified in future works.

Fourth, we presented results for 2D systems, in the final part of this review. Since the inclusion of just one more spatial dimension is already a numerical challenge, only time-independent calculations were performed. Fermionic systems with Coulomb interaction were studied with unrestricted Hartree-Fock calculations. At this, it was shown that the breathing frequency provides a diagnostic tool for the shell structure of the orbitals. The observed frequency minima follow similar characteristics as, for example, the addition energies which are measured in experiments with quantum dots [13]. Finally, to demonstrate the capabilities of the sum rules, the analysis was extended to dipolar Bose particles. Compared to the typical sizes of Bose-Einstein condensates (e. g., $N = 25000$ [129]), the systems in this work are relatively small. Nevertheless, the frequencies are nearly exact and provide a starting point for the extension to larger systems.

Our fifth main point was to highlight the surprisingly different asympotic behavior of the breathing frequency for large N and large λ in 1D and 2D Coulomb systems. While the strong coupling limit, $\lambda \to \infty$ at $N = \mathrm{const}$, yields always the classical value of $\omega_{\rm rel}$, the limit $N \to \infty$ at $\lambda = \mathrm{const}$ is different in different dimensions. While in 1D, $\omega_{\rm rel} \to 2\Omega$, i.e. $\omega_{\rm rel}$ approaches its ideal quantum limit, in all considered 2D systems $\omega_{\rm rel}$ was found to converge to its strongly coupled classical asymptotic [125], i.e., to $\sqrt{3}\,\Omega$, for Coulomb interaction and $\sqrt{5}\,\Omega$, for dipole interaction. A physical explanation of this behavior was given from an analysis of the degree of localization of the particles which is governed by the competition of interparticle repulsion and potential (trap) energy. To measure the degree of localization, we introduced a localization parameter that indicates how much the spatial extension of the entire particle "cloud" deviates from the extension of a non-interacting system, i.e., $\chi = \sigma/\sigma_{\rm ideal}$. It was demonstrated that the breathing frequency and χ exhibit very similar behaviors: in 1D (2D), both quantities are constant along lines $N \sim \lambda^{2.45}$ ($N \sim \lambda^{-4}$).

These scalings have been obtained from mean field type (Hartree-Fock and Thomas-Fermi) models, and it remains an interesting question for future investigation, what is the effect of correlations. While, for bosons, path integral Monte Carlo methods are well suited to answer this question, for strongly degenerate fermions they are hampered by the fermion sign problem. Here, possible approaches include multiconfiguration Hartree-Fock and restricted active space methods, e.g. [40,83,130,131], nonequilibrium Green functions [82,132], diffusion Monte Carlo [133] or path integral Monte Carlo in configuration space [134].

To summarize our main conclusion, the behavior of strongly correlated quantum systems in traps is rather complex as it depends on many parameters: the coupling parameter, the form of the interaction potential, the spin statistics and system dimensionality [56]. Moreover, as we have shown also the precise particle number is important (except for the maroscopic limit). The frequency of the radial "breathing-type" excitation of these systems is sensitive to all these properties and, thus, provides a useful tool for the diagnostics of trapped quantum systems. The idea of using the breathing frequency as a novel type of spectroscopy for these systems was demonstrated on the example of the mean kinetic, potential and interaction energy [37]. These quantitites are not directly accessible in experiments, yet all of them can be reconstructed directly from a measurement of the breathing frequency, as we showed in Sec. 3.3. With all contributions of the total energy at hand all ground state properties are known. It is expected that a similar approach is possible at finite temperature since from the energy the free energy (or the grand potential) and, hence, all thermodynamic properties can be computed.

Acknowledgements We are greatful to A. Filinov for providing path integral Monte Carlo data for 2D dipolar bosons and to H. Thomsen for classical Monte Carlo results. We acknowledge many stimulating discussions with (former) members of our group, in particular, K. Balzer, S. Bauch, D. Hochstuhl, A. Filinov and H. Kählert and with C. McDonald and T.

Brabec (Ottawa). This work is supported by the Deutsche Forschungsgmeinschaft via SFB-TR24 "Fundamentals of Complex Plasmas", project A5 and by a grant for CPU time at the North-German Supercomputing alliance (HLRN).

A Appendix

A.1 Perturbation theory

Some parts of this work refer to time-independent as well as time-dependent perturbation theory. We, therefore, recall the basic ideas and results and set up the notation used in the main text.

A.1.1 Time-independent perturbation theory

The time-independent perturbation theory aims at solving the eigenvalue problem

$$\hat{H}|\Psi_i\rangle = E_i|\Psi_i\rangle \ , \tag{210}$$

where the Hamiltonian $\hat{H} = \hat{H}_0 + \eta\hat{\Lambda}$ consists of an unperturbed part $\hat{H}_0$ and a perturbation $\eta\hat{\Lambda}$. The operator $\hat{\Lambda}$ remains unspecified, and η is a sufficiently small real parameter. It is assumed that $\hat{H}_0$ is diagonalized by the eigenfunctions $|\Psi_k^{(0)}\rangle$ with the non-degenerate eigenvalues $E_k^{(0)}$. The basic idea is to expand the i-th eigenfunction of $\hat{H}$ and its eigenvalue in the perturbation series

$$|\Psi_i\rangle = |\Psi_i^{(0)}\rangle + \sum_{k=1}^{\infty} \eta^k |\Psi_i^{(k)}\rangle \quad \text{and} \quad E_i = E_i^{(0)} + \sum_{k=1}^{\infty} \eta^k E_i^{(k)} \ .$$

Inserting these series into Eq. (210) yields a hierarchy of equations which determine the corrections in each order. Skipping the details of further calculations, the result for the correction of the energy in first order reads

$$E_i^{(1)} = \langle \Psi_i^{(0)}|\hat{\Lambda}|\Psi_i^{(0)}\rangle \ .$$

The corresponding correction of the wave function is given by

$$|\Psi_i^{(1)}\rangle = \sum_{k\neq i} \frac{\langle \Psi_k^{(0)}|\hat{\Lambda}|\Psi_i^{(0)}\rangle}{E_i^{(0)} - E_k^{(0)}} \ |\Psi_k^{(0)}\rangle \ .$$

It is obvious that this equation cannot hold if the energy $E_i^{(0)}$ is degenerate. In the following, the case of an n-fold degenerate eigenvalue $E^{(0)}$ is regarded. The wave functions with this eigenvalue are denoted by $|1\rangle, \ldots, |n\rangle$. In order to obtain the corrections in first order, the subspace spanned by these vectors has to be diagonalized, according to the eigenvalue problem $\mathbf{\Lambda c} = E^{(1)}\mathbf{c}$ or, equivalently,

$$\sum_{\alpha=1}^{n} \langle\beta|\hat{\Lambda}|\alpha\rangle \, c_\alpha = E^{(1)} c_\beta \ , \qquad \beta = 1, \ldots, n \ .$$

The first-order energy corrections for each of the states $|1\rangle, \ldots, |n\rangle$ are thus given by the n eigenvalues $E_{[1]}^{(1)}, \ldots, E_{[n]}^{(1)}$.

A.1.2 Time-dependent perturbation theory

The starting point of time-dependent perturbation theory is the TDSE

$$\mathrm{i}\hbar \frac{\mathrm{d}}{\mathrm{d}t}|\Psi(t)\rangle = \left(\hat{H}_0 + \eta\hat{\Lambda}(t)\right)|\Psi(t)\rangle \ . \tag{211}$$

The operators have the same properties as in the previous case of stationary perturbation theory, except for the fact that $\hat{\Lambda}$ is now explicitly time-dependent. Using the complete basis $\left\{|\Psi_k^{(0)}\rangle\right\}$, which is formed by the eigenfunctions of the stationary Hamiltonian $\hat{H}_0$, one can apply the expansion

$$|\Psi(t)\rangle = \sum_k c_k(t)\, \exp\left\{-\frac{\mathrm{i}E_k^{(0)}t}{\hbar}\right\} |\Psi_k^{(0)}\rangle \; .$$

Inserting this expansion into Eq. (211) and multiplying with $\langle\Psi_i^{(0)}|$ from the left, one arrives at

$$\mathrm{i}\hbar\frac{\mathrm{d}}{\mathrm{d}t}c_i(t) = \eta\sum_k c_k(t)\, \exp\left\{\frac{\mathrm{i}}{\hbar}\left(E_i^{(0)} - E_k^{(0)}\right)t\right\} \langle\Psi_i^{(0)}|\hat{\Lambda}(t)|\Psi_k^{(0)}\rangle \; . \tag{212}$$

This equation is still equivalent to the TDSE in Eq. (211). For sufficiently small η, one can make an expansion similar to those of the time-independent theory,

$$c_i(t) = \sum_{j=0}^{\infty} \eta^j c_i^{(j)}(t) \; . \tag{213}$$

It is now assumed that the system is at the initial time $t = t_0$ in the state $|\Psi(t_0)\rangle = |\Psi_n^{(0)}\rangle$. Without loss of generality, one can set $t_0 = 0$. The expansion coefficients obey the initial conditions with the choices $c_i^{(0)}(0) = \delta_{in}$ and $c_i^{(j)}(0) = 0$ for all $j \geq 1$. Inserting Eq. (213) into Eq. (212) and respecting the initial conditions, one obtains $c_i^{(0)}(t) = \delta_{in}$, and for the first-order correction of the expansion coefficients

$$c_i^{(1)}(t) = -\frac{\mathrm{i}}{\hbar}\int_0^t \mathrm{d}t'\, \exp\left\{\frac{\mathrm{i}}{\hbar}\left(E_i^{(0)} - E_n^{(0)}\right)t'\right\} \langle\Psi_i^{(0)}|\hat{\Lambda}(t')|\Psi_n^{(0)}\rangle \; .$$

A.2 Calculation of the cubic energy-weighted moment

The goal is to calculate the commutator in the expression

$$m_3 = \frac{1}{2}\langle 0|[[\hat{Q},\hat{H}_0],[\hat{H}_0,[\hat{H}_0,\hat{Q}]]]|0\rangle = -\frac{1}{2}\langle 0|[[\hat{H}_0,\hat{Q}],[\hat{H}_0,[\hat{H}_0,\hat{Q}]]]|0\rangle$$

for the observable $\hat{Q} = \sum_{i=1}^N \hat{\mathbf{r}}_i^2$ that is related to the breathing mode and for the generic Hamiltonian $\hat{H}_0 = \hat{T} + \hat{V} + \hat{W}$. One can start by evaluating

$$[\hat{H}_0,\hat{Q}] = [\hat{T},\hat{Q}] = -\mathrm{i}\sum_{i=1}^N \left\{\hat{\mathbf{p}}_i\hat{\mathbf{r}}_i + \hat{\mathbf{r}}_i\hat{\mathbf{p}}_i\right\} \; .$$

Now the commutator $[\hat{H}_0,[\hat{H}_0,\hat{Q}]]$ is evaluated for $\hat{T}$, $\hat{V}$ and $\hat{W}$ separately, starting with

$$-\mathrm{i}\sum_{i=1}^N [\hat{T},\hat{\mathbf{p}}_i\hat{\mathbf{r}}_i + \hat{\mathbf{r}}_i\hat{\mathbf{p}}_i] = -2\sum_{i=1}^N \hat{\mathbf{p}}_i^2 \; .$$

One concludes that

$$-\mathrm{i}\sum_{i=1}^N [\hat{\mathbf{p}}_i\hat{\mathbf{r}}_i + \hat{\mathbf{r}}_i\hat{\mathbf{p}}_i, -2\hat{\mathbf{p}}_i^2] = -8\hat{\mathbf{p}}_i^2 \; , \quad \text{and, hence,} \quad -\frac{1}{2}\langle 0|[[\hat{H}_0,\hat{Q}],[\hat{T},[\hat{H}_0,\hat{Q}]]]|0\rangle = 8\langle\hat{T}\rangle \; .$$

Similarly, one derives

$$-\mathrm{i}\sum_{i=1}^N [\hat{V},\hat{\mathbf{p}}_i\hat{\mathbf{r}}_i + \hat{\mathbf{r}}_i\hat{\mathbf{p}}_i] = 2\sum_{i=1}^N \hat{\mathbf{r}}_i^2 \quad \text{and} \quad -\mathrm{i}\sum_{i=1}^N [\hat{\mathbf{p}}_i\hat{\mathbf{r}}_i + \hat{\mathbf{r}}_i\hat{\mathbf{p}}_i, 2\hat{\mathbf{r}}_i^2] = -8\hat{\mathbf{r}}_i^2 \; .$$

Consequently,

$$-\frac{1}{2}\langle 0|[[\hat{H}_0,\hat{Q}],[\hat{V},[\hat{H}_0,\hat{Q}]]]|0\rangle = 8\langle\hat{V}\rangle,$$

is valid. The evaluation for the operator $\hat{W}$ is more complicated. Defining

$$U(\mathbf{r}_i) := \sum_{k\neq i}\frac{\lambda}{|\mathbf{r}_i-\mathbf{r}_k|^\alpha}, \quad \text{and} \quad \mathbf{G}_{ij} := \lambda(\mathbf{r}_i-\mathbf{r}_j)\frac{1}{|\mathbf{r}_i-\mathbf{r}_j|^{\alpha+2}}\ ,$$

we switch to the coordinate representation and evaluate

$$\begin{aligned}-\mathrm{i}\sum_{i=1}^{N}[W(\mathbf{r}),\mathbf{p}_i\mathbf{r}_i+\mathbf{r}_i\mathbf{p}_i] &= -\mathrm{i}\sum_{i=1}^{N}[U(\mathbf{r}_i),\mathbf{p}_i\mathbf{r}_i+\mathbf{r}_i\mathbf{p}_i]\\ &= 2\sum_{i=1}^{N}\frac{\partial U(\mathbf{r}_i)}{\partial\mathbf{r}_i}\mathbf{r}_i = -2\alpha\sum_{i=1}^{N}\sum_{j\neq i}\mathbf{G}_{ij}\cdot\mathbf{r}_i\\ &= -2\alpha\sum_{i<j}\mathbf{G}_{ij}\cdot(\mathbf{r}_i-\mathbf{r}_j) = -2\alpha\hat{W}\ .\end{aligned} \tag{214}$$

With this, one obtains

$$-\mathrm{i}\sum_{i=1}^{N}[\hat{\mathbf{p}}_i\hat{\mathbf{r}}_i+\hat{\mathbf{r}}_i\hat{\mathbf{p}}_i,-2\alpha\hat{W}] = -4\alpha^2\hat{W}$$

and

$$-\frac{1}{2}\langle 0|[[\hat{H}_0,\hat{Q}],[\hat{W},[\hat{H}_0,\hat{Q}]]]|0\rangle = 2\alpha^2\langle\hat{W}\rangle\ .$$

Adding up the terms, one arrives at the desired result,

$$m_3 = 8\langle\hat{T}\rangle + 8\langle\hat{V}\rangle + 2\alpha^2\langle\hat{W}\rangle\ . \tag{215}$$

References

[1] E. Lipparini and S. Stringari, Physics Reports **175**, 103-261 (1989).
[2] S. Stringari, Phys. Lett. B **108**, 232-236 (1982).
[3] O. Bohigas, A. Lane, and J. Martorell, Physics Reports **51**, 267-316 (1979).
[4] J. Martorell, O. Bohigas, S. Fallieros, and A. Lane, Phys. Lett. B **60**, 313-316 (1976).
[5] R. Davidson, Physics of Nonneutral Plasmas (World Scientific, 2001).
[6] D. Dubin and T. O'Neill, Rev. Mod. Phys. **71**, 87-172 (1999).
[7] F. Baletto and R. Ferrando, Rev. Mod. Phys. **77**, 371-423 (2005).
[8] S. Giorgini, L. P. Pitaevskii, and S. Stringari, Rev. Mod. Phys. **80**, 1215-1274 (2008).
[9] F. Dalfovo, S. Giorgini, L.P. Pitaevskii, and S. Stringari, Rev. Mod. Phys. **71**, 463-512 (1999).
[10] I. Bloch, Nature Physics **1**, 23-30 (2005).
[11] A.V. Filinov, M. Bonitz, and Y.E. Lozovik, Phys. Rev. Lett. **86**, 3851-3854 (2001).
[12] A. Filinov, Y. Lozovik, and M. Bonitz, physica status solidi (b) **221**, 231-234 (2000).
[13] S.M. Reimann and M. Manninen, Rev. Mod. Phys. **74**, 1283 (2002).
[14] R.C. Ashoori, Nature **379**, 413-419 (1996).
[15] S. Amiranashvili, M.Y. Yu, and L. Stenflo, Phys. Rev. E **67**, 016408 (2003).
[16] V.A. Schweigert and F.M. Peeters, Phys. Rev. B **51**, 7700-7713 (1995).
[17] S.A. Tatarkova, A.E. Carruthers, and K. Dholakia, Phys. Rev. Lett. **89**, 283901 (2002).
[18] A. Ivlev, H. Löwen, G. Morfill, and C.P. Royall, Complex Plasmas and Colloidal Dispersions: Particle-resolved Studies of Classical Liquids and Solids (World Scientific, 2012).
[19] A. Filinov, N.V. Prokof'ev, and M. Bonitz, Phys. Rev. Lett. **105**, 070401 (2010).
[20] A. Filinov and M. Bonitz, Phys. Rev. A **86**, 043628 (2012).

[21] A. Filinov, M. Bonitz, and Y.E. Lozovik, Contrib. Plasma Phys. **41**, 357 (2001).
[22] J. Schleede, A. Filinov, M. Bonitz, and H. Fehske, Contrib. Plasma Phys. **52**, 819-826 (2012).
[23] P. Harmann, Z. Donko, and G. Kalman, Eur. Phys. Lett. **72**, 396-402 (2005).
[24] P. Ludwig, K. Balzer, A. Filinov, H. Stolz, and M. Bonitz, New J. Phys. **10**, 083031 (2008).
[25] A. Filinov, P. Ludwig, M. Bonitz, and Y.E. Lozovik, J. Phys. A: Math. Gen. **42**, 214016 (2009).
[26] J. Böning, A. Filinov, and M. Bonitz, Phys. Rev. B **84**, 075130 (2011).
[27] M. Bonitz, C. Henning, and D. Block, Rep. Prog. Phys. **73**, 066501 (2010).
[28] A. Olivetti, J. Barré, B. Marcos, F. Bouchet, and R. Kaiser, Phys. Rev. Lett. **103**, 224301 (2009).
[29] C. Henning, K. Fujioka, P. Ludwig, A. Piel, A. Melzer, and M. Bonitz, Phys. Rev. Lett. **101**, 045002 (2008).
[30] E. Wigner, Phys. Rev. **46**, 1002-1011 (1934).
[31] A. Filinov, J. Böning, M. Bonitz, and Y.E. Lozovik, Phys. Rev. B **77**, 214527 (2008).
[32] M. Bonitz, P. Ludwig, H. Baumgartner, C. Henning, A. Filinov, D. Block, O. Arp, A. Piel, S. Käding, Y. Ivanov, A. Melzer, H. Fehske, and V. Filinov, Physics of Plasmas **15**, 055704 (2008).
[33] A. Melzer, A. Schella, T. Miksch, J. Schablinski, D. Block, A. Piel, H. Thomsen, H. Kählert, and M. Bonitz, Contrib. Plamsa Phys. **52**, 795-803 (2012).
[34] J. Meichsner, M. Bonitz, A. Piel, and H. Fehske, Contrib. Plamsa Phys. **52**, 789 (2012).
[35] H. Moritz, T. Stöferle, M. Köhl, and T. Esslinger, Phys. Rev. Lett. **91**, 250402 (2003).
[36] C. Menotti and S. Stringari, Phys. Rev. A **66**, 043610 (2002).
[37] C.R. McDonald, G. Orlando, J.W. Abraham, D. Hochstuhl, M. Bonitz, and T. Brabec, Phys. Rev. Lett. **111**, 256801 (2013).
[38] W. Kohn, Phys. Rev. **123**, 1242 (1961).
[39] M. Bonitz, K. Balzer, and R. van Leeuwen, Phys. Rev. B **76**, 045341 (2007).
[40] R. Schmitz, S. Krönke, L. Cao, and P. Schmelcher, Phys. Rev. A **88**, 043601 (2013).
[41] J.W. Abraham, K. Balzer, D. Hochstuhl, and M. Bonitz, Phys. Rev. B **86**, 125112 (2012).
[42] S. Bauch, D. Hochstuhl, K. Balzer, and M. Bonitz, Journal of Physics: Conference Series **220**, 012013 (2010).
[43] S. Peotta, D. Rossini, M. Polini, F. Minardi, and R. Fazio, Phys. Rev. Lett. **110**, 015302 (2013).
[44] M.N. Harakeh, K. vander Borg, T. Ishimatsu, H.P. Morsch, A. vander Woude, and F.E. Bertrand, Phys. Rev. Lett. **38**, 676-679 (1977).
[45] D.H. Youngblood, C.M. Rozsa, J.M. Moss, D.R. Brown, and J.D. Bronson, Phys. Rev. Lett. **39**, 1188-1191 (1977).
[46] D.H. Youngblood, H.L. Clark, and Y.W. Lui, Phys. Rev. Lett. **82**, 691-694 (1999).
[47] F. Chevy, V. Bretin, P. Rosenbusch, K.W. Madison, and J. Dalibard, Phys. Rev. Lett. **88**, 250402 (2002).
[48] F. Dalfovo, S. Giorgini, M. Guilleumas, L. Pitaevskii, and S. Stringari, Phys. Rev. A **56**, 3840-3845 (1997).
[49] S. Stringari, Phys. Rev. Lett. **77**, 2360-2363 (1996).
[50] M.O. Mewes, M.R. Andrews, N.J. van Druten, D.M. Kurn, D.S. Durfee, C.G. Townsend, and W. Ketterle, Phys. Rev. Lett. **77**, 988-991 (1996).
[51] A. Altmeyer, S. Riedl, C. Kohstall, M.J. Wright, R. Geursen, M. Bartenstein, C. Chin, J.H. Denschlag, and R. Grimm, Phys. Rev. Lett. **98**, 040401 (2007).
[52] T.N. De Silva and E.J. Mueller, Phys. Rev. A **72**, 063614 (2005).
[53] J. Kinast, A. Turlapov, and J.E. Thomas, Phys. Rev. A **70**, 051401 (2004).
[54] B. Partoens and F.M. Peeters, Journal of Physics: Condensed Matter **9**(25), 5383 (1997).
[55] C. Henning, Ground State and Excitation Properties of Yukawa Balls, Phd thesis, University of Kiel, 2009.
[56] S. Bauch, K. Balzer, C. Henning, and M. Bonitz, Phys. Rev. B **80**, 054515 (2009).
[57] N.G. Parker and D.H.J. O'Dell, Phys. Rev. A **78**, 041601 (2008).
[58] W. Bao, Y. Cai, and H. Wang, Journal of Computational Physics **229**, 7874-7892 (2010).
[59] D.H.J. O'Dell, S. Giovanazzi, and C. Eberlein, Phys. Rev. Lett. **92**, 250401 (2004).
[60] C. Eberlein, S. Giovanazzi, and D.H.J. O'Dell, Phys. Rev. A **71**, 033618 (2005).
[61] Y.E. Kim and A.L. Zubarev, Phys. Lett. A **289**, 155-159 (2001).
[62] W. Greiner, Theoretische Physik 04. Quantenmechanik 1, Theoretische Physik (Deutsch Harri GmbH, 2005).
[63] D.H.E. Dubin and J.P. Schiffer, Phys. Rev. E **53**, 5249-5267 (1996).
[64] H.E. Montgomery, G. Campoy, and N. Aquino, ArXiv e-prints 0803.4029 (2008).
[65] S. Al-Jaber, International Journal of Theoretical Physics **47**, 1853-1864 (2008).
[66] R. Yá nez, W. Van Assche, R. González-Férez, and J.S. Dehesa, J. Math. Physics **40** (1999).
[67] K. Balzer, M. Bonitz, R. van Leeuwen, A. Stan, and N.E. Dahlen, Phys. Rev. B **79**, 245306 (2009).
[68] K. Balzer, Nonequilibrium Green's function approach to artificial atoms, Diploma thesis, University of Kiel, 2007.
[69] M. Girardeau, Journal of Mathematical Physics **1**, 516-523 (1960).
[70] M. Taut, Journal of Physics A: Mathematical and General **27**, 1045 (1994).
[71] M.R. Geller and G. Vignale, Phys. Rev. B **53**, 6979-6980 (1996).
[72] N. Kwong and M. Bonitz, Phys. Rev. Lett. **84**, 1768 (2000).
[73] V. Adamyan and I. Tkachenko, Contrib. Plasma Phys. **43**, 252-257 (2003).
[74] F. Reiche and W. Thomas, Zeitschrift für Physik A Hadrons and Nuclei **34** (1925).
[75] W. Kuhn, Zeitschrift für Physik A Hadrons and Nuclei **33**, 408-412 (1925).

[76] H. Bethe, Annalen der Physik **397**, 325-400 (1930).
[77] S. Wang, Phys. Rev. A **60**, 262-266 (1999).
[78] A. Olivetti, J. Barr, B. Marcos, F. Bouchet, and R. Kaiser, Transport Theory and Statistical Physics **39**, 524-551 (2010).
[79] P. Ludwig, W. Miloch, H. Kählert, and M. Bonitz, New J. Phys. **14**, 053016 (2012).
[80] D. Block, J. Carstensen, P. Ludwig, W. Miloch, F. Greiner, A. Piel, M. Bonitz, and A. Melzer, Contrib. Plamsa Phys. **52**, 804 (2012).
[81] F. Schwabl, Quantenmechanik (Qm I): Eine Einführung, Springer-Lehrbuch (Springer, 2004).
[82] K. Balzer and M. Bonitz, Nonequilibrium Green's Functions Approach to Inhomogeneous Systems, Lecture Notes in Physics, Vol.867 (Springer, 2013).
[83] D. Hochstuhl, Multiconfigurational methods for the numerical simulation of photoionization processes of many-electron atoms, Phd thesis, University of Kiel, 2013.
[84] S. Kvaal, ArXiv e-prints 0810.2644 (2008).
[85] T.N. Rescigno and C.W. McCurdy, Phys. Rev. A **62**, 032706 (2000).
[86] K. Balzer, S. Bauch, and M. Bonitz, Phys. Rev. A **81**, 022510 (2010).
[87] K. Balzer, Solving the Two-time Kadanoff-Baym Equations. Application to Model Atoms and Molecules, Phd thesis, University of Kiel, 2011.
[88] T. Helgaker, J. Olsen, and P. Jorgensen, Molecular Electronic-Structure Theory (Wiley, 2013).
[89] A. Szabó and N. Ostlund, Modern Quantum Chemistry: Introduction to Advanced Electronic Structure Theory, Dover Books on Chemistry Series (Dover Publications, 1996).
[90] M. Bonitz and D. Semkat (eds.), Introduction to computational methods in many body physics (chapter by M. Bonitz and A. Filinov) (Rinton Press, Princeton, 2006).
[91] N. Metropolis, A.W. Rosenbluth, M.N. Rosenbluth, A.H. Teller, and E. Teller, J. Chem. Phys **21**, 1087-1092 (1953).
[92] M. Boninsegni, N.V. Prokof'ev, and B.V. Svistunov, Phys. Rev. E **74**, 036701 (2006).
[93] E. Baerends, D. Ellis, and P. Ros, Chemical Physics **2**, 41-51 (1973).
[94] C. Bunge, J. Barrientos, and A. Bunge, Atomic Data and Nuclear Data Tables **53**, 113-162 (1993).
[95] M. Bonitz, Quantum Kinetic Theory (B.G. Teubner, Stuttgart/Leipzig, 1998).
[96] F. Jensen, Introduction to Computational Chemistry (John Wiley & Sons, 2007).
[97] L. Rosenthal, Greensfunktionszugang zu Elektron-Loch-Bilayern, Diploma thesis, University of Kiel, 2009.
[98] W. Ritz, Journal für die reine und angewandte Mathematik **135**, 1-61 (1909).
[99] C.C.J. Roothaan, Rev. Mod. Phys. **23**, 69-89 (1951).
[100] G.G. Hall, Proceedings of the Royal Society of London. Series A. Mathematical and Physical Sciences **205**, 541-552 (1951).
[101] J.A. Pople and R.K. Nesbet, J. Chem. Phys **22**, 571-572 (1954).
[102] P. Kramer and M. Saraceno, Geometry of the time-dependent variational principle in quantum mechanics, in: Group Theoretical Methods in Physics, edited by K. Wolf, Lecture Notes in Physics Vol.135 (Springer Berlin / Heidelberg, 1980).
[103] M. Bonitz, N. Horing, and P. Ludwig (eds.), Introduction to Complex Plasmas (chapter by K. Balzer), Springer Series on Atomic, Optical, and Plasma Physics (Springer, 2010).
[104] P.A.M. Dirac, Mathematical Proceedings of the Cambridge Philosophical Society **26**, 376 (1930).
[105] J. Frenkel, Wave mechanics: advanced general theory, The International series of monographs on nuclear energy: Reactor design physics (The Clarendon Press, 1934).
[106] D.B. Boercker and J.W. Dufty, Annals of Physics **119**, 43-70 (1979).
[107] Y.L. Klimontovich, D. Kremp, and W.D. Kraeft, Kinetic Theory for Chemically Reacting Gases and Partially Ionized Plasmas (Advances in Chemical Physics, John Wiley & Sons, Inc., 2007).
[108] N.N. Bogolyubov, Problems of Dynamical Theory in Statistical Physics (Gostekhisdat (russ), 1946).
[109] N. Bogolyubov, in: Studies in Statistical Mechanics, Volume 1, edited by G. Uhlenbeck and J. deBoer (North-Holland, Amsterdam, 1961).
[110] L.H. Thomas, Mathematical Proceedings of the Cambridge Philosophical Society **23**, 542-548 (1927).
[111] E. Fermi, Rend. Accad. Naz. Lincei **6**, 602 (1927).
[112] L. Spruch, Rev. Mod. Phys. **63**, 151-209 (1991).
[113] N. March, Advances in Physics **6**, 1-101 (1957).
[114] E.H. Lieb and B. Simon, Phys. Rev. Lett. **31**, 681-683 (1973).
[115] E.H. Lieb and B. Simon, Advances in Mathematics **23**, 22-116 (1977).
[116] H. Kunz and R. Rueedi, Phys. Rev. A **81**, 032122 (2010).
[117] G.E. Astrakharchik and M.D. Girardeau, Phys. Rev. B **83**, 153303 (2011).
[118] R. Pino, Phys. Rev. B **58**, 4644-4648 (1998).
[119] S. Sinha, Physica E: Low-dimensional Systems and Nanostructures **8**, 24-39 (2000).
[120] J. Kiefer, Proc. Amer. Math. Soc. **4**, 502-506 (1953).
[121] G.V. Shpatakovskaya, Physics-Uspekhi **55**, 429-464 (2012).
[122] K. Schönhammer, Journal of Physics: Condensed Matter **25**, 014001 (2013).

[123] G.E. Astrakharchik, Phys. Rev. A **72**, 063620 (2005).
[124] E.Y. Loh, J.E. Gubernatis, R.T. Scalettar, S.R. White, D.J. Scalapino, and R.L. Sugar, Phys. Rev. B **41**, 9301-9307 (1990).
[125] J.W. Abraham, M. Bonitz, C. McDonald, G. Orlando, and T. Brabec, New J. Phys. **16**, 013001 (2014).
[126] J. Wrighton, H. Kählert, T. Ott, P. Ludwig, H. Thomsen, J. Dufty, and M. Bonitz, Contributions to Plasma Physics **52**, 45-48 (2012).
[127] D. Landau and K. Binder, A Guide To Monte Carlo Simulations In Statistical Physics (Cambridge University Press, 2005).
[128] D. Meschede and C. Gerthsen, Gerthsen Physik: Dieter Meschede, Springer-Lehrbuch (Springer-Verlag, 2003).
[129] T. Koch, T. Lahaye, J. Metz, B. Fröhlich, A. Griesmaier, and T. Pfau, Nature Physics **4**, 218-222 (2008).
[130] D. Hochstuhl and M. Bonitz, Phys. Rev. A **86**, 052424 (2012).
[131] D. Hochstuhl, C. Hinz, and M. Bonitz, European Physical Journal Special Topics (2014).
[132] M. Bonitz, S. Hermanns, and K. Balzer, Contrib. Plamsa Phys. **53**, 778-787 (2013).
[133] G.H. Booth, A.J.W. Thom, and A. Alavi, J. Chem. Phys **131**, 054106 (2009).
[134] T. Schoof, M. Bonitz, A. Filinov, D. Hochstuhl, and J. Dufty, Contributions to Plasma Physics **51**, 687-697 (2011).